FEDERAL UNIVERSITY OF TECNOLOGY - PARANÁ

POSTGRADUATE PROGRAM IN MECHANICAL AND MATERIALS ENGINEERING

LUIS HUMBERTO QUITIAN ARDILA

RHEOLOGICAL AND THERMAL CHARACTERIZATION OF THE EFFECTS OF HIGH PRESSURE AND HIGH TEMPERATURE ON THE PROPERTIES OF WATER-BASED DRILLING FLUIDS WITH XANTHAN GUM

MASTER THESIS

CURITIBA

2021

LUIS HUMBERTO QUITIAN ARDILA

RHEOLOGICAL AND THERMAL CHARACTERIZATION OF THEEFFECTS OF HIGH PRESSURE AND HIGH TEMPERATURE ON THE PROPERTIES OF WATER-BASED DRILLING FLUIDS WITH XANTHAN GUM

Caracterização Reológica e Térmica Dos Efeitos de Alta Pressão e Alta Temperatura nas Propriedades de Fluidos de Perfuração à Base de Água com Goma Xantana

MSc thesis presented to the Postgraduate Program in Mechanical and Materials Engineering from the Federal University of Technology – Paraná, as fulfillment of the requirements for Master degree in Engineering. Concentration area: Thermal Engineering.

Supervisor: Prof. Dr. Admilson Teixeira Franco

CURITIBA

2021

Ministério da Educação
Universidade Tecnológica Federal do Paraná
Câmpus Ponta Grossa

LUIS HUMBERTO QUITIAN ARDILA

RHEOLOGICAL AND THERMAL CHARACTERIZATION OF THE EFFECTS OF HIGH PRESSURE AND HIGH TEMPERATURE ON THE PROPERTIES OF WATER-BASED DRILLING FLUIDS WITH XANTHAN GUM

Trabalho de pesquisa de mestrado apresentado como requisito para obtenção do título de Mestre Em Engenharia da Universidade Tecnológica Federal do Paraná (UTFPR). Área de concentração: Engenharia Térmica.

Data de aprovação: 04 de maio de 2021.

Prof. Admilson Teixeira Franco, Doutorado - Universidade Tecnológica Federal do Paraná
Prof. Cezar Otaviano Ribeiro Negrao, Doutorado - Universidade Federal do Paraná
Profa. Luciana Viana Amorim, Doutorado - Universidade Federal de Campina Grande
Prof. Moises Alves Marcelino Neto, Doutorado - Universidade Federal do Paraná

I dedicate this work to my family who have always taught
me how to build the path to success and who, thanks to
their efforts, have made it so far.

ACKNOWLEDGEMENTS

I acknowledge my parents, who gave me the most precious teaching, for their support and guidance. My mother has always been my motivation and has encouragement bestowed upon me. To my father, who taught me to work hard every day to build my way. And to my sisters and niece who have always given me the best emotional support so as not to give up on my dreams.

To my supervisor, Admilson T. Franco, and my co-supervisor, Jonathan F. Galdino, for the opportunity, guidance, dedication, patience, and confidence in my capacity.

The colleagues of LabReo - CERNN, who was present throughout the experimental stage, and the researchers for their invaluable support in doing this work. I would like to thank Petrobras for the economic support in the first months of my master's degree.

Finally, this study was financed in part by the Coordenação de Aperfeiçoamento de Pessoal de Nível Superior - Brasil (CAPES) - Finance Code 001

The risk of moving toward your dreams is much lower
than the slow, everyday punishment you inflict on
yourself by suppressing your dream.
(Mel Robbins, 2015).

ABSTRACT

QUITIAN, Luis Humberto. **Rheological and Thermal Characterization of the Effects of High Pressure and High Temperature on the Properties of Water-Based Drilling Fluids with Xanthan Gum**. Master of Science Dissertation. Postgraduate Program in Mechanical and Materials Engineering, the Federal University of Technology – Paraná, Curitiba, Brazil, 136 pages, 2021.

The water-based drilling fluid with xanthan gum and limestone under high-pressure and high-temperature conditions is investigated in the following experimental study using an Anton Paar MCR 702TD rheometer with pressure cell. A wide range of mud suspensions is commonly used in the oil well drilling process. Water-based drilling fluid is used in some stages during the drilling process due to its low environmental impact and costs. HPHT conditions have several effects on the rheological behavior of water-based drilling fluids. For a better understanding of the process and knowledge of the implications of under HPHT conditions work, rheological and thermal analyzes were performed. Flow curves, flow start-up, time, and shear stress oscillatory sweeps were obtained in order to study the rheological behavior in a temperature range of 4 to 125 °C and 10 to 800 bar pressures. Also, thermal stability was investigated through 16 hours' dynamic thermal aging tests on Rover Oven Fann at temperatures of 55, 70, 90, 100, and 125 °C) in order to analyze the effects of thermal aging on its rheological properties. In addition to that microcalorimeter, tests were performed to determine the xanthan gum's transition temperature, which was the first indication of a decrease in drilling fluid viscosity. The viscosity suffered a decrease due to temperature growth and increased with pressure increment. A methodology was proposed to obtain HPHT measurements for water-based drilling fluid with xanthan gum, considering a change in the xanthan gum's conformation with increasing temperature. The static yield stresses obtained from the dynamic modules crossing were higher than the dynamic yield stress. Besides, temperature and pressure showed a decrease and a gain in the fluid structure, respectively. Next, an apparent viscosity fit was developed as a function of pressure, temperature and shear rate, based on experimental models. The experimental results showed that viscosity is sensitive to downhole conditions. Finally, the increase of the xanthan gum concentration in the drilling fluid was analyzed, presenting favorable characteristics in terms of transition temperature growth and fluid capacity considering operational scenarios.

Keywords: Water-based drilling fluids. Xanthan gum. HPHT. Thermal stability. Visco-elastoplastic fluid.

RESUMO

QUITIAN, Luis Humberto. **Caracterização Reológica e Térmica Dos Efeitos de Alta Pressão e Alta Temperatura nas Propriedades de Fluidos de Perfuração à Base de Água com Goma Xantana**. Dissertação de Mestrado. Programa de Pós-Graduação em Engenharia Mecânica e de Materiais, Universidade Tecnológica Federal do Paraná, Curitiba, Brasil, 136 páginas, 2021.

O seguinte estudo experimental investiga o fluido de perfuração à base de água com goma xantana e limestone sob condições de alta pressão e alta temperatura utilizando o reômetro Anton Paar MCR 702TD com célula de pressão. Uma ampla gama de suspensões de argila é comumente usada no processo de perfuração de poços de petróleo. O fluído de perfuração à base de água é utilizado em algumas etapas durante o processo devido ao seu baixo impacto ambiental e baixo custo. As condições HPHT têm vários efeitos no comportamento reológico de fluídos de perfuração à base de água. Para compreender melhor o processo e estudar as implicações do trabalho em condições HPHT, análises reológicas e térmicas foram realizadas. Para estudar o comportamento reológico em uma faixa de temperatura de 4 a 125 °C e pressões de 10 a 800 bar, foram medidas curvas de escoamento, reinício de escoamento, testes oscilatórios de varreduras de tempo e tensão de cisalhamento. Além disso, com o intuito de analisar os efeitos do envelhecimento térmico nas propriedades reológicas do fluído, a estabilidade térmica foi investigada através de testes de envelhecimento térmico dinâmico de 16 horas em Forno Fann Rover em temperaturas de 55, 70, 90, 100 e 125 °C. Adicionalmente, foram realizados testes de micro calorímetro para determinar a temperatura de transição da goma xantana, que foi o primeiro indício de uma diminuição na viscosidade do fluído de perfuração. Neste sentido, notou-se que a viscosidade diminui com ao aumento da temperatura e cresce com incremento da pressão. O presente estudo propõe uma metodologia para obter medições do fluido de perfuração a base de água com goma xantana sob condições HPHT, considerando a ocorrência de uma alteração em sua conformação como resposta ao aumento da temperatura. A TLEs (Tensão Limite de Escoamento) estática, obtida a partir do cruzamento dos módulos dinâmicos, foi superior à TLEs dinâmico. Além disso, temperatura e pressão apresentaram, respectivamente, diminuição e aumento na estrutura do fluído. Em seguida, foi desenvolvido um ajuste de viscosidade aparente em função da pressão, temperatura e taxa de deformação, com base em modelos experimentais. Os resultados experimentais mostraram que a viscosidade é sensível às condições existentes no fundo do poço de perfuração. Por fim, foi analisado o aumento da concentração de goma xantana no fluido de perfuração, apresentando características favoráveis em termos de aumento da temperatura de transição e capacidade de fluido em relação aos cenários operacionais.

Palavras-chave: Fluidos de perfuração a base de água. Goma xantana. HPHT. Estabilidade térmica. Fluido viscoelastoplástico.

LIST OF FIGURES

LIST OF TABLES

LIST OF ABBREVIATIONS AND ACRONYMS

ANP	Agência Nacional do Petróleo
API	American Petroleum Institute
BOP	Blowout preventer
BHP	Bottom Hole Pressure
CFD	Computational Fluid Dynamics
CGA	Colloidal Gas Aphron
CNT	Carbon Nano-Tubes
ECD	Equivalent Circulating Density
GDP	Gross Domestic Product
HPHT	High-Pressure High-Temperature
LiCl	Lithium Chloride
OBM	Oil Based Mud
KCl	Potassium Chloride
QSP	Qualified SWPPP Practitioners
NaCl	Sodium Chloride
SWPPP	Storm Water Pollution Prevention Plans
SBM	Synthetic Based Mud
TIPS	Thermally Induced Phase Separation
WBM	Water-Based Mud
CMC	Carboxy Methyl Cellulose
LVR	Linear Visco-elastoplastic Region
GON	Graphene Oxide Nanoparticles
VTF	Vogel-Tammann-Fulcher
WLF	Williams-Landel-Ferry

PVT	Pressure-Volume-Temperature
DSC	Differential Scanning Calorimetry
ASTM	American Society for Testing and Materials
AARD	Absolute Average Relative Deviation

NOMENCLATURE

Roman letters and symbols

m	Consistency coefficient	$[Pa \cdot s^n]$
n	Flow behavior index	$[-]$
t	Time	$[s]$
P	Pressure	$[bar]$
T	Temperature	$[°C]$
T_m	Transition Temperature	$[°C]$
P_{ref}	Pressure of reference	$[bar]$
k_0	Yield stress for the Casson model	$[Pa]$
k_1	High shear viscosity for the Casson model	$[Pa \cdot s]$
v_k	Specific speed constant of a chemical reaction	$[-]$
A	Frequency factor	$[-]$
E_a	Activation energy	$[kJ \cdot mol]$
R	Ideal gas constant	$[J \cdot K^{-1} mol^{-1}]$
C	Pressure coefficient	$[bar^{-1}]$
D	Constants in Arrhenius equation	$[Pa \cdot s]$
B	Constants in Arrhenius equation	$[Pa \cdot s]$
A_n	Pre-exponential factor	$[Pa \cdot s]$
B'	Model Constant equation 3.4	$[bar^{-1}]$
C'	Model Constant equation 3.4	$[bar^{-1}]$
T_∞	The Vogel temperature	$[°C]$
D_f	Fragility parameter	$[-]$
T_{ref}	Temperature of reference	$[°C]$
c_1	WLF constant	$[-]$
c_2	WLF constant	$[°C]$
a_p	Pressure shift factor	$[-]$
B''	Model Constant equation 3.6	$[-]$
f_0	The fraction of the fractional volume at reference	$[-]$
f	The fraction of the fractional volume	$[-]$
K^*	The bulk modulus at zero pressure	$[-]$
k	Empirical constant bulk modulus at pressure	$[-]$
k_e^*	The bulk module of the entire volume	$[-]$
k_ϕ^*	The bulk module of the occupied volume	$[-]$
k_e	Proportionality constant	$[-]$

k_ϕ	Proportionality constant	$[-]$
C''	Proportionality constant of equation 3.10	$[-]$
E	Least squares error	$[-]$
G'	Storage modulus	$[Pa]$
G''	Loss modulus	$[Pa]$
M	Torque	$[Pa]$
L	Height of cylindrical part of the rotor	$[mm]$
C_L	End effect correction factor	$[-]$
r_e	The outer radius of the rotor	$[mm]$
r_i	The inner radius of the cup	$[mm]$
N	Speed	$[rpm]$
R^2	Correlation coefficient	$[-]$
C_{XG}	Xanthan Gum Concentration	$[-]$
X_i	The shear stress filtered at any time	[Pa]
$X_{i+50sec}$	The shear stress filtered after 50 seconds	[Pa]
t_{obs}	The observation time of the phenomenon	$[sec]$
De	Deborah's number	$[-]$

Greek letters

τ	Shear stress	$[Pa]$
γ	Shear rate	$[s^{-1}]$
μ	Newtonian fluid dynamic apparent viscosity	$[Pa \cdot s]$
η	Viscoplastic fluid apparent viscosity	$[Pa \cdot s]$
τ_0	Yield stress	$[Pa]$
η_B	Apparent viscosity for the Bingham model	$[Pa \cdot s]$
τ_0^B	Yield stress for the Bingham model	$[Pa]$
τ_0^H	Yield stress for the Herschel-Bulkley model	$[Pa]$
γ	Strain	$[Pa]$
β	Piezoviscous coefficient	$[Pa^{-1}]$
η_{ref}	Apparent viscosity at the reference temperature	$[Pa \cdot s]$
η_c	Apparent viscosity for the Casson model	$[Pa \cdot s]$
α	Packing factor	$[-]$
ϕ	Solid fraction	$[-]$
β_p	Isothermal compressibility	$[bar^{-1}]$
η_∞	Apparent viscosity at the Vogel temperature	$[Pa \cdot s]$
θ	Material-dependent empirical parameter	$[C]$
α_v	Expansivity of the free volume	$[-]$
α_ϕ^*	Expansivity of the occupied volume at zero differential pressure	$[-]$

α_f^*	Expansivity of the free volume at zero differential pressure and temperature of the reference	$[-]$
τ_{out}	Final Yield stress	$[Pa]$
τ_{in}	Initial Yield stress for the Bingham model	$[Pa]$
μ_{oil}	Apparent viscosity for oil	$[Pa \cdot s]$
η_{mud}	Apparent viscosity for mud	$[Pa \cdot s]$
η_{red}	Reduced viscosity	$[Pa \cdot s]$
ω	Angular velocity	$[rad \cdot s]$
δ	Radius ratio	$[s]$
λ	The relaxation time of the material	$[sec]$

Superscripts and Subscripts

$(\,)_T$	Evaluated at a constant temperature

Operators

$(\partial ln/\partial ln)$	Coefficient logarithmic of sensitivity for a variable

CONTENTS

1 INTRODUCTION

1.1 CONTEXT

The world economy was strongly dependent on oil for over a hundred years, which is currently responsible for approximately 2.5% of the world's Gross Domestic Product (GDP) and represents one-third of humanity's primary energy supply. The oil production development began with subsequent advances in drilling technology, when oil was extracted in only small amounts, usually from shallow or naturally exposed oil wells, until the mid-19th century. From the second half of the 19th and 20th centuries, the demand for oil, and especially its components, began to rise due to the incremented use of engines and other industrial developments.

As the energy demand for oil and gas worldwide rapidly rose in the 20th century, the oil companies are always pursuing new hydrocarbon reservoirs once the conventional reserves are being depleted. Therefore, companies are now focusing their effort to drill and explore deeper wells. Nowadays, the oil and gas companies are dealing with the challenges presented by the sea's extreme depths and high variation of geological conditions that increase drilling difficulty. Some of them are the large gradients of temperature and pressure.

According to Westwood Wildcat Service (2018), the region with the most significant number on offshore well exploration in 2019, with at least 100 million barrels of oil, was Central and South America, represented by Brazil and Mexico, followed by Europe, Africa, North America, Middle East, Asia, and Australia. In Brazil, the largest oil company in the country, PETROBRAS, predicts high-pressure and high-temperature zones in its future wells in the Pre-Salt region, in Santos, Campos, and Espírito Santo basins. According to the Brazilian National Agency of Petroleum (2018), the number of conventional offshore and pre-salt wells is increasing rapidly. For instance, there was an increase of 160% in oil production in the Pre-Salt compared 2014 to 2017, demonstrating that Brazil will be one of the four countries responsible for covering the world demand growth up to 2025. Despite the increment, new wells explored in offshore environments present more challenging conditions, requiring technologies capable of reducing production costs and increasing environmental safety.

Seymour, MacAndrew et al. (1993) proposed the definition of the high-pressure and high-temperature drilling wells, which are wells with blowout preventer system equipment (BOP) that has a working rating pressure up to 690 bar, and the bottom hole temperature exceeds 149 °C as is shown in Figure 1.1, which presented ranges of pressures and temperatures in the international system units (upper) and English units (lower), which are those implemented mainly by the companies responsible for drilling. Also, other levels were defined, due to the presence of even more extreme conditions at the bottom hole than those presented by HPHT definition, Level I (HPHT); Level II (Ultra HPHT); Level III (Extreme HPHT). The most used definition is proposed by Schlumberger (DONG; CHEN, 2017), with temperatures from 149 to 204 °C and pressures from 690 to 1378 bar (TELESFORO; ANTONIO, 2017).

The drilling process involves several necessary steps, such as constructing the hole, casing, completion, production, and abandonment of the well. During construction of the hole, a drill bit and

Figure 1.1 – HPHT classification system as a function of temperature and pressure.

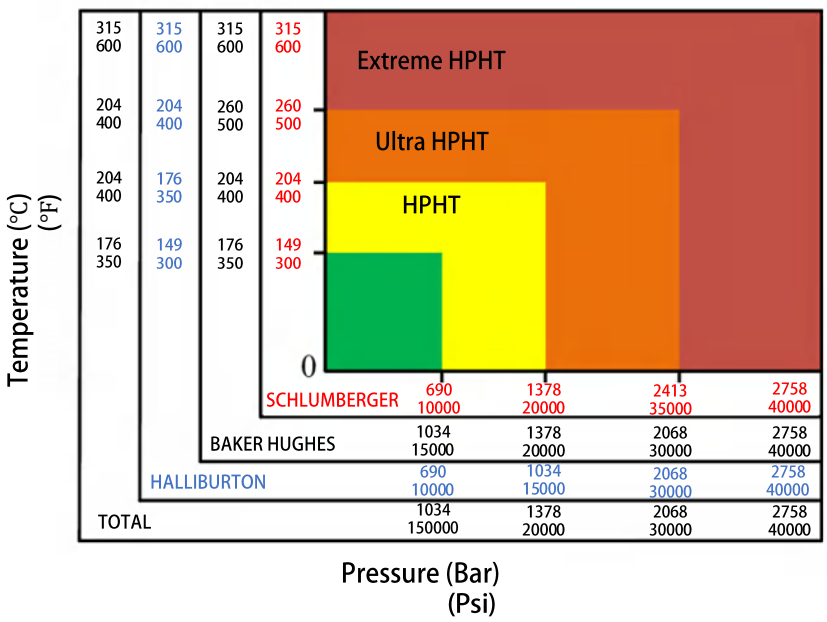

Source: Adapted from Dong e Chen (2017).

drill string are used to create a vertical or horizontal hole into the ground, requiring a circulation system with drilling fluids capable of removing cuttings during the construction process, among other essential functions. The oil and gas industry analysts consider that the drilling fluid significantly impacts petroleum wellholes' total costs, varying between 15 and 18% (ALCÁZAR-VARA; CORTÉS-MONROY, 2018). Therefore, successful drilling depends remarkably on a broad understanding of the drilling fluids' properties, which must be designed to adapt to the formation conditions during the entire drilling process (HERMOSO et al., 2014). Formulating drilling fluids suitable for HPHT operations in areas such as pre-salt contributes to more efficient processes. One of the main problems in drilling in such areas is the alteration of drilling fluids' properties. Pressure and temperature affect several variables, such as apparent viscosity, yield stress, and density (IBEH, 2007).

In the early days of oil exploration, water-based drilling fluid was pioneered due to its capacity to carry cuttings from the bottom of the well to the surface and, at the same time, to serve as well controllers. However, many other news challenges appeared with harsher and operation conditions, such as high-pressure and high-temperature, causing the degradation of the water-based drilling fluid. As a consequence, new types of drilling fluids were developed, such as oil-based and synthetic-based ones.

Today, due to scientific advances, water-based drilling fluids are overcoming their limitations at HPHT conditions by the addition of new compounds, such as nanoparticles or viscosifiers. The use of new viscosifiers has been the best and most economical solution. Over the years, various viscosifiers such as bentonite, laponite, and other clay have been the most widely used in water-based drilling fluid. However, in recent years, various viscosifiers based on synthetic and natural polymers such as polysaccharides (starch, CMC, and mainly xanthan gum) have been used due to their biodegradability and

more stable rheological properties. The formulation of new drilling fluids and the use of new viscosifiers has been shown to improve their rheological properties allowing deeper well-drilling (ANOOP et al., 2019; MOHIDEEN; SAHEED; MOHAMED, 2019). Therefore, water-based drilling fluids are returning to be used by the oil and gas industry in deep areas, bringing costs reduction of drilling with less environmental impact when compared to the oil-based ones.

1.2 PROBLEM ASSESSMENT

The success recorded in offshore exploration and drilling operations has encouraged oil companies to drill deeper and new areas. These new reserves are very challenging to explore due to the harsh conditions at the bottom hole. Drilling fluids are essential to reach these high depths. Thus, to reach great depths and carry out successful drilling of the well, a comprehensive analysis of the properties and a good selection of the fluid used in the drilling process is required (HERMOSO; MARTÍNEZ-BOZA; GALLEGOS, 2014).

Drilling fluids are complex materials that display elastoviscoplastic and thixotropic characteristics. Drilling fluids present a reversible time-dependent decreasing viscosity under shear and display yield stress that characterizes the transition from a structured state to an unstructured one induced by shear stress. Drilling fluids have various functions, such as carrying cuttings created by the drilling process and facilitating their exit to the surface, cool and lubricating the drill bit, and preserving the walls' stability (CAENN; CHILLINGAR, 1996). Additionally, one of the main functions of drilling fluids is to hold in suspension the cuttings when the flow is interrupted. The drilling fluid must form a gelled structure to maintain the cutting in suspension, allowing maintenance stoppages and the drill bit change without precipitating the cuttings. Otherwise, the particulate material may bury the drill bit and, consequently, makes it difficult to restart the drilling process. This capacity of forming a gelled structure and the degree of gelification are directly related to the drilling fluid rheology.

Another vital function of the drilling fluid is the pressure control. An overbalanced drilling is desired in most cases, in which the wellbore pressure is kept above the pore pressure, but without exceeding the fracture pressure. When good pressure control is not carried out during drilling, phenomena such as kick appear, i.e., an influx of gas from the formation into the well (CARLSEN; NYGAARD; NIKOLAOU, 2013). If gas kicks are not adequately controlled, they may escalate to blowouts, i.e., the uncontrolled influx from the formation into the wellbore to the surface (VAJARGAH; OORT, 2015). A blowout can result in loss of life, immeasurable damages to the environment, and financial losses to the oil company (AHMED; HEGAB; SABRY, 2016; CHERU, 2017). Simultaneously, the wellbore pressure cannot exceed the fracture pressure, or the formation will suffer a mechanical failure with consequent fluid loss (MITCHELL; MISKA et al., 2011).

The bottom hole pressure may fall below the pore pressure or be above the fracture pressure due to changes in the drilling fluid rheology, and these changes can be caused by pressure and temperature variations. The drilling process has a wide variation in the working conditions, and all these conditions significantly affect the density and the rheology of the drilling fluid. Therefore, the major challenge for offshore oil industries in the drilling of HPHT wells is the choice of drilling fluid technology. The wrong selection can cause lost drilling time, problems related to well stability, circulation losses, and especially

well control situations.

For these reasons, several experimental studies performed fluid rheology measurements under HPHT conditions to predict the drilling fluid's behavior during drilling correctly. The studies observed that the viscosity is directly related to the depth of the well. Pressure gains tend to increase compressibility by decreasing the free-volume between the macromolecules, causing a growth in the fluid's viscosity, while higher thermal gradients boost Brownian movements due to a high molecular interaction. Thus, the viscosity and other rheology properties decrease or increased(IBEH, 2007). In recent years, there has been a growth in studies investigating which model best represents the drilling fluid rheological behavior in HPHT conditions. Some authors concluded that the Arrhenius equation related to activation energy represents best the effect of temperature and Barus equation to pressure, for some fluids, the theoretical models as the free-volume theory describe fairly well temperature and pressure of viscosity dependency (HERMOSO; MARTÍNEZ-BOZA; GALLEGOS, 2014; BALED et al., 2016; HERMOSO; MARTÍNEZ-BOZA; GALLEGOS, 2017; GOKDEMIR; ERKEKOL; DOGAN, 2017; PANASETI et al., 2018).

Consequently, there is a need to understand the rheological behavior of the drilling fluid, especially regarding pressure modeling under high-temperature conditions. Furthermore, no studies were found in the literature that investigated the combined effect of pressure and temperature with rheometers in water-based drilling fluids with xanthan gum.

The new technological challenges motivate the Center for Research in Rheology and Non-Newtonian Fluids (CERNN) to carry out experimental studies to investigate the effects of high-pressure and high-temperature on the rheological properties of water-based drilling fluids. The investigation of the influence of pressure and temperature was developed through Anton Paar MCR 702TD rheometer using a Couette geometry with a pressure cell that reaches 1000 bar.

1.3 OBJECTIVES

The objective of the present study is to investigate and analyze the effects of high-pressure and high-temperature on water-based drilling fluids' rheological properties with xanthan gum and limestone. A methodology is developed for the measurements of rheological properties under HPHT conditions, and the experimental data of the viscosity under HPHT conditions are fitted to theoretical models of free volume. Besides, the increase in the xanthan gum concentration under high-temperature conditions is understood and verified. As a result, this work supports the proper formulation and selection of drilling fluid for the oil well drilling design.

Specific aims were accomplished to reach this objective:

- Develop a methodology for conducting rheological tests with water-based drilling fluids with a concentration of 0.71 g/l of xanthan gum and limestone. That allow obtaining rheological measurements in conditions of high-pressure and high-temperature, to be useful for the design of drilling projects;
- Measure the influence of temperature (4 to 125 °C) at constant pressure (atmospheric pressure and 10 bar) and the effects of pressure (10 to 800 bar) at different temperatures (25, 55, and 100 °C)

on viscosity and the yield stress in drilling fluid. Through tests of flow curves and time and stress amplitude oscillatory sweeps;

- Analyze the influence of thermal history on the rheology of drilling fluids through aging tests (55, 70, 90, 100, and 125 ºC for 16 hours) by implementing the API standard;
- Understand and analyze the transition temperature of the xanthan gum contained in the drilling fluid through micro-calorimetry tests;
- Fit the experimental data of the behavior of viscosity as a function of temperature, pressure, and shear rate through theoretical models of free volume proposed in the literature for drilling fluids;
- Analyze the influence of xanthan gum concentration and high-temperature in the water-based drilling fluid, adding 0.5, 1, and 2% by weight to the base drilling fluid under study;

1.4 DOCUMENT OUTLINE

The work's content is structured into six chapters; the present chapter is a brief introduction contextualizing the oil industry scenario and solving the challenges that arise in drilling deep areas. In this chapter, the general objective of this work is also defined.

Chapter 2 depicts the theoretical framework about non-Newtonian fluids' flow, drilling fluids, and dependence pressure and temperature on drilling fluids. These concepts are necessary for the proper understanding of the following chapters.

Chapter 3 presents a literature review of water-based drilling fluids under HPHT conditions showing relevant previous experimental studies and also was proposed experimental review related to the xanthan gum solutions with sodium chloride.

The material and methods are depicted in Chapter 4, encompassing the fluid to was used, the different rheological equipment, and the methodology defined for the rheological tests.

Chapter 5 presents the results evaluating temperature effects and pressure on the rheological properties of water-based drilling fluid.

Chapter 6 summarizes the main conclusions from this project and the purposes and the expectations of this experimental study are emphasized.

Finally, the appendixes show results obtained from the sample evaporation effects in the rheological tests at atmospheric pressure. In the same way, the verification of the equipment is displayed. Validation was carried out through a solution of xanthan gum and sodium chloride to verify the methodology for using the microcalorimeter.

2 THEORETICAL FRAMEWORK

This chapter introduces fundamental concepts providing a contextualization regarding Non-Newtonian fluids' behavior, their effects under the action of a shear rate, time, and strain. Also, a contextualization is depicted on the drilling fluids, mainly water-based ones. In the end, mathematical models to describe the dependence of viscosity as a function of temperature and pressure are presented.

2.1 FLUID BEHAVIOR

The following section describes basic concepts about the behavior of several types of fluids. First, it focuses on non-Newtonian fluids, mainly on generalized Newtonian fluids, which present different models for describing their behavior, time dependence, and finally, the fluids that present viscoelastic behaviors.

2.1.1 Non-Newtonian Fluids

Newtonian fluids are low molecular weight organic and inorganic liquids that can be described by Newton's law of viscosity, where there is a constant proportionality ratio between the shear stress and the shear rate, being only a function of the material, at some specific temperature and pressure (CHHABRA, 2010). According to Bird et al. (1987), Newton's law can be expressed as:

$$\underline{\boldsymbol{\tau}} = \mu \underline{\dot{\boldsymbol{\gamma}}} \tag{2.1}$$

where $\underline{\boldsymbol{\tau}}$ is the shear stress of Cauchy stress tensor, $\underline{\dot{\boldsymbol{\gamma}}}$ is shear rate tensor in the direction of interest and μ is dynamic viscosity that can be understood as the resistance to gradual deformation by the shear stress sensed for an infinitesimal fluid layer or a measure of internal resistance of liquids. However, the Newtonian fluid is not the case for drilling fluids (CAENN HCH DARLEY, 2017).

Many industrial significance substances, especially of multi-phase nature with emulsions, dispersions, suspensions, and polymeric melts, do not conform to the Newtonian postulate of the linear relationship between shear stress and shear rate in simple shear. Accordingly, these fluids are known as non-Newtonian, non-linear, complex, or rheologically complex fluids (CHHABRA; RICHARDSON, 2011). For a non-Newtonian fluid, the relationship between the shear stress tensor and the shear rate tensor is not linear, and can even depend on time, shear history, thermal history, or the viscoelastic behavior of the material. Therefore, a constant viscosity coefficient cannot be defined. For non-Newtonian fluids, the resistance to fluid movement is known as apparent viscosity, defined as η (MORRISON et al., 2001).

The apparent viscosity of certain materials can be a function of the flow conditions (shear rate, time, etc.), the temperature and pressure to which the sample is subjected, and the aging time. According to Deshpande (2010), non-Newtonian materials are traditionally separated into three different groups. Their classification constitutes a gross simplification of rheological behaviors due to rheological properties, which are extremely dependent on the experimental conditions under which the measurements are made.

Fluids whose viscosity only depends on the shear rate are known as *Generalized Newtonian Fluids*. The fluids that depend on time are called *Time-Dependent Fluids*, and for materials that exhibit the behavior of both a viscous and elastic fluid, presenting recovery and structural relaxation effects are known as *Viscoelastic*.

2.1.2 Generalized Newtonian Fluids

The generalized Newtonian fluids are characterized by the rate's dependence on the shear stress only (CHHABRA; RICHARDSON, 2011), i.e., there is no effect of memory or history in shear rate. The fluids that present this behavior satisfy the following rheological equation:

$$\underline{\boldsymbol{\tau}} = \eta(\dot{\gamma})\underline{\dot{\boldsymbol{\gamma}}} \tag{2.2}$$

where $\eta(\dot{\gamma})$ is the scalar function and $\dot{\gamma}$ is equal to the magnitude of the tensor $\dot{\gamma} = |\underline{\dot{\boldsymbol{\gamma}}}|$.

Depending on their behavior, generalized Newtonian fluids can be subdivided into shear-thinning, shear-thickening, or viscoplastic fluids. The shear-thinning behavior is characterized by decreasing apparent viscosity with increasing shear rate (BREIT, 2017). Shear-thickening behavior on the contrary, increases the viscosity with shear rate (MEZGER, 2015). The viscoplastic fluid presents a peculiar characteristic, it deforms irreversibly when the minimum shear stress is exceeded, causing the fluid to start to flow. TThis minimum shear stress is known as yield stress (τ_0). Figure 2.1 shows a comparison of the Newtonian, shear-thinning, shear-thickening and shear-thinning with yield stress fluid behavior. The picture shows the shear stress as a function of the shear rate to different generalized Newtonian fluids. The flow index (n) relates to the behavior of fluids and (α) represents the constant viscosity of Newtonian fluids that behave according to Newton's law viscosity (BREIT, 2017). In the literature, many mathematical models can be found describing these behaviors. The most common models are the Cross model, the Carreau-Yasuda model, the Ellis fluid model, the Bingham model, the Herschel-Bulkley model, and power-law model.

Figure 2.1 – Flow curves for fluids: (1) Newtonian; (2) Shear-thinning; (3) Shear-thickening; (4) Viscoplastic.

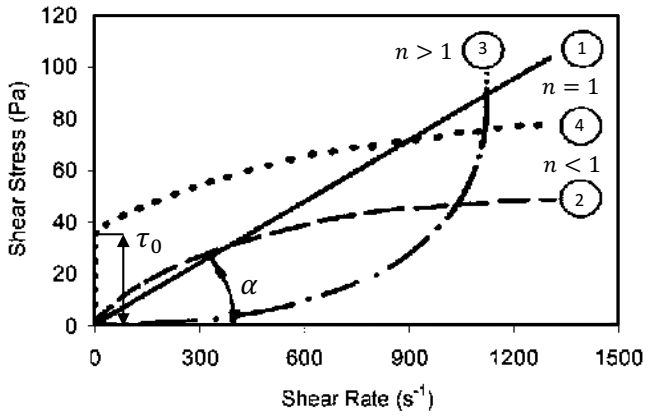

Source: Adapted from Bird et al. (1987).

One of the models that adequately represent shear-thinning fluids' behavior is the power-law. It is essential to describe non-Newtonian fluids' behavior without yield stress. The power-law or Ostwald (1925) model describes the apparent viscosity as a function of shear rate. This mathematical relationship is helpful because of its simplicity. The power-law model is shown in Equation 2.3 and consists of two parameters to describe the fluid behavior (MORRISON et al., 2001).

$$\eta(\dot{\gamma}) = m\,\dot{\boldsymbol{\gamma}}^{n-1} \tag{2.3}$$

where, m is the consistency coefficient, n the flow behavior index (dimensionless), and $\eta(\dot{\gamma})$ apparent viscosity. The behavior of shear-thinning fluids is characterized by a value of n smaller than unity ($n < 1$).

An example of this behavior can be seen in polymer systems, such as polymer melts and solutions, the disentanglement of polymer chains causes shear-thinning during flow. At rest, high molecular weight polymers are entangled and randomly oriented. However, when sheared at a high enough rate, these highly anisotropic polymer chains start to disentangle and align along the shear direction, leading to less molecular/particle interaction and a larger amount of free space, decreasing the viscosity (BARNES, 2000).

Shear-thickening fluids its exponent is $n > 1$, typical examples of this behavior are dense suspensions of particles in a liquid. If a shear rate is applied to these particles, they need to reorder to reduce the shear rate's influence. By doing so, the overall shear force can be reduced. If the shear rate applied is small, the particles have enough time to reorder. However, if a high shear rate is applied, the particles do not have the required time to reorganize, and a significant shear force is built up (RAPP, 2016).

Another standard behavior of non-Newtonian fluids is the viscoplastic one. The existence of threshold stress characterizes this type of non-Newtonian fluid behavior, called yield stress (τ_0), which must be exceeded for the fluid to deform (shear) or flow (CHHABRA; RICHARDSON, 2011). Materials that present an elastic limit are not deformed if the stress is below this critical value, represented by existing models that are idealized models to represent this type of behavior. However, these materials can present elastic deformation below the yield stress. However, when the critical value is exceeded, the material may exhibit downright viscous behavior with or without shear thinning characteristics.

A fluid with a linear flow curve for $|\underline{\boldsymbol{\tau}}| > \tau_0$ is called a Bingham plastic fluid and is characterized by a constant value of plastic viscosity η_B. Thus, in one-dimensional shear, the Bingham model is written as:

$$\begin{aligned} |\underline{\boldsymbol{\tau}}| &= \tau_0^B + \eta_B\,(\dot{\boldsymbol{\gamma}}) \qquad && \text{for} \quad |\underline{\boldsymbol{\tau}}| > \tau_0^B \\ |\underline{\dot{\boldsymbol{\gamma}}}| &= 0 && \text{for} \quad |\underline{\boldsymbol{\tau}}| < \tau_0^B \end{aligned} \tag{2.4}$$

On the other hand, visco-plastic fluids that show shear-thinning behavior when the yield stress is exceeded (τ_0^H) is known as a shear-thinning with yield stress fluid, and its behavior is frequently approximated by the so-called Herschel-Bulkley fluid model:

$$\begin{aligned} |\underline{\boldsymbol{\tau}}| &= \tau_0^H + m\,(\dot{\boldsymbol{\gamma}})^n \qquad && \text{for} \quad |\underline{\boldsymbol{\tau}}| > \tau_0^H \\ |\underline{\dot{\boldsymbol{\gamma}}}| &= 0 && \text{for} \quad |\underline{\boldsymbol{\tau}}| < \tau_0^H \end{aligned} \tag{2.5}$$

For most practical purposes, the Herschel-Bulkley model can account for the steady-state rheological performance of most viscoplastic fluids, especially drilling fluid's (HERZHAFT et al., 2002; KELESSIDIS; DALAMARINIS, 2009).

2.1.3 Time-Dependent Behavior

When left long periods of rest and subjected to a constant value of shear rate, many substances exhibit a gradual decrease or increase in viscosity over time as the internal structures are broken down (CHHABRA; RICHARDSON, 2011; MENDES; THOMPSON, 2019). For this reason, they are also called materials with memory (DESHPANDE ABHIJIT P., 2010). The apparent viscosities of time-dependent fluids are functions of the applied shear stress or the shear rate and the duration for which the fluid has been subjected to shearing and their previous kinematic history. For instance, the way the sample is loaded into a viscometer, by pouring or by injecting using a syringe, etc.; influences the resulting values of shear stress or shear rate. It makes the behavior of the fluid more challenging to predict or even unpredictable.So, it is evident that time-dependent fluid rheological properties can impact the different operation's success (PIBER et al., 2006).

Materials that have reversible time dependence can be classified as thixotropic or rheopectic fluids (DESHPANDE ABHIJIT P., 2010). Thixotropy addresses materials whose viscosity drops with time when the mechanical stress is imposed, whereas rheopexy contemplates materials that increase viscosity when applying mechanical stress.

According to Mewis e Wagner (2009), thixotropy can be defined as the continuous decrease of viscosity with the flow time in material previously at rest and the recovery of viscosity when the flow is stopped. The thixotropic effects are observed in several materials of industrial interest, such as drilling fluids. The conditions necessary to obtain the thixotropy effect can also be satisfied with various types of colloidal particles and can be achieved in low concentrations for bentonite suspensions (HUYNH; ROUSSEL; COUSSOT, 2005) and synthetic laponite suspensions (MEWIS; WAGNER, 2009). The effect of thixotropy can be observed in ramp tests of shear rates or shear stress. The test result is called a hysteresis area and is a widely used way to check and quantify the material's thixotropy (DIVOUX; GRENARD; MANNEVILLE, 2013).

2.1.4 Viscoelastic Materials

Hooke's law and Newton's law describe solid materials and viscous fluids very well, but like any other model, their definitions are idealized to represent real materials' behavior. A good part of the materials behaves neither as elastic solids nor as viscous fluids, but they present an intermediate response between these two behaviors, these materials are called viscoelastic. Reiner (1964) defined one of the most important dimensionless numbers in rheology, Deborah's number, De, expressed by equation 2.6 that defines the relaxation time of the material λ and the observation time of the phenomenon t_{obs} or characteristic time under analysis. Therefore, materials with long periods of relaxation are considered elastic solids and materials with short times as viscous fluids. Consequently, viscoelastic materials have an intermediate classification between elastic solids and viscous fluid.

$$De = \frac{\lambda}{t_{obs}} \tag{2.6}$$

Viscoelastic materials exhibit behavior that combines both elastic and viscous characteristics. The stress required to maintain a constant strain applied to the material diminishes gradually with time or relaxes for these materials.

The study of viscoelastic materials implies determining a constitutive equation related to stress, strain, and time. When both strain and stress are small enough, and microstructure is conserved during the experiment, the relationship between magnitudes can be described by linear differential equations with constant coefficients, and the material is in a linear viscoelastic regime (FERRY, 1980). In this case, the stress-strain relation is simply a function of time and not of stress magnitude (DARBY, 1976; DEALY, 1982). Otherwise, viscoelastic behavior is called nonlinear.

Viscoelastic properties can be characterized by experiments that examine the relationship between stress and strain, and shear rate in time-dependent experiments.

Dynamic mechanical analysis is the most widely used method for characterizing viscoelastic behavior. Dynamic or oscillatory tests may be performed in stress-controlled or strain-controlled modes. In oscillatory tests, the sample is deformed sinusoidally by applying a sinusoidal shear deformation or stress, and the resultant stress or strain is monitored with time.

During the drilling process, cuttings-suspension function depends on the viscoelastic behavior of drilling fluids; therefore, it is crucial to know the deformation energy stored in fluids during the shear process, determine the capacity to keep the cuttings in suspension, and the energy required to start-up the flow (SOHM; TADROS, 1989).

2.2 ELASTOVISCOPLASTIC AND THIXOTROPIC FLUIDS

In most cases, many materials exhibit one or more of the behaviors previously classified. In other words, a material can have time-dependent, viscoplastic, and viscoelastic characteristics, presenting an increasing complexity in the study of its rheological properties. Elastoviscoplastic materials deform irreversibly and flow at stresses above the limit stress, and some simultaneously present thixotropic characteristics. Elastoviscoplastic fluids behave as viscoelastic solids when the fluids are gelled and as viscous fluids when it is subjected to high rates of deformation sufficient to destroy their internal structure, starting to flow presenting a continuous and reversible decrease in their viscosity during their flow (Frey et al., 2015; Souza Mendes e Thompson, 2013).

2.3 DRILLING FLUIDS

The definition of drilling fluid is expressed in different ways, differing among authors. However, drilling fluids are complex mixtures of liquids, solids, and, in some cases, gases, which may assume suspension, colloidal dispersion, or emulsion aspects, depending on the chemical composition, and physical state of its components (MITCHELL, 2006). Due to many functions, drilling fluids are considered one of the main variables in well hydraulic projects, and the drilling activities are only possible with proper fluid formulation (DARLEY; GRAY, 1988). Therefore, the selection of drilling fluid is the key to overcoming the most challenges presented in offshore well. Drilling fluids require various additives, such as weighting materials, viscosifiers, filtration control additives, pH/alkalinity control chemicals,

dispersants/deflocculants/thinners, surfactants, emulsifiers, shale inhibitors, corrosion inhibitors/oxygen scavengers/hydrogen sulfide (H_2S) scavengers, lubricants, and bridging agents/lost circulation materials, to improve the rheological properties of the drilling fluid.(NEFF, 2005). The addition of several chemicals causes the drilling fluid to present a non-Newtonian fluid behavior (CAENN HCH DARLEY, 2017). Usually, the drilling fluids are designed to be shear-thinning, reducing friction pressure losses while circulating at high flow rates. Yield stress and gel behavior provide a solid carrying capacity on static conditions. However, most drilling fluids present thixotropy, meaning that the fluid rheology exhibits a transient response to changing shear conditions, demonstrating that fluids' rheological properties are sensitive to recent shear history (CAENN; CHILLINGAR, 1996).

2.3.1 Classification of Drilling Fluids

Darley e Gray (1988) classified drilling fluids according to their composition, using as criteria the main constituent of the continuous phase, which is the most relevant component that forms the dispersing phase. Drilling fluids can be broadly classified into three categories based on their constituent: water-based drilling fluids (WBM), oil-based drilling fluids (OBM), and pneumatic fluid, as shown in Figure 2.2. The most used type of drilling fluid is based on liquids fluids, which their classification is based on their continuous phase, being able to be emulsions, suspensions, and colloidal solutions. The fluids oil-based are mainly emulsions. The most popular oil base known are Diesel oils, Mineral oils, and synthetic oils, the most widely used being those on olefins-based. The fluids with water in their continuous phase are generally are suspensions, either with colloidal clay's, free-clays, synthetic polymers, or bio-polymers mud. Currently in the drilling industry 50% of the most widely used drilling fluids in the world are water-based drilling fluids (IADC, 2014).

Figure 2.2 – Classification of drilling fluids.

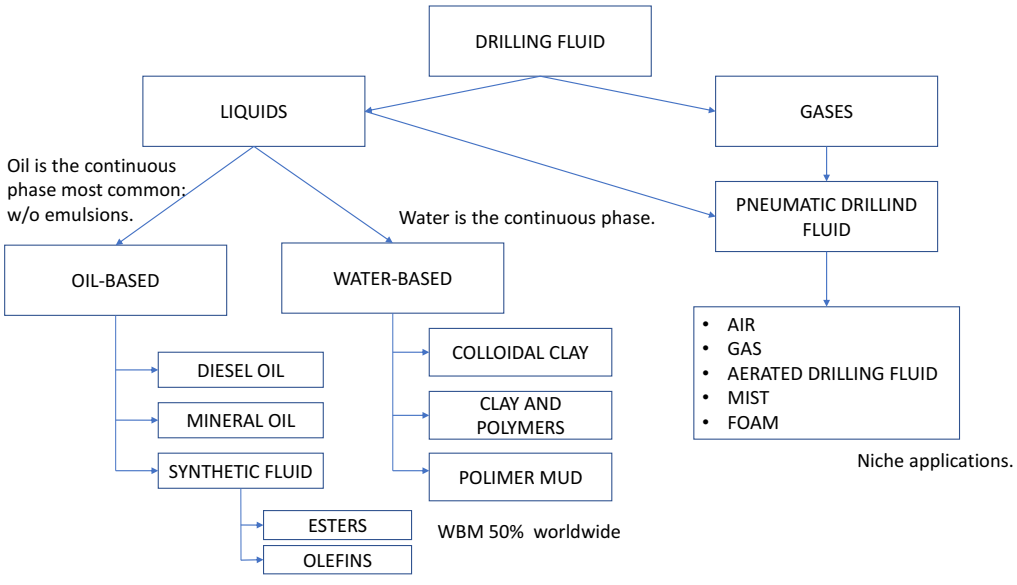

Source: Adapted from Chilingarian e Vorabutr (1983), Ibeh (2007)

2.3.1.1 Water-Based Drilling Fluid

Water-based drilling fluids have solid particles suspended according to the water's nature (fresh, salty, brine, or saturated brine), and some chemical additives used in the formulation. The solids particles consist of clays and organic colloids added to provide the necessary viscous and filtration properties for the drilling processes, as heavy minerals (usually barite or limestone) are added to increase the mud weight. Water-based drilling fluids are used most frequently in offshore drilling, where usually is used seawater to generate the top hole and start drilling more deeply. After that, it is replaced by a non-aqueous fluid (CAENN HCH DARLEY, 2017).

Naturally, the rise in clay or polymer concentration leads to a growth in some rheological properties, such as the yield stress and viscosity (ABEND; LAGALY, 2000), but the excessive concentration gain can also bring unwanted operational problems. Therefore, it is essential to characterize the fluid rheologically and classify them according to their best applications.

Water-based drilling fluids are classified into different types of fluids depending on the dissolved substances in the aqueous-based or on the soluble or dispersive materials in the rocky formations to be drilled. Thus, it can further be subdivided into four types (CAENN; CHILLINGAR, 1996):

- **Non-Dispersed**: these are suspensions that have not been chemically treated to disperse any clays present. These are generally fresh-water muds with bentonite clay and no barite.
- **Dispersed Bentonitic**: these are fluids used as the well is drilled deeper, requiring greater control of its properties, i.e., weight, rheology, and fluid loss. They require alkalinity control, so significant caustic soda is used to maintain the proper pH level.
- **Calcium Treated**: calcium-based fluids use calcium chloride brine as the base fluid or additions of lime or gypsum to make lime mud or gyp mud. These fluids were designed to assist in wellbore stability as they give high levels of soluble calcium to minimize clay swelling. They are contaminant resistant but can experience high gel strengths, especially at high temperatures.
- **Polymer Systems**: a polymer system uses an organic, usually long chain and high molecular weight, natural or synthetic material used to control one or more fluid properties. The polymer replaces the traditional water-based additives such as bentonite and chemical thinners, exhibiting remarkably reducing friction properties depending on the concentration and polymer structure (ZHOU; SHAH, 2004; CAENN HCH DARLEY, 2017).

Water-based drilling fluids are widely used in drilling operations throughout the world in different industries. However, in wells with HPHT conditions, there are some caveats to be made, as WBM does not have good thermal stability (CAENN HCH DARLEY, 2017). Nowadays, there is a need to provide WBM with greater thermal stability in wells with more severe conditions. It has led several researchers to carry out a series of formulations with resistant polymers, such as polysaccharides, polyanionic cellulose (PAC), and amides with polyglycols in WBM. Oort et al. (1996) concluded that polyglycols decrease fluid degradation at high temperatures. Furthermore, currently, formulations with nanoparticles that have higher thermal conductivity and efficient mechanical properties are being implemented, increasing the maximum allowed temperature to 150 ºC.

2.3.2 Pressure and Temperature Effects on Drilling Fluids

Hermoso et al. (2014) presented some effects generated by the high-pressure and high-temperature scenario that changes the rheological behavior of both water-based and oil-based drilling fluids differently:

- **Physically**: decreases in temperature and/or rises in pressure influence the mobility of drilling fluid, leading to an increase of apparent viscosity. In oil-based systems, the effect of pressure on rheological properties is expected to be greater than water-based drilling fluids due to their oil phase compressibility, which is higher than the water compressibility. On the other hand, fluids with polymers present transition processes of physical changes in their polymer chains due to temperatures gain, generating rheological modifications.
- **Chemically**: at temperatures above 94 °C, all hydroxides react with clay minerals, resulting in a modification of the structure, changes in the drilling fluid rheology, and highly alkaline muds.
- **Electrochemically**: temperature rising intensifies the ionic activity of any electrolyte, as well as the solubility of any partially soluble salts present in the drilling fluid. The variation of ion and base exchange balance alters the equilibrium between interparticle attractive and repulsive forces and the degree of dispersion and flocculation.

Due to the large number of variables involved, the behavior under high pressure and high temperature of drilling fluids, particularly WBM, are difficult to predict. Therefore, they require a more complex analysis. Minor differences in the fluid's chemical composition can cause considerable variations in rheological behavior (IBEH, 2007; RAVI, 2012; HERMOSO; MARTÍNEZ-BOZA; GALLEGOS, 2014; OLIVEIRA, 2016; TELESFORO; ANTONIO, 2017). Generally, the magnitude and direction of both temperature and pressure effects will vary as a function of the particular composition of a given drilling fluid.

2.4 CHAPTER SUMMARY

Chapter 2 presented the main concepts necessary to understand the work. First, basic concepts of rheology and mechanics of non-Newtonian fluids were presented. The drilling process was introduced in sequence, focusing on offshore environments and conditions of high pressure and temperature. Also, the definition and classification of drilling fluids were introduced, highlighting their primary functions. Finally, it was presented the effects of the high temperature and high pressure on water-based drilling fluids.

3 LITERATURE REVIEW

The following chapter presents a brief review of relevant studies of water-based drilling fluids' rheology at high-pressure and high-temperature. It also highlighted the experimental results obtained with different viscometers and rheometers, the influence of xanthan gum on the fluids' rheological behavior, and the mathematical models developed empirically and theoretically are presented as well.

3.1 WATER-BASED DRILLING FLUIDS BEHAVIOR ON HPHT

The study on drilling fluids started in the 1800s when water was the first drilling fluid, and its usage was documented back to the ancient Egyptian and Chinese cultures. The petroleum drilling in Corsicana, Texas (1890), and Spindletop, Texas (1901) indicated the use of natural drilling fluid (drilling fluid from the local clays) was an established part of rotary drilling by this time. Technical descriptions of the U.S. Bureau of Mines in 1913 and 1914 were the beginning of a long history of the science and engineering of drilling fluid usage (BARRETT, 2011).

Later on, 1930 was the real beginning of drilling fluid engineered in response to more profound and more difficult drilling conditions, where higher temperatures and pressure generated many issues during production processes. Oil companies developed significant research programs in drilling fluid design during this time frame.

One of the first published works was by Gray et al. (1952), dealing with temperature changes in drilling fluids. The authors investigated and discovered that temperatures above 150 ºC, showing that the lime-treated water-based drilling fluids underwent high gelation leading to solidification. In the study, the authors concluded that pressure does not significantly affect the fluid's viscosity when it is imposed at a high temperature and that the increase in temperature increments the fluid's acidity.

The previous event triggered that in 1956 many researchers announced that it was not yet well known how the rheological properties of drilling fluids, which were affected by temperature and pressure, sparked the curiosity of many researchers to study different types of compositions to generate more stable suspensions. Research on the use of oil and water-based drilling fluids was carried out jointly because these two bases were the most widely used globally, but each had a different reaction to drilling conditions (CAENN; CHILLINGAR, 1996).

One of the works starting this race for the generation of new technologies was Srini-Vasan, Gatlin et al. (1958), who studied the effect of temperature in a WBM in a temperature range of 25 to 80 ºC and where they converged that the viscosity, one of the essential rheological properties for the oil industry, decreased with the gain in temperature. The authors also verified the relationship between the drilling fluid's viscosity and its main base "water" when subjected to rises in temperature and observed that this proportion increased with increasing temperature.

At the beginning of the sixties, Olphen (1963) determined that because the drilling fluid are clay-water systems having an intermediate behavior between flocculated and deflocculated state, which are obtained naturally, this phenomenon was observed from Wyoming sodium clays that originally provided

viscoplastic behavior, which served as the basis for creating concepts of apparent and plastic viscosity in API standards. The main components of water-based drilling fluids used for its preparation were water, bentonite, and polymers. Determining that the main components of the water-based drilling fluids used for their preparation were water and a viscosifier composed of clays known at the time, but that over the years and with the discovery of new materials became bentonite and polymers.

In conclusion, Olphen (1963) demonstrated that deflocculated systems have high apparent and plastic viscosities. The flocculated systems were divided into a flocculated gel with high apparent viscosity and low plastic viscosity, having anisometric clay particles forming a face-to-edge micro-configuration as a house of cards, and flocculated with phase separation, where the anisometric clay particles have a face-to-face micro-configuration. Besides, the author determined that bentonite has an excellent ability to improve viscosity and control filtration during drilling since it has many particles present in the aqueous phase, which depend on the degree of hydration and the associated interparticle forces (AL-MARHOUN; RAHMAN, 1988).

Hiller et al. (1963) proposed an explication about the rheological properties' variations under HPHT conditions of water suspensions. The authors implemented a rotational Couette viscometer with a cell in which pressure and temperature could be controlled. Measurements were performed up to 160 °C and 700 bar to investigate HPHT conditions' effects on a simple homo-ionic clay's properties. The authors used bentonite suspended in distilled water for six months, then diluted to 1% by weight and centrifuged to obtain a stable and homogeneous solution. For recognizing the effects of salts on drilling fluids rheology, two suspensions with different salt concentrations were used. The first sample contained an excess of 4% suspension of pure sodium montmorillonite with an excess of sodium hydroxide and a 13% suspension of pure calcium montmorillonite. The difference between the two suspensions' behavior was that the first sample decreased the yield stress with increasing temperature, keeping the pressure constant, as can be seen from Figure 3.1 (a). The opposite occurred with the calcium montmorillonite suspension increased the yield stress with increasing temperature, shown in Figure 3.1 (b). Moreover, it was observed that a pressure increment lowered the yield stress in the calcium montmorillonite suspension and rose in pure sodium montmorillonite.

Hiller et al. (1963) detected two behavior types in suspensions of sodium montmorillonite in the measurements developed. One suspension showed that both plastic viscosity and Bingham yield stress decreased with increasing temperature and increased slightly with increasing pressure. According to the authors, this behavior is probably because of partial destruction of the hydration shell than are the spherical conformations of water molecules around each dissolved Ion. The calcium montmorillonite suspensions tended to be thixotropic, especially at high temperatures, where the yield stress rose with temperature and dropped with high pressure. The researchers concluded that the effect of increasing temperature and pressure on the dispersed suspensions of sodium montmorillonite could be explained by a simple weakening of the strength of the bonds between particles. Due to the high thermal energy, the suspension medium's viscosity decreased, and associated clay micelles' dispersion increased. The mentioned above was concluded through studies carried out by Foster, Savins e Waite (1954), then detected the suspensions subjected to high pressure reduced the sample's hydration, which caused an increment of the particles' symmetry and lower yield stress. Moreover, other factors were observed that influence the balance of symmetry between the suspended particles, such as Van Der Waal's attractive forces, once the

Figure 3.1 – (a) Consistency curves for a 4% suspension of pure sodium montmorillonite to which excess of sodium hydroxide have been added, measured at various temperatures and pressures; (b) Consistency curves for a 13% suspension of pure calcium montmorillonite at various temperatures and pressures.

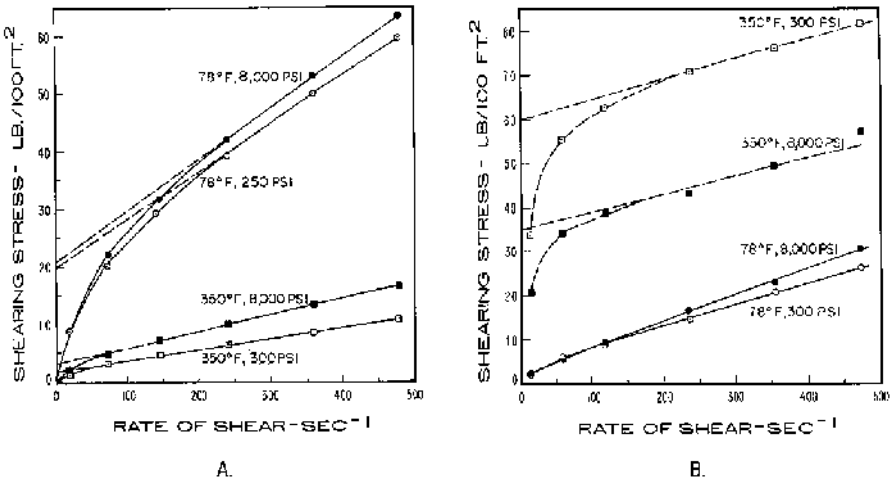

Source: Adapted from Hiller et al. (1963).

reorientation increases the structure's links in suspension until at a given solids concentration. Therefore, the total interaction energy is a function of the attractive Van Der Waal's forces, the repulsive double-layer interaction, and the absorbed molecules' steric interactions.

Some years later, Annis et al. (1967) investigated the changes in the apparent viscosity and yield stress with time and temperature, becoming one of the essential properties in drilling, mainly in water-based drilling fluids formulated with bentonite. The results showed that with increasing temperature, the yield stress grows and the viscosity decreases. Incorporation of electrolytes such as NaCl into drilling fluid at 150 ºC provided a marked gain of shear stress compared to formulated drilling fluids without salt. The results suggested that high temperatures lead to the bentonite particles' flocculation process, and the flocculation process depends on the electrolyte content. Since the drilling was carried out each year, the conditions at the bottom hole increased; therefore, water-based drilling fluids began to diminish and be replaced mainly through oil-based drilling fluids, which were highly aggressive with the environment but satisfied the functions in high-temperature conditions. Chesser, Enright et al. (1980) indicated that drilling of HPHT wells with water-based drilling fluids was limited due to a lack of additives to maintain the desired rheological properties at elevated temperature and high electrolyte flux. The authors also stated the non-existence of a standard method available to determine the effects of the drilling fluid components' instabilities.

Chesser, Enright et al. (1980) and Hille et al. (1985) were some of the first works that used water-based fluids with limestone, bentonite, electrolytes such as NaCl, polymers, and deflocculant based on synthetic polymers such as low molecular weight Copolymer. The use of bentonite and polymers in the drilling fluids with temperature growths caused an increment of apparent viscosity, promoting gelation. However, beyond 120 ºC, the viscosity began to fall sharply.

Al-Marhoun e Rahman (1988) concluded that the initial increase in apparent viscosity and a gradual fall in yield stress with augmenting temperature was attributed to polymer degradation and consequent dehydration of clay platelets. As the polymer degraded, its ability to flocculate the clay platelets also decreased. As a result, the platelets approach one another so closely that the attractive forces predominate, thus giving rise to a state of dispersion with edge-to-face contact of the platelets, forming gels. Therefore, the studies carried out by Chesser, Enright et al. (1980), Hille et al. (1985) showed that in water-based drilling fluids with bentonite and polymers they required a deflocculant such as a copolymer, which caused a thermal stability gain of the fluid above 200 ºC, lowered the flocculation of the clays present in the fluid and reduced the loss of fluid by filtration.

Guven et al. (1988) studied water-based drilling fluids with different clays (bentonite, saponite, and sepiolite) for a temperature range of 149 up to 316 °C under appropriate confining pressures to simulate the conditions encountered while drilling deep oil and gas wells. The rheological and filtration properties of the fluids were measured before and after autoclaving. The hydrothermal reactions of the clays in these fields were studied with X-ray diffraction and electron microscopy. Salts and hydroxides of sodium (Na), potassium (K), and calcium (Ca) were found to undergo chemical reactions with the clays at high temperatures, and vastly changing the properties rheological of the drilling fluids, significantly reducing the apparent viscosity and increasing fluid losses. The addition of low and high molecular weight polymers, such as sodium polyacrylates, improved the rheology and filtration control properties of the clay fluids.

In addition to the fact that the high temperature had adverse effects on the water-based drilling fluid, the pressure also had to be analyzed to know its effect. Therefore Alderman et al. (1988) performed rheological measurements under HPHT conditions for water-based drilling fluids at temperatures up to 130 ºC and pressured up to 1000 bar. The water-based drilling fluids were based on suspensions of bentonite clay. The authors separated the effects of temperature and pressure on the rheology from those of the shear rate. The results showed that yield stress was essentially independent of pressure and dependent on temperature due to the particles' weak associations, leading to flocculation processes, causing changes in the rheological properties. An extensive study of the effect of temperature, time, and shear-energy input during the preparation process showed that this particular procedure produced suspensions with thermal/shear-history characteristics reversible. Results of rheological measurement presented a pressure-temperature dependence in the viscous characteristics of water-based drilling fluids. Therefore, it appears to be qualitatively similar to that observed for oil-based drilling fluids (HOUWEN; T GEEHAN, 1986). The authors concluded that the Casson's apparent viscosity decreased with increasing temperature similarly for all the drilling fluids examined and increased with pressure. Its behavior is primarily governed by the viscosity and compressibility characteristics of the continuous phase.

In the early in Saudi Arabia, Ali, Al-Marhoun et al. (1990) wrote the first thesis investigating the effect of high temperatures (up to 255 °C) and high pressures (up to 700 bar) on the properties of the water-based drilling fluid, in an HPHT Fann Model 70 viscometer, due to the various accidents that had been reported in subsequent years on oil rigs. The results showed a reduction in apparent viscosity, static, and dynamic yield stress with increasing temperature. The pressure climb caused an amplification of the drilling fluid's apparent viscosity and dynamic yield stress.

Rommetveit, Bjorkevoll et al. (1997) studied water-based drilling fluid formulations at temperatures up to 200 °C and pressures up to 1200 bar, using the Fann 70 viscometer, the effects of pressure were less than the effects of temperature, at 1000 bar and 150 °C, the viscosity decreased linearly for water-based drilling fluids.

Rossi et al. (1999) performed an experimental study about sodium bentonite suspensions, or technically Na^+-montmorillonites, a key component in water-based drilling fluids. To know of the rheological properties in the presence and absence of different electrolytes (NaCl, KCl, LiCl) and polyethylene oxide (PEO), the authors performed measurements in Haake-Searle type HPHT viscometer able to operate within a range of 0 - 1130 s^{-1} and maximum shear stress of 60 Pa, where the pressure can be adjusted up to 1000 bar with temperature ranging from 25 to 120 °C. The results showed that the temperature increased the yield stress for clay suspensions, generally above 60 °C, in a similar way, as it was described in earlier studies (HILLER et al., 1963; ANNIS et al., 1967; ALDERMAN et al., 1988; BRISCOE; LUCKHAM; REN, 1994). The behavior was attributed to the particles' swelling at higher temperatures and the dissolution of Na^+ cations from the clay surface into the medium. Moreover, pressure generally incremented the clay suspension's plastic viscosity due to volume changes in the continuous phase. Furthermore, the hysteresis loop of thixotropy was significantly reduced in the presence of NaCl, indicating a quicker recovery of the gel structure than without NaCl. On the other hand, pressure growth led to a dramatic drop of the shear stress by at least three orders of magnitude and had an irreversible effect over the Na^+-montmorillonite flocculated suspension containing NaCl and PEO. Simultaneously, suspensions containing KCl did not exhibit hysteresis loops, as the ramp-up and ramp-down curves were practically superimposed. The authors observed a reduction in the clay suspension yield stress that may be explained in terms of the transition from a well-developed gel structure to a predominantly aggregated face-to-face association. Hence, the suspensions in the presence of KCl were less sensitive to pressure variations at high temperatures, owing to a more compact and more robust structure. Finally, Rossi et al. (1999) concluded that in the suspension of Na-montmorillonite, the combined effect of inflammation and flocculation induced by the clay particles generates an improvement in the clay suspension's gel structure increasing the yield stress values. However, such as other studies, the plastic and the high shear viscosity decrease continuously with temperature and grows with pressure. The latter effect is due to the volume change of the liquid under pressure and an increment of the suspension's effective clay content.

Due to the revolution in computer systems in the nineties, the number of publications investigating the effects of high-pressure and high-temperature increased, being an essential and significant role for the scientific community due to the availability of a large number of sophisticated devices for measuring the rheological properties of fluids that could perform accurate and reliable tests at high pressures and temperatures. In the first decade of the twenty-first century, the publication of articles referring to water-based drilling fluids was scarce since the industry was focused on oil-based and synthetic drilling fluids that presented greater profitability in the face of the new challenges faced by the oil and gas industry. Some researchers like Bland et al. (2002) were trying to encourage research into water-based fluids with new additives and viscosifiers to improve against HPHT conditions. Only until 2007 many publications began to focus on water-based drilling fluids due to several accidents that generated high environmental impacts, mainly in offshore wells that began to present greater demand, which generated stricter restrictions regarding the use of drilling fluids (BLAND et al., 2002; KELESSIDIS, 2007; ROSE,

2009).

Furthermore, the use of bio-polymers began its career in the oil and gas industry when Salimi, Sadeghy e Kharandish (2000) investigated the rheological behavior of several polymer-extended water-based drilling fluids at different temperatures and pressures, simulating their proper working conditions in a deep oil well. The bases studied were suspensions of bentonite and distilled water, to which were added bio-polymers such as PHPA (PartiallyHydrolysed Poly-Acrylamide), XC (Xanthan Gum), and CMC (Carboxy Methyl Cellulose). A Fann 50C commercial viscometer was used to obtain the flow curve of all test fluids. All experiments were done at five distinctive pressures ranging from 6.9 to 34.5 bar, and temperatures from 43.4 to 148.9 °C. The experiments showed that the shear stress rose non-linearly with the shear rate for all test fluids at any given pressure and temperature. Additionally, for all polymer extended drilling fluids, a decrease in shear stress was observed when the temperature or the pressure was increased. It was found that the effect of temperature on the flow curve was more severe than the effect of pressure.

Later Hamed e Belhadri (2009) studied two drilling fluids formulated with different bio-polymers, one with scleroglucan and the other with xanthan gum, which were dissolved in distilled water. Also, starch and a bactericide were added at constant concentrations. Other materials as clay, calcium carbonate, and potassium chloride varied with different concentrations. All measurements were executed at 25 °C through the Rheostress 600 of ThermoHaake. The present study determined the different effects of additives in water-based drilling fluids, where all fluids exhibited shear thinning behavior with low yield stress and high permeability. Furthermore, this study was favorable to understand better the chemical action of these drilling mud systems.

In the last nine years, the publication of articles, dissertations, and thesis published referring to water-based drilling fluids increased exponentially, especially those with viscosifiers based on bentonite and bio-polymers on high-pressure and high-temperature conditions.

Amani, Al-jubouri et al. (2012) analyzed different drilling fluids' compositions to find the temperatures where the drilling fluids failed when subjected to constant high pressure and several shear rate cycles. The authors also observed the rheological behavior for two fluids with different densities. In conclusion, under high temperature, the thermal degradation of the solid, polymers, and other components of the drilling fluid samples occur, causing the expansion of the molecules, decreasing the fluid resistance to flow.

In the same year, Amani e Al-Jubouri (2012) published another work presenting an investigation about the effects of salinity on water-based drilling fluids rheology with polymers, barite, lime, sodium chloride (NaCl), and potassium chloride (KCl). Three levels of concentration were used to observed the effects of pressure and temperature. The no-salt sample presented a shear-thinning behavior at ambient conditions. However, once pressure and temperature went above 2413 bar and 232 °C, the fluid started to follow the Bingham model. On the other hand, samples with salt behaved slightly differently. Figure 3.2 shows the eight different cases, where each case corresponds to the combination of pressure and temperature, two suspensions with different electrolytes are shown.

For the sodium chloride, as shown in Figure 3.2 (a), at room conditions and a slight increase in pressure (case 1 and 2), the fluid maintained the same behavior. In case 3, the fluids had lower shear

stress at the middle to low range of shear rate. In case 4, the shear stress dropped significantly, and the relationship was linear with the shear rate. Case 5 and 6 had the lowest shear stress for given shear rates among all the cases. There was an almost identical additional pressure growth when above 2068 bar and temperature above 232 °C resulted in higher yield stresses. As for the second type of salt sample, the potassium chloride as shown in Figure 3.2b was generally similar to sodium chloride at low temperatures and pressures; the fluids have power-law properties (Case 1 and 2). When the pressure and temperature increase, the shear stresses at high shear rates drop down significantly, and it begins to have a linear curve (case 3 and 4) no apparent changes in the shear stress between the conditions of cases 5 and 6. After the condition of case 7, the yield point of the curves starts to climb in a large step.

Figure 3.2 – Flow curve for Water-based drilling fluid with, (a) 7% NaCl salt; and (b) 7% KCl salt at different pressures and temperatures.

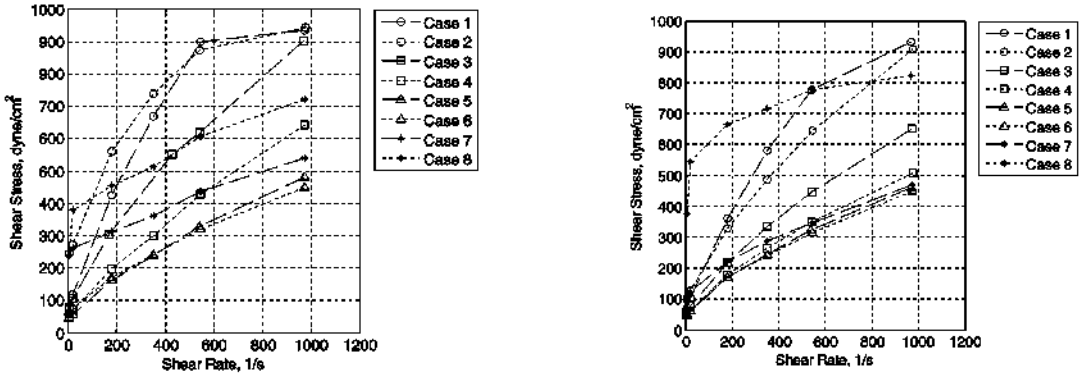

Source: Adapted from Amani, Al-jubouri et al. (2012).

In conclusion, increments of temperature and pressure for a particular electrolyte concentration show the same rheological behavior. However, as the electrolyte concentration increases, the shear-thinning behavior was maintained either by increasing or decreasing the shear stress and the yield stress. NaCl suspensions with better rheological capacity predominated. However, when exceeding 1379 bar and 143 ºC, fluids started to follow the Bingham model, but at 2400 bar and 232 ºC, there was a jump in shear-stress shear-rate curves of KCl at high concentration compared with WBM.

Xu et al. (2013)investigated the effects of HPHT conditions on the water-based drilling fluid applied in the exploration of oil wells in the Yuanba region in southwest China. The researchers realized that the pressure exerted a more significant influence on the rheological properties at higher temperatures and at lower shear rates, a result contrary to what the literature had until then, in which the impact of pressure was more evident at low temperatures and high shear rates. Xu et al. (2013) also observed that the apparent and plastic viscosities exhibited small changes with increasing pressure at a constant temperature. However, the apparent and plastic viscosities exhibited a notable decline with the increase in temperature at constant pressure.

William et al. (2014) investigated water-based drilling fluids on high-pressure and high-temperature conditions using the nanofluids of CuO and ZnO (size < 50 nm) in a xanthan gum aqueous solution as a fluid base, where the enhancement in thermal and electrical properties was studied. High-pressure rheo-

logical studies were conducted to understand nanofluids' effect on the rheological properties at varying temperatures (25, 70, 90, and 110 ºC) and pressures (1 bar and 100 bar). In conclusion, an incremented concentration of nanoparticles further enhances the electrical and thermal properties of drilling fluids, and the effect of pressure on the rheology of fluid is more significant at higher temperatures and indicated better viscosity stability at higher temperatures. Additionally, the experimental data obtained were fitted to the classical drilling fluid rheological models with a power-law model, Bingham plastic model, and Herschel-Bulkley model, being the Herschel-Bulkley model the best fit-model for rheological behavior.

Jain, Mahto e Sharma (2015) developed rheological, filtration, salt tolerance, shale inhibition, and formation damage studies, which were carried out to evaluate synthesized nanocomposite as a potential additive in the developed water-based drilling fluid system. The synthesized nanocomposite had a significant effect on the rheological parameters such as plastic viscosity (17-26 mPa.s), apparent viscosity (25-41 mPa.s), yield point (8-15 Pa), and gel strength (0.66-3.83 Pa) of the developed based drilling fluid formulations due to the enhanced hydrogen bonding in the developed drilling fluid system. Also, high thermal stability, good salt tolerance (18.0 wt/v%), and aids in the better shale inhibition property to mitigate wellbore instability problems. The drilling fluid system developed with nanocomposite had a relatively high return permeability value (74%), indicating less formation damage effect of nanocomposite system due to the less permeable filter cake formation.

The effects of high pressure on drilling fluids were analyzed by Gokdemir, Erkekol e Dogan (2017), who investigated a colloidal system, a mixture of the base fluid and special chemicals. The authors formulated five different drilling fluids, one oil-based, two synthetic-based, and two water-based ones. All five fluids were subjected to a pressure increase from 1 to 827 bar at constant temperatures of 25, 50, and 75 °C, monitoring changes in rheological properties. Anton Paar MCR 302 Rheometer was used with a limiting temperature up to 300 °C and 1000 bar (14500 psi) pressure. Water-based drilling fluids were assumed as incompressible fluids to see whether the pressure can affect the rheological behavior. Various experiments were conducted in the literature to integrate the temperature or the pressure effects in the fluid system's viscosity and rheological parameters. Most of them used Arrhenius equations in the developed models (ROYER; DESIMONE; KHAN, 2001). Amani e Al-Jubouri (2012) used a similar approach for pressure and also established a temperature term in the viscosity. In conclusion, the rheology of drilling fluid systems formulated using incompressible fluid was not affected by pressure change at a constant temperature. On the other hand, conventional mathematical rheological models do not include pressure in the equations. Other models that are dependent on pressure do not adequately represent its rheological effects. Like other previous studies, the viscosity was increased by pressure in a small proportion. Finally, the author indicated that more accurate rheological test results are obtained using the HPHT Rheometers than HPHT viscometers.

For the years 2018 and 2019, the water-based drilling fluids' use grew dramatically; thus, studies were conducted to enhance water-based drilling fluid's rheological and thermal properties under HPHT conditions. Owing to their enhanced thermo-physical properties and stable nature, it was recommended to use suspensions of nanoparticles along with drilling fluids for these conditions (ELKATATNY et al., 2018; ECHT; PLANK, 2019). In 2019, Anoop et al. (2019) studied Graphene Oxide Nanoparticles (GON) and Aramendiz et al. (2019) carbon nanotube particles. Both works reported that nanoparticle-based drilling fluid usage improved the rheological stability and reduced its differential pipe sticking nature. They also

observed that the nano-mud suspension was superior to the bentonite fluids in reducing mud filtration and improved rheological characteristics. There was an increase in plastic viscosity, yield stress, and thermal conductivity for water-based drilling fluid with nanoparticles compared to the base fluid. Anoop et al. (2019) performed a formulation using water-based drilling fluid and nanoparticle CNT.

The authors demonstrated that viscosity tends to increase for a colloidal suspension with a pressure gain, which they considered an expected trend. Moreover, a similarity in the results was observed with Anoop et al. (2019) for alumina particles-silicon oil nanofluids. Figure 3.3 shows the viscosity variation for different samples with different CNT concentrations, where was imposed a temperature gain from ambient temperature until approximately 125 °C. The authors observed that the samples could withstand high temperatures without thermal degradation in a greater range than fluids without nanoparticles. However, a breakpoint in this trend is identified around 150 °C, after which the viscosity values seem to be fluctuating severely. Additionally, Anoop et al. (2019) observed that the variation of relative viscosity with temperature had reduced the cohesive attraction forces between the molecules of bentonite and nanoparticles, affecting the fluid's overall performance with a gradual decrease in its viscosity. In the same way, it was a perceived increase in viscosity with pressure growth. However, the authors observed that the reduced viscosity dropped as more particles were added to the samples, creating a trend leaning towards the water when the CNT concentration was incremented.

Figure 3.3 – (a) Normalized viscosity variation with the temperature at 1710 bar pressure; and (b) normalized viscosity variation with the pressure at 26 °C for measurement shear rate of 1021 s^{-1}.

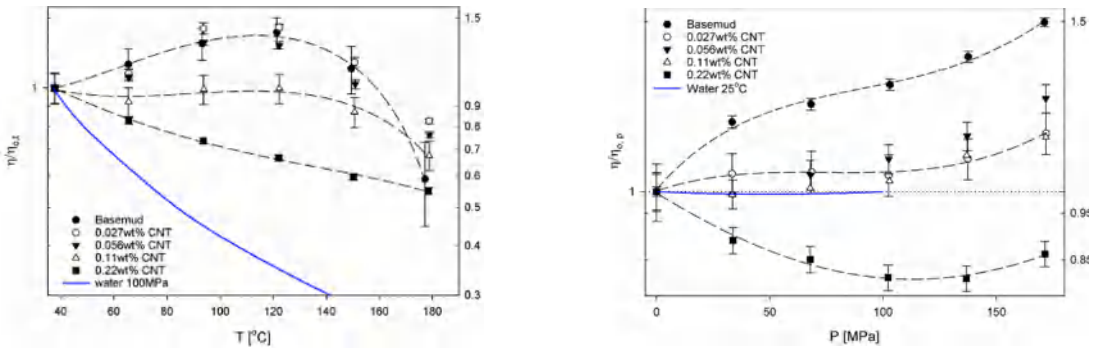

(a) (b)

Source: Adapted from Anoop et al. (2019).

Finally, Echt e Plank (2019) developed a new test protocol using a sepiolite water-based fluid and a xanthan gum-based reference system designed for drilling high-temperature wells. The author measured the suspension capacity of drilling cuttings to different aging times and temperatures, through static aging tests, following the API RP 13B-1 2004 standards. The newly proposed test protocol allows for a better assessment of fluid performance under actual downhole conditions such as when drilling in temperature granite and emphasizes the importance of testing under these conditions. While in the conventional test, the xanthan gum fluid displayed a similar yield point and low shear rate values than the sepiolite fluid, it performed significantly worse than the sepiolite fluid when tested at actual high temperature, under dynamic, and even much more under static conditions.

The primary investigations used to study drilling fluids are summarized in Table 3.1 presenting in chronological order, highlighting the type of fluid and viscosifier, the range of temperature and pressure, the equipment used, the type of electrolyte contained in the solution, and the main results. After analyzing the different studies, it was observed that variations strongly influence water-based drilling fluids' viscosity in temperature and pressure and the type of salt. In conclusion, it was observed that the viscosity decreases with rising temperature and increases with rising pressure, this being to a lesser degree. Another critical point observed over the years was that depending on the type of viscosifier, it provided some strong advantages or disadvantages for its application. Therefore, a literature review of the xanthan gum viscosifier in drilling fluid adapted to HPHT conditions in the offshore environment with high salt content.

Table 3.1 – Summary of major research in chronological order from 1952 to 2020 on the rheology of drilling fluids in HPHT.

Article	Fluid and Viscosifier Type	Temperature-Pressure Range	Equipment	Salt Type	Main Conclusions
Gray et al. (1952)	WBM; limestone	25 a 200 ºC Atmosphere Pressure	Viscometer Coaxial cylinders	–	Temperatures above 150 ºC, the fluid under going high gelation leading to solidification and pressure, do not significantly affect the viscosity.
Srini-Vasan (1958)	WBM	25 to 80 ºC Atmosphere Pressure	Viscometer Fann Coaxial Cylinders	–	Viscosity decreases with increasing temperature.
Olphen (1963)	WBM; Bentonite; Polymers.	–	–	–	Bentonite has a good ability to improve viscosity and control filtration during drilling.
Hiller et al. (1963)	Water suspensions bentonite.	25 to 160ºC 1 to 700 bar	Rotational Couette Viscometer HPHT	Sodium / Calcium Montmorillonite	The dynamic yield stress and plastic viscosity of the sodium bentonite suspension decreased with increasing temperature. The calcium bentonite suspension showed a different behavior, the dynamic yield stress and the plastic viscosity increased with temperature.
Annis et al. (1967)	WBM; Bentonite	25 a 150 ºC Atmosphere Pressure	Viscometer Fann Coaxial cylinders	NaCl	As the temperature increased, the dynamic yield stress increased and the viscosity decreased.
Chesser et al.(1980); Hille et al. (1985); Al-Marhoun and Rahman (1988)	WBM; Limestone; Bentonite; Polymers; Deflocculant.	25 a 200 ºC Atmosphere Pressure	–	NaCl	The use of bentonite and polymers in the drilling fluids with temperature increases, caused an increase in apparent viscosity, causing gelation. However, beyond 120 ºC, the viscosity began to decrease sharply.
Guven et al. (1988)	WBM bentonite; saponite; sepiolite.	149 to 316 °C	Fann 50C HPHT Viscometer	Salts and hydroxides (Na), (K), (Ca)	Salts and hydroxides were found to undergo chemical reactions with clays at high temperatures and greatly change drilling fluids' rheological and wall building properties.

(continued)

Article	Fluid and Viscosifier Type	Temperature-Pressure Range	Equipment	Salt Type	Main Conclusions
Alderman et al. (1988)	WBM; Bentonite	25 to 130 ºC; 1 to 1000 bar	Haake D1000/300 Rheometer; Coaxial Cylinders	–	Viscosity decreases with increasing temperature, and increases with pressure depending on the density of the fluid. The dynamic yield stress does not depend on the applied pressure, showing weak dependence on the temperature below a critical temp.
Ali, Marhoun et al.(1990)	WBM	25 to 255 ºC; 1 to 700 bar	HPHT Fann Model 70 Viscometer	–	A reduction in apparent viscosity, static, and dynamic yield stress with increasing temperature. The increase in pressure caused an amplification of the values of apparent viscosity and dynamic yield stress of the drilling fluid.
Rommetveit et al. (1997)	WBM	25 to 200 °C; 1 to 1200 bar	Fann 70 Viscometer	–	The effects of pressure were less than the effects of temperature, at 1000 bar and 150 ° C the viscosity decreased linearly
Rossi et al. (1999)	Sodium bentonite suspensions.	25 to 120 ºC; 1 to 1000 bar	HPHT Haake Viscometer; Coaxial Cylinders.	NaCl KCl LiCl PEO	The electrolytes and the increase in temperature lead to an increase in yield stress, due to the flocculation of the bentonite suspension. The properties of PEO stabilized bentonite suspensions containing KCl were little affected by HPHT.
Salime et al. (2000)	WBM; PHPA; Xanthan Gum; CMC.	43.4 to 148.9 °C; 6.9 to 34.5 bar	Fann 50C Viscometer	–	All polymer extended drilling fluids, a decrease in shear stress was observed when either the temperature or the pressure was increased.
Later Hamed and Belhadri (2009)	WBM; Xanthan Gum; scleroglucan.	25ºC; Atmosphere Pressure	Rheostress 600 of ThermoHaake	–	All fluids exhibited shear thinning behavior with low yield stress and high permeability and favorable to understand better the chemical action.
Amani et al.(2012)	OBM; WBM	65 to 315 ºC; 1 to 2750 bar	Chandler 3600 HPHT Viscometer; Coaxial Cylinders	–	Under high temperature, the thermal degradation of the solid and polymers of the drilling fluid samples take place, causing the molecules' expansion decreasing the resistance of the fluid to flow.

(conclusion)

Article	Fluid and Viscosifier Type	Temperature-Pressure Range	Equipment	Salt Type	Main Conclusions
Amani and Al-Jubouri (2012)	WBM	65 to 315 ºC; 1 to 2750 bar	Chandler 3600 HPHT Viscometer;	NaCl; KCl	Increases in temperature and pressure for particular electrolyte concentration show the same rheological behavior, but the shear-thinning behavior increases as the electrolyte concentration increases.
Xu et al. (2013)	WBM	60 to 180 ºC; 150 to 1000 bar	Fann IX77 Viscometer	–	The apparent and plastic viscosities exhibited small changes with increasing pressure, at constant Temp.
William et al. (2014)	WBM; nanofluids CuO and ZnO	25 to 110 ºC; 1 to 100 bar	Anton Paar MCR 52 Rheometer; Coaxial Cylinders.	–	An increased concentration of nanoparticles further enhances electrical and thermal properties of WBM and the effect of pressure on the rheology of fluid is more significant at higher temperatures and indicated better stability the viscosity.
Jain, Mahto & Sharma (2015)	WBM; Xanthan Gum.	25 ºC; Atmosphere Pressure	Fann VG model 35	KCl	Nanocomposite as a potential additive in the developed WBM system. WBM demonstrated high thermal stability , good salt tolerance, and it aids in the better shale inhibition property to mitigate instability problems.
Gokdemir (2017)	WBM; OBM; SBM.	25ºC to 300 ºC; 1 to 1000 bar	Anton Paar MCR 302 Rheometer.	–	Some fluid was not affected by pressure change at a constant temperature and rheological models do not include pressure terms in the equations that are dependent do not represent its rheological effects.
Anoop et al. (2019); Aramendiz et al. (2019)	WBM; OBM; Graphene Oxide; Carbon Nanotube Particles.	26 °C to 175 °C. 1 to 171 MPa	HPHT Viscometer Chandler Viscometer	–	The nano-mud suspension was superior to the bentonite fluids in reducing mud filtration and improved rheological characteristics.
Echt e Plank (2019)	WBM; Sepiolite; Xanthan Gum.	25ºC to 150 ºC; 1 to 35 bar	Chandler 3500LS Viscometer	KCl	The sepiolite fluid is characterized by a low plastic viscosity and high low shear rheology indicating a high carrying capacity.

Source: Author (2021).

3.2 XANTHAN GUM SUSPENSIONS HPHT

Xanthan gum is the most extensively used natural polysaccharide (Xanthomons Campestris) for a long time in industrial processes of food, cosmetics, and pharmaceutics, due to its high molecular weight, which increases the viscosity (KRUMEL; SARKAR, 1975; SPEERS; TUNG, 1986; URLACHER; NOBLE, 1997; BERCEA; MORARIU, 2020; AHMED; RAMASWAMY, 2004; KATZBAUER, 1998; EREN; SANTOS; CAMPANELLA, 2015). One of the industries that revolutionized the biopolymers' use was the oil and gas industry, where xanthan gum is used in the water-based drilling fluid, improving its operational capacity. (BROOKEY et al., 1998; KURU et al., 2008; ARABLOO; SHAHRI; ZAMANI, 2013). The pseudo-plasticity of its solutions allows a high capacity of suspending cuttings in the annulus due to the high viscosity at a low shear rate, and also allows a high drill bit penetration rate, because of the low viscosity at a high shear rate (ROSALAM; ENGLAND, 2006).

Among the xanthan gum, physicochemical characteristics are good water-solubility, excellent bio-compatibility, and high molecular weight polysaccharides having branched polymeric chains. When hydrated in either freshwater or brine solution, the aqueous phase tend to associate, and the long-chain backbones wrap around each other, thereby forming relatively massive dispersed packets. These packets greatly slow down any particle settling that tends to occur. When dispersed, xanthan gum forms a double helix molecular arrangement, as shown in Figure 3.4. The xanthan gum's primary structure consists of 1,4-linked βD-glucose residues having a trisaccharide side chain attached to alternate D-glucose residues(LAPASIN; PRICL, 1995). The backbone of xanthan gum is similar to that of cellulose. The side chains are β-Dmannose-1,4- β-D-glucosyl acid-1,2-α-D-mannose. The secondary structure of xanthan gum has been shown to consist of a five-fold helical structure. Most researchers (HOLZWARTH; PRESTRIDGE, 1977; CAMESANO; WILKINSON, 2001) suggest a right-handed double-helical state for native xanthan gum molecule, which is stabilized by intermolecular and intramolecular hydrogen bonds (OGAWA; YUI, 1998).

Figure 3.4 – Schematic representation of the xanthan gum monomer.

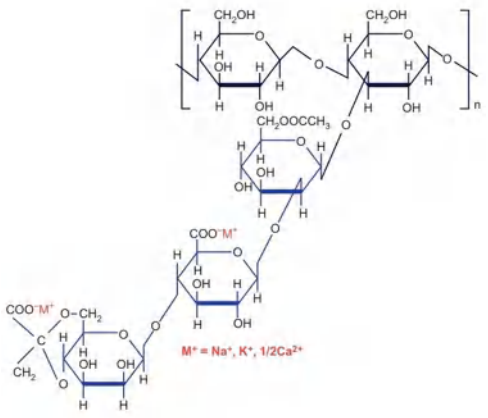

Source: Adapted from Rosalam e England (2006).

Today many of the water-based suspensions used for drilling fluid formulation contain a viscosifier, an electrolyte, and a liquid base. Knowing the isolated behavior of the suspension without the additives that are added to stabilize some rheological properties in critical situations allows one to

conclude some phenomena that are observed in more complex fluids. Many of the studies of xanthan gum in aqueous solutions were developed in recent years due to several of its properties, which are useful in the application of industries such as food, pharmaceutical, and oil & gas industry, the latter being interested in the viscosifying behavior, fluid loss, shale stabilization, and mainly for being environmentally friendly in offshore well.

One of the first works that attempted to understand the rheological effects of xanthan gum under salinity conditions, temperature, and the strain was Rochefort e Middleman (1987), who developed steady-state and oscillatory tests on suspensions of xanthan gum with distilled water and sodium chloride. The authors used a Rheometries Fluids Rheometer (Model RFR 7800) to develop oscillatory tests to obtain the storage and loss modulus and tests to measure the steady-state shear viscosity transient shear stress. Experiments were done in the Couette geometry using a 1.0 mm gap. In all the experiments, a layer of light mineral oil was placed along the fluid's outer edge to prevent evaporation.

First, the effectiveness of dynamic oscillatory shear measurements for studying solutions with structure has been demonstrated. The rheological study concluded that the suspension is affected by salt and in different ways, depending on the concentration regime. The xanthan gum's transition temperature was studied, through dynamic tests measurements with oscillatory frequency superposition, demonstrating that there is a transition from order to disorder conformation drive-by temperature ($helix\ coil$) at T 50 - 60 °C for low salt. Moreover, the transition was increased to higher temperatures ($T > 80$ °C) when high salt. Finally, frequency/temperature superposition has been demonstrated for xanthan gum in high salt in a temperature range of 30 to 800 ºC. Once again, it illustrates the usefulness of dynamic measurements in studying solutions with structure, being the semi-dilute solution rheology of xanthan gum is controlled by intermolecular associations (which are affected by the molecular conformation). However, the rheology of "dilute" solutions is primarily controlled by intramolecular conformation changes.

Once the drilled rock formations contain increasingly higher amounts of salt, the use of polysaccharides (CMC or PAC) in base drilling fluid sensitive to high salinity conditions was replaced by anionic polysaccharides such as xanthan gum. Therefore, Xie e Lecourtier (1992) developed a study focused on the stability of clay/xanthan-gum suspensions, rheological properties analysis, and thermal stability in the presence of various salts, where he used three different types of xanthan gum, sodium chloride, and one clay of 70% sodium montmorillonite and 30% calcium montmorillonite. The measurements were carried out through Rotovisco RV20 coaxial viscometer at 30 ºC and the thermal stability of the xanthan solutions was characterized by measuring sample viscosity before and after aging inside a cell was subjected to rolling in an oven for 24 hours. The author concluded that Xanthan is a suitable polymer for stabilizing water-based drilling mud under high salinity and/or hardness conditions due to its rigid structure. Additionally, the stability of clay/xanthan-gum suspensions depends on the nature and concentration of electrolytes, and there is a minimum xanthan gum concentration required to stabilize the suspension. The xanthan gum solution's thermal stability and the clay/xanthan-gum suspension depend on the xanthan gum conformation affected by temperature and salinity. The xanthan gum solution and suspension are very stable below the transition temperature, but the suspension is not stable. Xanthan gum degradation is accelerated when it is in its disordered single-stranded conformation, and with an appropriate salinity, the clay/xanthan-gum suspension is stable up to 120 °C.

Pelletier et al. (2001) developed oscillatory shear, steady-state flow curves, and extensional flow experiments at different temperatures. The results determined the order-disorder transition through differential scanning calorimetry (DSC). The methodology used to corroborate the transition temperature was based on the various experiments that reflect changes on the molecular scale and slight modification of the physical network structure. It was possible to determine when the fluid generates these changes in structure through the heat peaks that microcalorimeters measure thermal analysis. Figure 3.5 shows a DSC heating curve of the xanthan gum solution of 1% w/w and containing 0.008M NaCl. The curve shows a broad endothermic peak starting at 45 °C and ending at 65 °C. The midpoint transition temperature T_m, is 52 °C. The value of T_m for the xanthan gum in 0.08M NaCl is approximately 90 °C. In conclusion, the temperature range knowledge where the transition from order to xanthan gum disorder helps define rheological behavior variations, defining this range as a critical zone for some high-temperature applications.

Figure 3.5 – Order-disorder transition of xanthan gum (1% w/w, 0.008M NaCl) monitored by differential scanning calorimetry (scan rate 1 °C.min^{-1}).

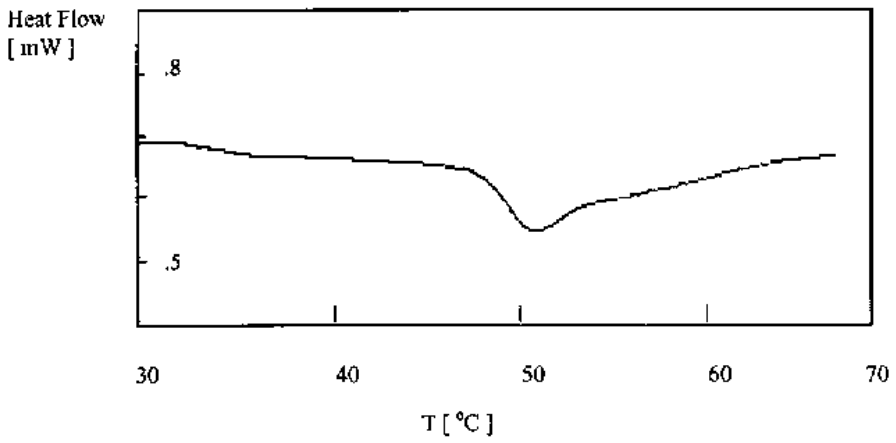

Source: Adapted from Pelletier et al. (2001).

Song, Kim e Chang (2006) concluded that xanthan gum solutions have a shear-thinning behavior and the results for different concentrations were fitted appropriately for the Herschel-Bulkley and power-law model. Furthermore, concentrated xanthan gum solutions exhibit a quite important elastic flow behavior which acts as a significant factor for many industrial applications.

The effects of temperature are widely shown for xanthan gum suspensions, but the effects of pressure are not studied, only Gulrez et al. (2012) developed a study on the effects generated by various industrial treatments typically found in their applications. Treatments such as heating, autoclaving, high-pressure homogenization, and irradiation were subjected to the same sample. Different experiments based on visualization of atomic force microscopy, gel permeation chromatography, and light scattering to properly account for all fractions present in xanthan gum solutions concluded that thermally treated xanthan gum solution in the semidilute region leads to an order-disorder transition. Similarly, irradiation of xanthan gum solution results in an order-disorder transition together with the production of single-strand

low molecular weight molecules. The xanthan gum changes the polymeric chains' structures before and after being subjected to heat treatments and high-pressure homogenization. When xanthan gum undergoes a temperature change, a modification in chain dissociation from a double helix chain to a standard helix is marked by the transition temperature order-disorder conformation of the biopolymers. On the other hand, the high-pressure homogenization treatments cause degradation of xanthan gum, where the polymer chains go from a double helix state expanded with flexibility for the chains' degradation generating a destabilization of the suspension more quickly. The renatured xanthan gum is degraded into smaller molecules that retain its double-helical conformation.

On the other hand, Reinoso et al. (2019) investigated suspensions of xanthan gum in chloride and formate potassium brine at high temperature, just as in previous studies. The authors found that with an electrolyte increment, the conformation transition temperature increases. Moreover, it demonstrated that the suspension exhibits viscoelastic behavior and shear-thinning in a specific temperature range greater than for NaCl.

Moura e Moreno (2019) analyzed the same suspensions of xanthan gum with NaCl, intending to fit their experimental data to the Arrhenius equation that has been used in several studies for polymer solutions, relating the changes in viscosity with temperature, which demonstrating that xanthan gum exhibits high thinning behavior in the semi-diluted region.

In recent years, the xanthan gum solutions' study presents an increasing trend due to its use in drilling fluids and the food industry, presenting several unresolved questions. Most of the works are dedicated only to obtain flow curves to analyze the behavior of the fluid. Therefore, the use of oscillatory and transient tests to characterize the rheological properties are not studied, such as critical yield stress and strain, linear viscoelastoplastic region (LVR), and overshoot stress. Table 3.2 describes the main studies that were the basis for the construction of this dissertation. This chapter presented the lack of methodologies for measuring water-based drilling fluid with xanthan gum and limestone and other unknowns due to the effects of high-pressure and high-temperature on the drilling fluid's rheology.

Table 3.2 – Summary of major research in chronological order from 1987 to 2019 on rheology of xanthan gum suspensions.

Article	Fluid and Viscosifier Type	Temperature-Pressure Range	Equipment	Main Conclusions
Rochefort and Middleman (1987)	Xanthan Gum; Distilled Water; Sodium Chloride.	25 to 100 ºC; Atmosphere Pressure	Rheometries Fluids Rheometer Model RFR 7800	The suspension is affected by the addition of salt, depending on the concentration regime. The transition order to disorder conformation of xanthan gum with temperature was demonstrated with frequency superposition.
Xie and Lecourtier (1992)	Xanthan Gum; Distilled Water; Sodium Chloride	30 ºC; Atmosphere Pressure	Rotovisco RV20 coaxial Viscometer	Xanthan is a suitable polymer for stabilizing WBM under high salinity and/or hardness conditions, due to its rigid structure.
Pelletier et al. (2001)	Xanthan Gum; NaCl	25 to 80 ºC; Atmosphere Pressure	Setaram Micro DSC II Carrimed CSL rheometer	The knowledge of the temperature range where the transition from order to disorder of xanthan gum takes place, defining this range as a critical zone for some high-temperature applications.
Song, Kim & Chang(2006)	Xanthan Gum	20 ºC; Atmosphere Pressure	ARES Rheometric	Yield stress increased concluded may come from the fact that a large number of hydrogen bonds in the helix structure result in a stable configuration.
Gulrez et al. (2012)	Xanthan Gum	–	AFMs GPC DLS	Thermally treated xanthan solution in the dilute region leads to an order-disorder transition and high-pressure homogenization treatments cause degradation of xanthan gum.
Reinoso et al. (2019)	Xanthan Gum; Chloride and formate potassium brines.	20 to 190ºC; 1 to 50 bar	MCR-301 Rheometer Anton Paar Haake Mars II Rheometer	Electrolyte the strength of the solution and shifts the order-disorder conformational thermal transition to higher temperatures, especially formate brine increases up to around 160 ºC.
Moura and Moreno (2019)	Xanthan Gum; NaCl	23 to 77 ºC; Atmosphere Pressure	HAAKE MARS III Rheometer	Depending on the concentration of xanthan gum there are two different non-Newtonian and Newtonian behaviors, in addition to the fact that saline solutions help increase the thermal capacity of the suspensions.

Source: Author (2021).

3.3 MODELS TO DESCRIBE VISCOSITY DEPENDENCE ON TEMPERATURE AND PRESSURE

The rheological properties of drilling fluids under downhole conditions can differ from those measured at ambient pressure and temperatures found at the surface. At depth, the pressure exerted by the mud column may be as much as 1400 bar. The temperature depends on the geothermal gradient and may be more than 260 °C at the bottom of the hole.

Fluid viscosity is not only dependent on parameters such as shear rate, strain, composition, or time. It is also highly dependent on temperature and pressure. The overall tendency is the apparent viscosity to be reduced with increasing temperature but increased with increasing pressure (BARNES, 1999).

For non-Newtonian fluids, the dependence of viscosity on temperature and pressure can be expressed as separate functions of shear rate (OSSWALD T., 2015). Empirical models are based on the data tendency, and their fitting parameters have not physical meaning. On the other hand, theoretical models are essentially based on molecular theories, such as free volume theory. In the latter case, their parameters have a physical interpretation.

Equation 3.1 is the exponential model proposed by Barus (1893) to describe the isothermal viscosity's evolution with pressure, where η_{ref} is the viscosity at the reference temperature and pressure, β is piezoviscous coefficient, P is the applied pressure and P_{ref} is the pressure of reference. Initially, in 1893, the model was proposed for marine glue and pitch, which change continuously from solid to liquid, and in which this change takes place at an enormously rapid rate and is complete within relatively few degrees, but in later years several works with which materials were used polymeric, suspensions, emulsions, and drilling fluids implemented the model reporting good adjustments (FILLERS; TSCHOEGL, 1977; MOONAN; TSCHOEGL, 1985; TSCHOEGL; KNAUSS; EMRI, 2002a; HERMOSO; MARTÍNEZ-BOZA; GALLEGOS, 2017). Barus' model is a proper equation to correlate viscosity pressure at low and moderate pressures (HERMOSO et al., 2014). The main limitation is the exponential increase in viscosity prediction at high pressures since viscosity shows either a change in the viscosity-pressure variation or limiting viscosity values reported elsewhere (BRIDGMAN, 1925; LAMB, 1978).

$$\boldsymbol{\eta} = \eta_{ref}\ exp\left[\beta\ (P - P_{ref})\right] \tag{3.1}$$

Houwen e T Geehan (1986) decided to investigate the variations of temperature and pressure on Herschel-Bulkley and Casson models' rheological parameters, where used Barus equation to model the effects of pressure with the dependence of shear rate. The authors found that the Casson model is more reliable for extrapolation purposes than the Herschel-Bulkley model, which was necessary due to the rheometer's limitations to measure low shear rates. Wherefore Houwen e T Geehan (1986) decided to investigate the Casson model, which several authors have claimed to give a good representation of the rheology of water-based drilling fluid (SUN et al., 1986).

The Arrhenius equation is shown in Equation 3.2, which correlates the variation of the speed constant of a chemical reaction with temperature. It was demonstrated that the order of greatness of the activation energy shows a dependence of the viscosity with the temperature (JR et al., 1975). Therefore,

Houwen e T Geehan (1986) suggested using the Arrhenius equation to represent the effects of pressure and temperature.

$$\boldsymbol{v_k} = A\, exp\left(\frac{-E_a}{R\,T}\right) \tag{3.2}$$

where R is the ideal gas constant, A is constant in the Arrhenius equation related to the frequency factor probability of an effective collision, and E_a is constant in the Arrhenius equation related to the activation energy.

Houwen e T Geehan (1986), Alderman et al. (1988), and Maglione et al. (1996) concluded that the influence of temperature and pressure on the viscous flow behavior is significant in drilling fluids. However, only the influence of temperature on the viscosity of drilling fluids is well known and can be modeled by equations based on the thermal activation theory, such as the Arrhenius equation, or on the free volume theory with WLF (Williams-Landel-Ferry) and FMT (Fillers-Moonan-Tschoegl) equations.

The effects temperature is frequently modeled through the WLF equation defining a reference temperature at constant pressure. Equation 3.3, where fitting parameters of rheological models dependent on shear rates are used, to fit the flow behavior with the effects of temperature. The model consists of the viscosity at the reference temperature η_{ref} and two setting parameters $c_1 - c_2$.

$$\boldsymbol{\eta} = \eta_{ref} \cdot\ 10^{-\left(\frac{c_1\,(T - T_{ref})}{c_2 + (T - T_{ref})}\right)} \tag{3.3}$$

Traditionally, the effect of pressure on fluid viscosity at constant temperature has been described by the empirical equation, such as the one proposed by Barus (1893). Alderman et al. (1988) extend the Arrhenius equation by considering the temperature and pressure effect with the high-shear viscosity variation. The proposed equation is shown in Equation 3.4, which combines Equation proposed by Houwen e T Geehan (1986).

$$\boldsymbol{\eta}(P,T) = A_n\,(1 + \alpha(\varphi)\beta_p(P)\ P)\,Exp\left[\frac{E_a + P(B'T - C')}{T}\right] \tag{3.4}$$

where the first bracket quantifies the change in volume fraction with pressure and the exponential term models of colloidal suspension rheology with the pressure coefficient of viscosity for aqueous systems, E_a is the activation energies, A_η is the pre-exponential factor, α is a packing factor which for drilling fluids' that can be taken as a fit factor which is a constant for a given mud having a solids fraction φ, $\beta(P)$ is the isothermal compressibility of the drilling fluid and B', C' are constants which characterize $(\partial ln_\eta/\partial lnP)_T$ for the continuous phase.

On the other hand, pressure-temperature-viscosity models can be obtained by combining different equations, such as the Andrade-Barus model and WLF-Barus model. Equation 3.5 shows the Andrade (1930) expression, an Arrhenius-like equation that describes the thermal dependence at temperatures near the boiling point and far from the glass transition temperature. Besides, it is not strictly an empirical

model since its parameters have a physical interpretation.

$$\boldsymbol{\eta} = \eta_{ref}\ exp\left[\frac{E_a}{R}\ \left(\frac{1}{T} - \frac{1}{T_{ref}}\right) + \beta_p\ (P - P_{ref})\right] \tag{3.5}$$

where η_{ref} is the viscosity at the temperature of reference, R is the gas constant, $\beta_p(P)$ is the thermal compressibility, and E_a is the activation energy to flow.

At the same time, Williams, Landel e Ferry (1955) originally proposed the WLF model, which represented a useful modification of the Vogel-Tammann-Fulcher model or VTF model and was coupled with the Barus' equation to model the pressure effects:

$$\boldsymbol{\eta} = \eta_{ref}\ exp\left(\beta\ (P - P_{ref})\right) \cdot\ 10^{-\left(\frac{c_1\ (T - T_{ref})}{c_2 + (T - T_{ref})}\right)} \tag{3.6}$$

where c_1 and c_2 are the WLF constants, η_{ref} is the viscosity at the temperature of reference, T_{ref}. This model is particularly valid for describing the low-temperature viscosity dependency where non-Arrhenius behavior is characteristic.

Hermoso et al. (2014) highlight that theoretical models can provide a more accurate framework for describing temperature and pressure of viscosity dependency. Many theories for modeling the effects of thermodynamics variables such as pressure or temperature on the time-dependent behavior of materials are based on the free-volume theory (TSCHOEGL; KNAUSS; EMRI, 2002b). The authors supposed that the variation in viscosity relies on the molecule-size holes in the fluid. The total sum of these holes describes the free-volume, which affects the mobility of the liquid molecules.

The FMT model is considered an extension of the WLF equation (FILLERS; TSCHOEGL, 1977; MOONAN; TSCHOEGL, 1985). In this model, both pressure and temperature are taken into account.

For polymeric materials, the free-volume models available based on the time-pressure-temperature-superposition principle has been extensively reviewed by Tschoegl, Knauss e Emri (2002a). The FMT model and modified WLF equations proposed by Tschoegl, Knauss e Emri (2002a) are based on the free volume concept to model the dependence of temperature and pressure on the behavior of rheological properties in suspension and polymeric materials in the linear viscoelasticity range (FILLERS; TSCHOEGL, 1977).

The FMT model is presented in Equation 3.7. Its different parameters can all be determined using non-linear regression techniques, allowing a broad context that can be used to model drilling fluids.

$$log\left(\frac{\boldsymbol{\eta}}{\eta_{ref}}\right) = -\frac{c_1^{00}(T - T_{ref} - \theta(P))}{c_2(P) + (T - T_{ref} - \theta(P))} \tag{3.7}$$

where c_1^{00} and c_2 as shown in Equation 3.9, are variables that depended on B'' is a constant that normally is taken to be 1, but maybe calculated only if Pressure-Volume-Temperature (PVT) data are available to determine the pressure dependence of the bulk modulus of the entire volume, $\alpha_v(P)$ separately is the

expansivity of the free volume, considered pressure-dependent and temperature independent, and f_0 is the fractional free-volume at the reference temperature.

$$\theta(P) = c_3(P) ln\left(\frac{1 + c_4 P}{1 + c_4 P_{ref}}\right) - c_5(P) ln\left(\frac{1 + c_6 P}{1 + c_6 P_{ref}}\right) \tag{3.8}$$

$$c_1^{00} = \frac{B''}{2,303 f_0};\ c_2(P) = \frac{f_0}{\alpha_v(P)};\ c_3(P) = \frac{1}{k_e \alpha_v(P)};\ c_4 = \frac{k_e}{k_e^*};\ c_5(P) = \frac{1}{k_\phi \alpha_v(P)};\ c_6 = \frac{k_\phi}{k_\phi^*} \tag{3.9}$$

$$\alpha_v(P) = \alpha_f^* \left[1 - \frac{C'' P}{K_e^* + k_e P}\right] - C'' \alpha_\phi^* P \left[\frac{1}{K_e^* + k_e P} - \frac{1}{K_\phi^* + k_\phi P}\right] \tag{3.10}$$

where k_e^* and k_ϕ^* are the bulk module of the entire and occupied volume, respectively, at zero pressure and the temperature of reference, k_e and k_ϕ are proportionality constants, which are independent of temperature and pressure, α_ϕ^* is the expansivity of the occupied volume at zero differential pressure, $\alpha_f^*(P)$ is the expansivity of the free volume at zero differential pressure and temperature of reference, and C'' is proportionality constant.

Generally, the parameter C'' is assumed to be the same value for either occupied or entire volume. However, this assumption might be erroneous when PVT data are employed, and different values of C'', for the occupied or entire volume, are required to estimate the evolution of expansivity with pressure correctly, as is reported elsewhere (MARTÍN-ALFONSO et al., 2007).

3.4 CHAPTER SUMMARY

The chapter presented a literature review on studies investigating the water-based drilling fluids' rheology under high pressure and high-temperature conditions. The literature review observed that drilling fluids have a wide range of rheological properties affected by different operational variables, such as temperature, pressure, density, physical-chemical composition, and even contaminants themselves lent along during drilling. The various investigations focused on observing the effects of temperature and pressure on viscosity and yield stress for several water-based drilling fluids, with different compositions found in offshore operations. Recently, the authors have focused on improving the rheological properties of drilling fluids, mainly due to the demanding environmental laws presented in the last two years. Therefore, the formulation of fluids with nanoparticles and additives that increase thermal stability in water-based drilling fluid with bio-polymers has stood out. On the other hand, to characterize and develop constitutive models of drilling fluids prepared in the laboratory, it is necessary to observe the fluids base matrix's main phenomena. In this research, the knowledge of xanthan gum behavior in distilled water subjected to high temperature and electrolyte, mixtures, characterize its possible behavior when mixed in more complex fluids. Therefore, some studies showed that the critical ranges of temperature and consent play an essential role in the fluid's rheology. Other studies also presented constitutive models representing the non-Newtonian behavior of drilling fluids, including the combined effects of temperature, pressure, and shear rate. The models are based on molecular and physical theories of fluid behavior. Observing what

was obtained in the various experimental studies shows viscosity decreases with temperature and slight increases with pressure.

In conclusion, this literature review shows the lack of studies that deepen in the argumentation of the influence of the thermal history effects, as well as the possible influence of the pressure history in water-based drilling fluids, as they are subjects that interrelate with various areas of study and requires a greater deepening. Furthermore, no studies were found for water-based drilling fluids that analyze transition temperature order-disorder conformation through modulated differential scanning calorimetry tests, which characterize the sample thermally behavior with different concentration solutions. The lack of rheological high pressure and high-temperature measurements was observed in water-based drilling fluids with xanthan gum and limestone. Likewise, there is a need to characterize a model that explains the effects of viscoelastoplastic, thixotropy, and high-pressure and high-temperature conditions on water-based drilling fluids, allowing to improve and solve problems in offshore operations.

4 MATERIALS AND METHODS

This chapter presents the materials, the experimental equipment, and the methodology used to obtain the water-based drilling fluid's rheological characteristics and to analyze the effects of pressure and temperature on its rheology.

4.1 DRILLING FLUID

Petrobras S.A kindly provided the water-based drilling fluid used for this study and is shown in Figure 4.1. The sample was stored at ambient temperature and has been at rest since arrival at the Federal University of Technology-Parana (UTFPR). Therefore, solids in the sample had considerably sedimented at the bottom of the tank, so the sample was homogenized with an Electric Mortar Mixer 1600W - WBR-888761 for 20 minutes and separated into 6 samples of 400 ml each.

Figure 4.1 – Water-based drilling fluid with xanthan gum and limestone.

Source: Author (2021).

The water-based drilling fluid used for the research comprises industrial water, NaCl brine, limestone and xanthan gum, the last one being the main viscosifier. The complete solution composition is shown on Table 4.1.

Besides, 3 samples of water-based drilling fluids of 400 ml were prepared with concentrations of 0.5, 1, and 2% of xanthan gum, keeping the other components of the fluid constant. The fluids were prepared using drilling fluid provided by Petrobras S.A. The fluid was homogenized for 15 minutes in an industrial mixer Hamilton Beach HMD200 at room temperature, then the xanthan gum was added to the water-based drilling fluid and finally, the fluid was left mixing constantly for 4 hours.

Table 4.1 – Chemical composition of water-based drilling fluid with xanthan gum and limestone.

Chemical Composition	
WBM/UTFPR	Industrial Water - QSP
	NaCl brine
	Anti-foamer (Polifoan)
	Xanthan Gum
	Starch HP
	Magnesium Oxide
	Lubricant (Liovac 4260)
	Bactericidal (Polibac TC)
	Magnesium Peroxide
	Rheological Modifier (BDF 990)
	Limestone $Ca(OH)_2$

Source: Petrobras S.A (2019).

4.2 EQUIPMENT

4.2.1 Rotational Rheometry

The rheological characterization of the drilling fluid was carried out in a controlled stress and strain rheometer Anton Paar MCR 702TD. The accuracy of the acquired data was verified comparing the results with those obtained with Haake Mars III and TA Instrument DHR 3 rheometers, which are shown in Figures 4.2 (a) and (c). The data validation of the tests is shown in Appendix A.

Figure 4.2 – (a) Haake Mars III; (b) Anton Paar MCR 702TD; and (c) TA instrument rheometer.

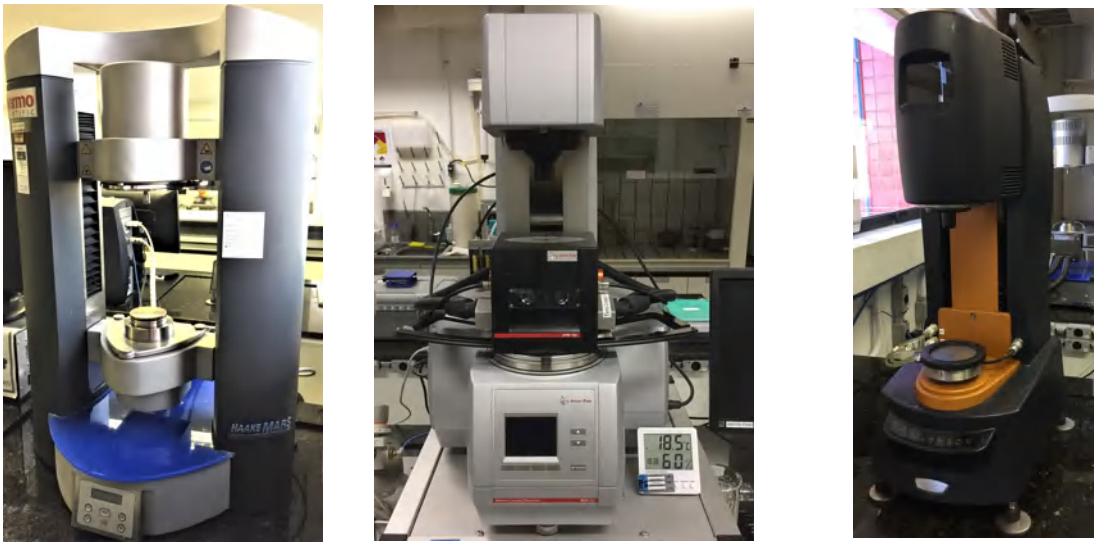

(a) (b) (c)

Source: Author (2021).

The viscous flow behavior and viscoelastic response of these materials was studied using conventional geometry coaxial cylinders at atmospheric pressure. The high-pressure rheological characterization was carried out with the pressure cell C-ETD 300/PR 1000 using also coaxial cylinders geometries. The rheological tests developed to characterize the water-based drilling fluid at atmospheric pressure were performed in the Anton Paar MCR 702TD rheometer with chamber CTD 180, which is shown in Figure 4.2 (b). The rheometer has wide applied torque range 10 to 230 $[mN \cdot m]$, angular velocity 10^{-7} to 628 rad/s, and temperatures -20 to 180 ºC with Peltier-based convection. The temperature control system have maximum heating rate of 18 ºC.min^{-1} and the maximum cooling rate is 10 ºC.min^{-1}. The temperature control can be made through forced air or for non-forced convection by a Peltier-based system in the chamber walls of the rheometer.

The geometries used were a serrated plate-plate geometry of 35 mm diameter (PP35/P2), as shown in Figure 4.3 (a), and sandblasted coaxial cylinders of 20 mm inner diameter with a radius ratio of 0.909 and a bottom gap of 4 mm (CC20/S and C-CC20/S/TD), as shown in Figure 4.3 (b). The annular gap was chosen according to the particle size considerations (ANNE-ARCHARD; MAROUCHE; BOISSON, 2006; CHHABRA, 2010; HERMOSO et al., 2014).

Figure 4.3 – (a) Serrated plate-plate geometry 35 mm diameter (PP35/P2); (b) Sandblasted coaxial cylinder geometry of 20 mm diameter (CC20/S and C-CC20/S/TD).

(a) (b)

Source: Author (2021).

The diameters of the analyzed drilling fluid particles can vary between 28 and 63 μm, as can be seen in Figure 4.4. The visualizations were performed through an Olympus BX51 microscope with magnifications between 1 and 100x and an image acquisition system (ImagePro-Plus®). Analyzing the different samples it was found out that the largest particle present in the fluid had 63 μm of diameter. Therefore, it was confirmed that there is no particle-wall interaction effects because the geometry of coaxial cylinders has an annular gap of 1 mm, fulfilling the criterion for particulate fluids, where the gap must be greater than 10 to 100 times the size of the largest particle in the fluid (ANNE-ARCHARD; MAROUCHE; BOISSON, 2006; CHHABRA; RICHARDSON, 2011; HERMOSO et al., 2014).

Figure 4.4 – Images of particles in the water-based drilling fluid taken through the Olympus BX51 microscope.

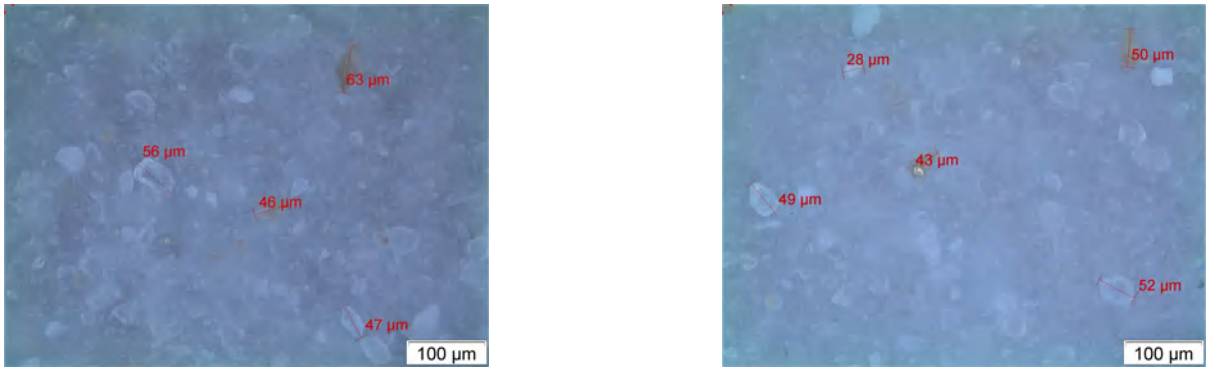

Source: Author (2021).

4.2.2 High-Pressure Rheometry

The Anton Paar MCR 702TD rheometer combined with the pressure cell C-ETD 300/PR 1000 system was used to reproduce the pressure and temperature conditions found in HPHT wells. The pressurization system is shown in Figure 4.5. The pressure cell works in the range from atmospheric pressure to 1000 bar and temperatures from 25 to 300 °C. Heating was performed by electrical control and integrated with the pressure cup, whereas cooling was performed with compressed air. The maximum heating rate is 30 ºC.min^{-1} and the maximum cooling rate is 3 ºC.min^{-1}. The pressurization source is external through a pump of 400 bar employing a valve system that allows increasing the pressure to 1000 bar in the measurement chamber. The measurement system consists of magnetic coupling with a coaxial cylinder. The torque acting on the rotor is transmitted to the rheometer by a magnetic clutch with a minimum torque of 4.0 x 10^{-4} [N.m] and a normal force resolution of 2.0 x 10^{-5} [N]. The pressure cell was also used to perform measurements at high temperatures, preventing the sample's evaporation above the boiling point.

Figure 4.5 – Pressure cell C-ETD 300/PR 1000 system for Anton Paar MCR 702TD Rheometer.

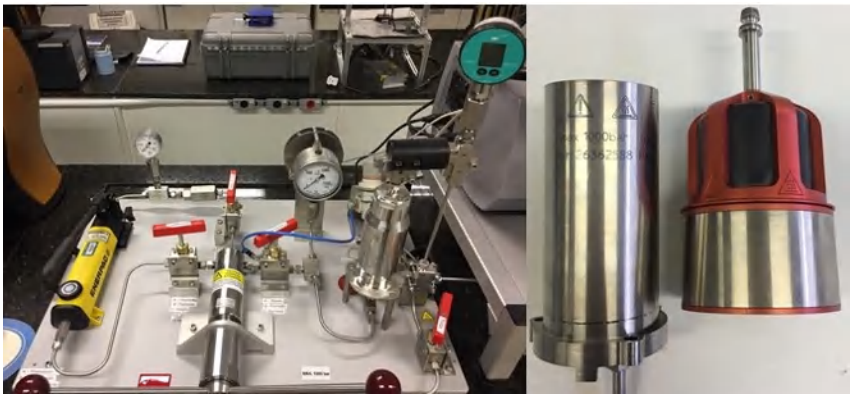

Source: Author (2021).

The rheological tests were made at high pressure with the water-based drilling fluid. The coaxial cylinders' geometry "helical profile cylinder B-CC28/PR1000/HR geometry" and "smooth CC-26 and CC-29 geometry" were used. The geometries are shown in Figures 4.6 (a) and (b). They were compared under the same conditions to verify if the smooth geometries presented a pronounced slip concerning the helical geometry since this type of helical geometry was not registered in the literature. The comparison can be seen in Appendix A. In conclusion, the variation was minimal concerning the measured shear stress. Therefore, for this research, helical geometry was used in all tests.

Figure 4.6 – (a) Helical profile cylinder B-CC28/PR1000/HR geometry; (b) Smooth CC-26, and CC-29 geometry.

(a) (b)

Source: Author (2021).

4.2.3 Roller Oven Fann Stove

Many constituents of water-based drilling fluids degrade slowly at high temperatures. Such degradation occurs while circulating but is more severe when the drilling fluid is left in the lower part of the hole, due to the higher temperature. Consequently, the effect of aging at elevated temperatures was observed on all water-based drilling fluid compositions. The thermal aging tests can simulate the conditions of the bottom hole temperature to investigate its effects. The test consists of letting the fluid within a stove at a high temperature for at least 16 hours statically or with the roller' in movements. The tests were carried out in the Roller Oven Fann stove, shown in Figure 4.7 (a). The maximum temperature allowed is 175 °C. For the test, the drilling fluid was inserted into a 500 ml stainless steel aging cell that is shown in Figure 4.7 (b), and placed on the rollers, where static or dynamic conditions can be applied. The dynamic condition simulates the flow at the annular zone when the well is in operation. The thermal aging tests were performed according to the conditions in Table 4.2, where the recommended values of volume and pressure required in aging tests with temperatures higher than the boiling point of water are shown. The aging cell is then cooled to room temperature and the rheological properties are measured and compared to the same properties before the aging process (CAENN HCH DARLEY, 2017).

Figure 4.7 – (a) Roller oven Fann; (b) Aging cell.

(a)

(b)

Source: Author (2021).

Table 4.2 – Drilling fluids volume and pressure for high-temperature aging.

Desired Aging Temperature [ºC]	Absolute Water Vapor Pressure [bar]	Sample Volume [ml]	Applied Pressure [bar]
100	1.03	364	1.72
121	2.06	370	3.45
149	4.62	380	6.89

Source: Adapted from Fann Instrument Company (2014).

4.2.4 Differential Scanning Microcalorimetry

For the thermal analysis measurements, the μDSC7 Evo microcalorimeter was used to study the samples (denaturation, transition, gelification, reaction, etc.) over a wide temperature range (-45 to 110 °C) with a programmable temperature scanning rate for heating and cooling is 0.001 to 2 ºC.min^{-1}. Differential scanning calorimetry (DSC) was used as an alternative method to precisely measure the transition temperature order-disorder confirmation of water-based drilling fluid. DSC provides valuable information about the sample's physical properties as crystalline or amorphous nature and demonstrates a possible interaction between particles and polymers in formulations.

Figure 4.8 – Differential Scanning Microcalorimetry μDSC7 Evo.

Source: Author (2021).

4.3 RHEOLOGICAL CHARACTERIZATION

This section describes rheological experiments that were performed and planned for the development of the dissertation. The following study considers three different analyses. The first situation are the sweep oscillatory tests. The second are the steady-state viscous flow curves of the drilling fluid and the third are flow start-up tests with different shear rates and an aging time of 600 seconds, recommended by 13B-1 (2016) standards.

4.3.1 Sweep Oscillatory Test

During the drilling fluid's characterization, it was necessary to perform some time and stress amplitude sweep oscillatory tests. The fluid's elastic and plastic characteristics at small strains allow knowing the capacity of the drilling fluids' main functions, also serving as a guide for carrying out other experiments.

Initially, the stress amplitude sweep oscillatory tests were developed. The tests are essential to properly determine the LVR (Linear Visco-elastic Region) to define a strain value that is a critical input parameter for subsequent frequency and time-based tests. The LVR indicates the range in which the test can be carried out without destroying the sample structure, indicating the sample's stability.

Through the stress amplitude sweep oscillatory tests also possible to obtain other parameters are an approximation of the minimum shear stress required to initiate flow for certain oscillatory conditions, known as the critical yield stress and the minimum strain to keep the material stable, this value is called critical strain. The critical yield stress and critical strain values can be obtained through the crossing of the stronger G' and loss G'' modulus. The tests were carried out imposing stress amplitude with logarithmically stepped increments from 0.01 to 100 Pa. Each stress is held on the material for a given amount of time and the data is acquired at 60 points per decades to have greater precision and a frequency of 1 Hz. In order to know the stability of the fluid in the linear regime, the tests were executed at temperatures of 4, 10, 25, 40, 55, and 70 ºC at atmospheric pressure, and also at high pressure of 100, 400, 600, 800 bar at 25 ºC.

Time sweeps oscillatory tests are important when testing materials such as suspensions, that may undergo macro- or micro-structural rearrangement with time. Depending on the sample, evaporation, dispersion settling and thixotropy data can take place. But once any of these cases actually occur, the material properties change so drastically that accurate and reproducible measurement becomes difficult. An oscillatory time sweep was used to select the adequate aging time to perform flow start-up tests, analyzing the influence of temperature and the xanthan gum's concentration at atmospheric pressure in the water-based drilling fluid. The tests allowed to verify the structural modifications of the material over time. The tests were conducted in all cases first by homogenizing the fluid for 10 minutes at a shear rate of 300 s^{-1} at 25 ºC. Straight ahead, the temperatures of 4, 10, 25, 40, 55, 70, and 90 ºC at atmospheric pressure were reached with temperature ramps at 4 ºC.min^{-1} at 300 s^{-1}. Then, the fluid was left for 300 seconds at the selected temperature so that the sample reached its thermal equilibrium before measurement, keeping the fluid-structure in balance. The tests were fulfilled with a constant strain of 0.001 and a frequency of 1 Hz for 3600 seconds.

For tests with the different concentrations of 0.25, 0.5, 1, and 2% xanthan gum, the duration was 7200 seconds at a constant temperature of 25 ºC and atmospheric pressure.

The methodology for constructing flow curves required the obtainment of the time sweep oscillatory tests at 4, 10, 25, 40, 55, 70, and 90 ºC at atmospheric pressure, due to evaporation and sedimentation phenomena that fluid suffices during measurements. Figure 4.9 shows the storage modulus G' and phase angle as a function of time. It was observed that for all temperatures the restructuring of the material occurs instantaneously, having a gelation time of about 300 seconds, this phenomenon is more evident when the experimental numerical data obtained are observed. Moreover, the test can identify the evaporation and sedimentation phenomena of the sample. These phenomena took place when the sample was left at rest, especially for 70 and 90 ºC, where it begins to suffer sedimentation or phase separation for both temperatures after 600 seconds of the test. Figure 4.9 makes it possible to observe that the storage modulus for temperatures from 4 to 55 ºC kept their values constant throughout the test. At 70 ºC, the modulus decreased from 3.7 to 2.63 Pa, indicating a weakening of the structure. At 90 ºC, it first suffered a fall from 2.7 to 1.46 Pa. After 2300 seconds of testing, the storage modulus increased to 5562 Pa, with two structural relaxation effects followed by a stiffness of the sample. The phase angle was observed, the sedimentation phenomenon was evident because the angle increases from 32º to 39º and from 36º to 47º at 70 and 90 ºC, respectively. As a result, there may be problems of obstruction or sedimentation of cuttings due to the structure's breakdown during operational stops in high-temperature sections. On the other hand, for the test at 90 ºC after 2000 seconds, problems of evaporation effects of the liquid phase during the test were evidenced. Evaporation was only observed at 90 ºC when the angle decreased from 47º to approximately 22º. One can notice the salt's crystallization on the geometry, as shown in other tests in Appendix B, causing data errors during measurement.

The results indicate that the construction of flow curves at temperatures higher than 70 ºC was only possible by using the rheometer with the pressure cell, avoiding erroneous measurements for high temperatures. The flow curves for temperatures of 90, 100, and 125 ºC were obtained with the pressure cell, in which a constant pressure of 10 bar was imposed, higher than the saturation pressure of water vapor for these temperatures.

Figure 4.9 – Time sweep at temperatures 4, 10, 25, 40, 55, 70, and 90 °C with 0.1% strain for 3600 seconds.

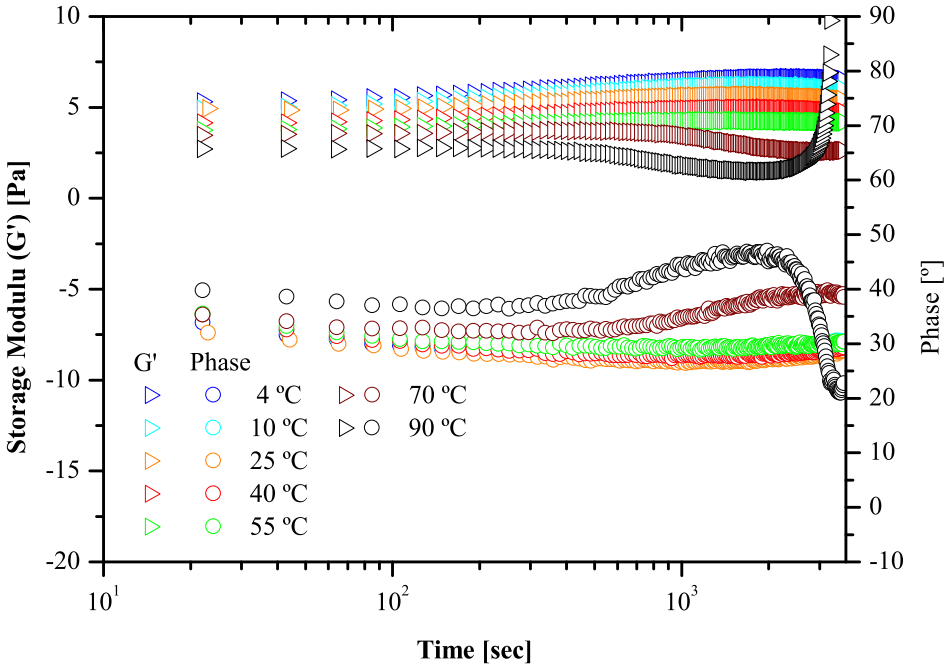

Source: Author (2021).

4.3.2 Flow Curves at Atmospheric and High Pressure

One way of knowing the drilling fluid's behavior is by obtaining the flow curve (COUSSOT; GAULARD, 2005). The experiment can be done by imposing a series of constant shear rate levels for sufficient time for the shear stress to reach a steady-state regime. It is recommended to start from the highest shear rates to the lowest ones to completely break the material down at the highest rates, favoring a faster achievement of the permanent regime at the lowest rates, especially if the material presents thixotropy (CRUZ et al., 2002; DIVOUX; GRENARD; MANNEVILLE, 2013).

In this analysis, one can divide the results into two parts. The first tests investigated the effects of temperature at atmospheric pressure. Flow curves were obtained for a temperature range of 4 to 70 ºC at atmospheric pressure for shear ranging from 400 to 0.1 s^{-1} with steps of 50 s^{-1} applied for 1000 seconds each until reaching steady-state shear stress. The steady-state criteria was based on the moving average with 50 seconds intervals, with variations less or equal to 1%. For temperatures of 90, 100, and 125 ºC, the flow curves were measured using the pressure cell C-ETD 300 under the same conditions of shear rate and time, but imposing pressure of 10 bar, as said in the previous subsection. After, the analysis of the effects of pressure at constant temperature was investigated. The range of pressure was from 100 to 800 bar while keeping the temperature constant at 25, 55, and 100 ºC for shear rates ranging from 400 to 50 s^{-1} with steps of 50 s^{-1}.

4.3.2.1 Atmosphere Pressure Measurement

Figure 4.10 presents the procedure for the rheological tests fulfilled at atmospheric pressure at temperatures of 4, 25, 40, 55, and 70 ºC. The procedure begins by inserting 7.5 ml of sample into the geometry using a measuring syringe; the starting conditions of each test were always 25 ºC for 5 minutes. Then temperature ramps were implemented to reach the test temperature at a rate of 4 ºC.min^{-1} for heating and 3 ºC.min^{-1} for cooling. Followed by a pre-shear of 600 s^{-1} for 10 minutes to eliminate possible flocculation and erase any shear history. Finally, the flow curve was obtained for different constant shear rates.

Table 4.3 – Temperatures for the construction of flow curves.

The temperatures at Atmospheric Pressure	The temperatures at 10 bar
4	90
10	100
25	125
40	-
55	-
70	-

Source: Author (2021).

In order to verify the measurements of the Anton Paar MCR702TD and determine which is the best geometry for measurements of water-based drilling fluids, flow curves were performed at 25 ºC using the procedure shown on Figure 4.10. The results were compared to the Anton Paar, Haake Mars III and TA Instruments DHR 3 rheometers, using geometries of concentric cylinders and parallel plates. The Appendix A shows the obtained results in detail. In conclusion, it was observed that the geometry of the concentric cylinders is the best since the fluid has low viscosity, which allows maintaining the fluid confined without mass loss to the surroundings, resulting in better results. On the other hand, a variation of the shear stress measurements was also found due to possible heating effects once the Anton Paar rheometer's Peltier cell is located at the chamber walls. Therefore, it requires more time for the heat transfer to homogenize the temperature in the sample, showing high thermal inertia that could be taken as thixotropy of the fluid. In these cases the Anton Paar MCR 702TD rheometer and the geometry with CC20/S sandblasted coaxial cylinders was used and provided better results. The effects of temperature and pressure were compared using the same rheometer and type of geometry. The water-based drilling fluid used for this research was a xanthan gum suspension and other additives prepared in industrial water-(QSP). Consequently, the use of Peltier-based temperature control systems with forced convection, such as the one used for the Anton Paar MCR 702TD rheometer, at high-temperature during long test time can generate evaporation. A methodology to avoid these problems during the measurements was developed to evaluate different specific situations, as shown in Appendix B. The tests where evaporation of the liquid phase was observed, there were based on the imposition of a constant shear rate of 100 s^{-1} for 14000 seconds. The test duration depended on the value of the shear stress, when it increased

Figure 4.10 – Proposed procedure for testing with temperatures.

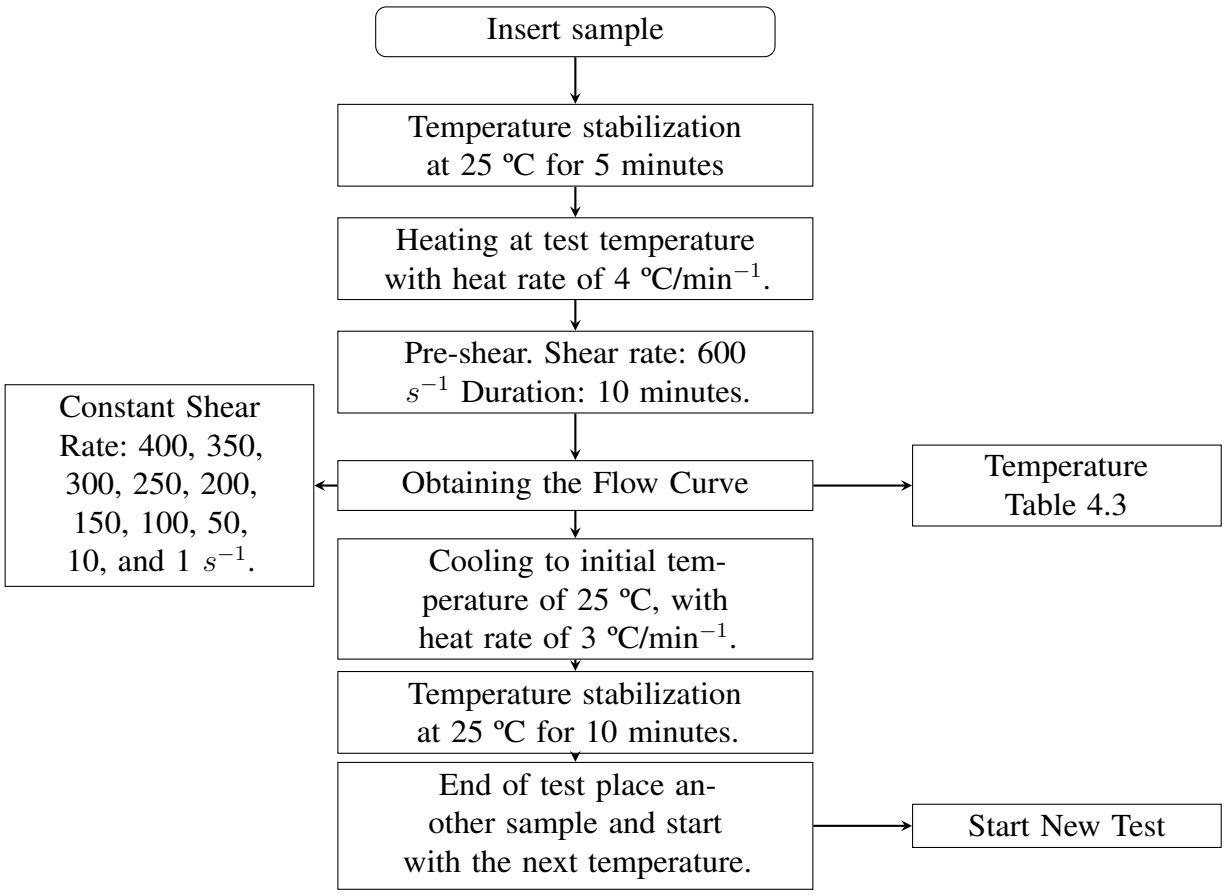

Source: Author (2021)

excessively the test was stopped. The tests were carried out at 25 and 55 °C at atmospheric pressure. The data acquisition was performed with four different settings. First, the convection temperature control system turned on, the second test was the Peltier-based heating temperature control system with turned off convection, the third was the convection system off but saturating the atmosphere inside the rheometer chamber, through cotton swabs moistened with water and the Peltier-based heating temperature control system, and finally, the convection system off under saturated atmosphere with a surface layer of SAE 25W-60 oil. The analysis suggests that the Peltier-based heating temperature control system with turned off convection and saturated atmosphere through damp pieces of cotton inside the rheometer's protective chamber presents greater stability for the acquisition of rheological data especially in the flow curve, which requires longer times and high temperatures. Therefore, this configuration is the one used in the subsequent tests at atmospheric pressure. The procedure for temperatures at 90, 100, and 125 ºC was similar at Figure 4.10, which were carried out with the rheometer with a pressure cell at 10 bar to avoid evaporation problems of the sample.

4.3.2.2 High-Pressure Measurement

Effects of the pressure on the rheology of water-based drilling fluid with xanthan gum were determined through pressure tests of 10, 100, 400, 600 and 800 bar at temperatures of 25, 55 and 100 ºC based on the procedure shown in Figure 4.11. The procedure consisted of placing the sample inside the

Figure 4.11 – Procedure of the rheological tests staggered with pressure increases.

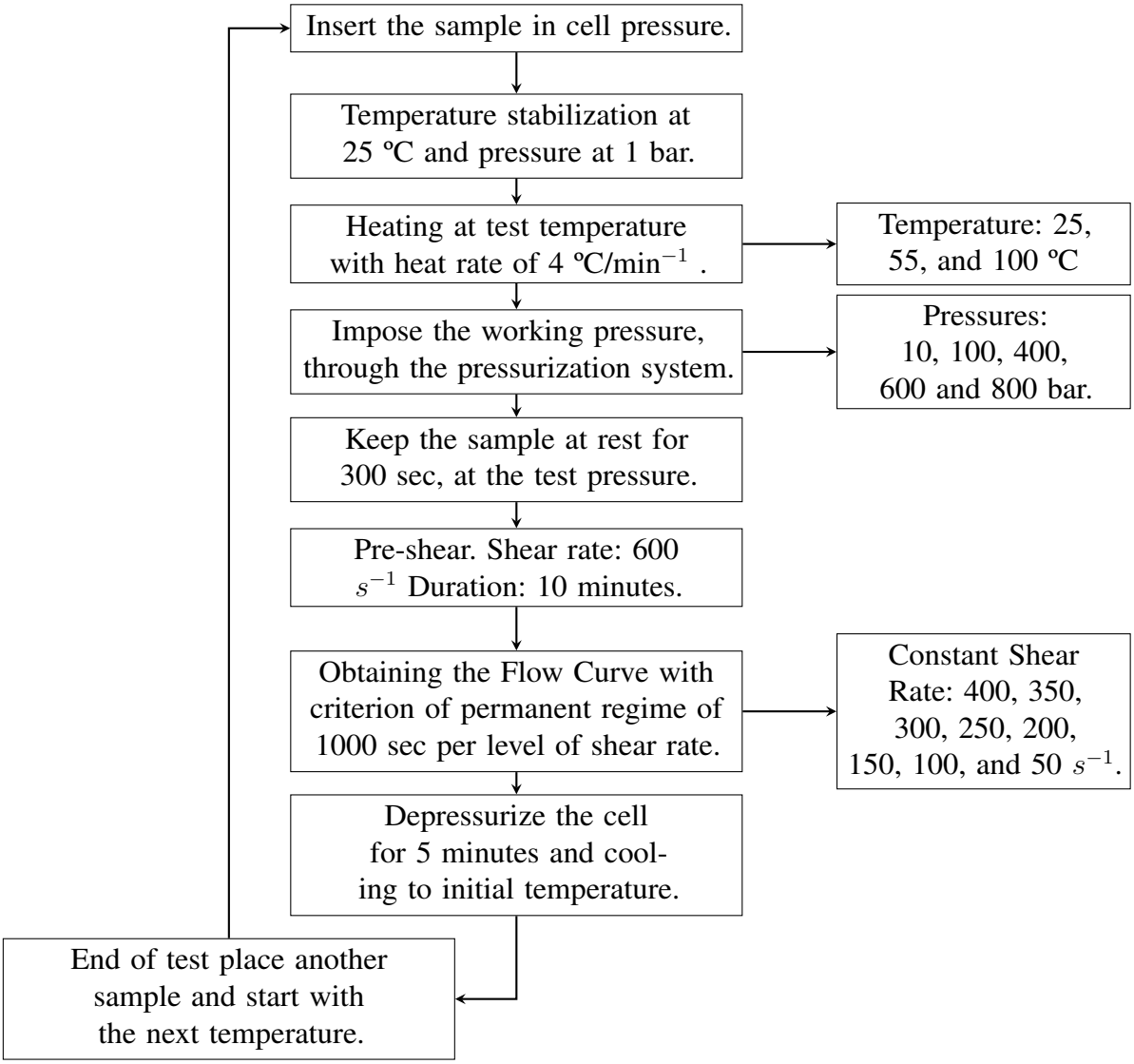

Source: Author (2021)

pressure cell with approximately 30 ml. Then, the system was pressurized at the measurement pressure for 2 minutes and after that placed at 25 ºC for 5 minutes. Temperature ramps were implemented to reach the test temperature with a rate of 4 ºC.min^{-1} for heating and 1 ºC.min^{-1} for cooling. Subsequently, a pre-shear of 600 s^{-1} for 10 minutes was performed. Finally, the flow curves were obtained at the different shear rates mentioned at the beginning of the section and under the same conditions. In the end, the cell was depressurized for 2 minutes.

Flow curves to 25 ºC at atmospheric pressure were obtained and compared to the normal rheometer measurements under the same conditions to verify the reliable range and validate the methodology described for the pressure cell tests. The torque was analyzed as a function of different shear rates. According to the manufacturer guide, the material's viscosity influences the maximum and minimum values of shear rates that can be applied in rheological tests with pressure. Figure 4.12 presents the result of the shear stress and torque values obtained as a function of the different shear rates, described in the methodology for water-based drilling fluid with xanthan gum.

Figure 4.12 – Flow curve of the water-based drilling fluid at 25 ºC and atmospheric pressure obtained on the Anton Paar rheometer in the standard configuration and with the pressure cell.

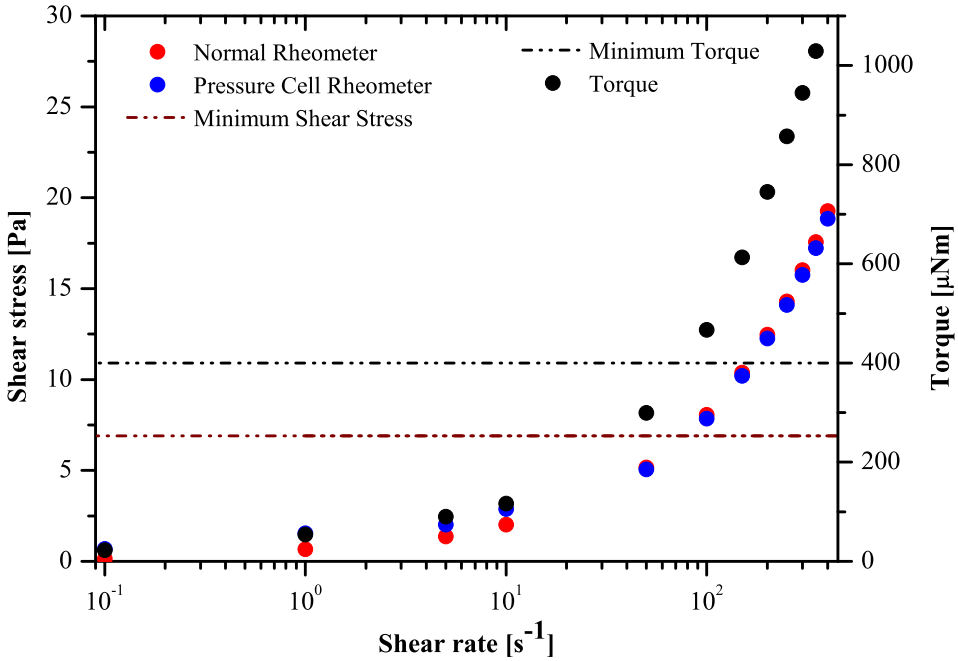

Source: Author (2021)

The manufacturer indicates that the minimum torque for reliable measurements for fluids with low viscosity is 400 μNm. One can note that in Figure 4.12, for shear rates lower than 100 s^{-1}, the measured torque is less than the minimum torque of the rheometer, compromising the reliability of measurements. On the other hand, when comparing the two rheometers' measurements, it was observed that for values obtained more than the shear rate of 50 s^{-1}, the shear stress value is less than 5% difference, and for lower shear rates, the difference increases considerably. This way, it verifies that the results obtained below shear rates of 50 s^{-1} were not reliable for the analysis.

4.3.3 Flow Start-Up Test

The flow start-up tests consist of a transient regime where constant shear rates are imposed after a particular aging time. Therefore, the start-up flow tests are of great help to determine the yield stress, which varies according to the aging time that the fluid has been subjected to. The yield stress indicates the fluid's ability to keep the drilling cuttings in suspension when the flow is relatively null within the well. The drilling fluid begins a transition from liquid-like to gel-like after the circulation stops, developing a micro-structure over time that must be broken to resume flow (CAENN; CHILLINGAR, 1996).

The procedure for executing start-up flow tests is based on API 13B-1 (2016) standards to determine drilling fluid's gel strength. The standard suggests aging times and shear rates. The aging time is defined as the time in which the fluid is left at rest for the internal structure of the fluid to reorganize. An oscillatory time sweep test was carried out at 25 ºC and atmospheric pressure, following the procedure in section 4.3.1 in order to select the best aging times.

Figure 4.13 shows the storage modulus G' and phases angle δ as a function of time, which helps observe the thixotropic recovery and phase separation of the sample (COUSSOT et al., 2002). It is observed that the G' tends to a constant value in less than 600 seconds, which may indicate that complete was restructuring the fluid. However, that the G' remaining constant does not indicate that the structure continues to be organized. Therefore, it is important to observe the phase angle to see other phenomena that cause the structure's variation when the sample is at rest.

Figure 4.13 – Oscillatory test of the sweep of time at 25 ºC and atmospheric pressure to determine the allowed aging time.

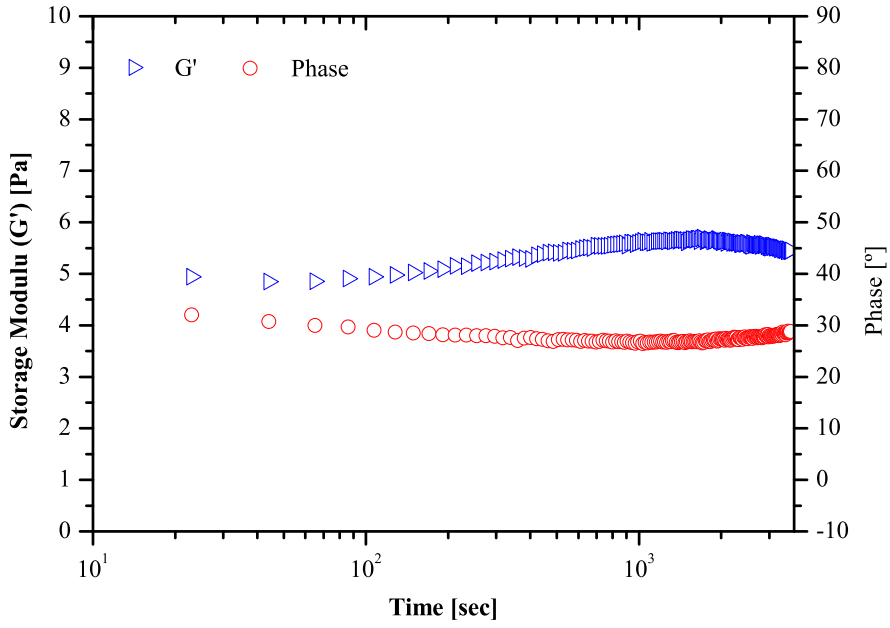

Source: Author (2021)

In this case, it was observed that the fluid remained fully structured for only approximately 600 seconds. The results indicated that the aging times for the flow start-up tests should be between 100 and 600 seconds. The flow start-up tests consisted of homogenizing the sample for 10 minutes in a low-capacity industrial mixer (Hamilton Beach HMD200). Then the sample was placed inside the geometry, which was left for 5 minutes at a constant shear rate of 600 s^{-1}. The aging time was of 600 seconds. Each tests were carried out with a new sample. The shear rates values were of 5, 10 and 50 s^{-1} with a duration of 10 minutes and their were chosen according to API standards.

4.4 THERMAL CHARACTERIZATION

Thermal analysis experiments that were performed to determine the effects of temperature over prolonged and instantaneous periods are described below. The first situation were the dynamic thermal aging tests for different temperatures during 16 hours according to the 13B-1 (2016) standard and scanning calorimetry tests according to standard ASTM D3418 (2012).

4.4.1 Thermal Aging Tests

The thermal aging tests were developed following the API 13B 2016 standard procedure for dynamic aging tests. First, the fluid was homogenized for 15 minutes; then a 400 ml sample was placed inside the pressure cell. After closing, a pressure of 6 bar was imposed. The cell was placed inside the Roller Oven Fann at the aging temperature. For this study, five tests were carried out at different temperatures (55, 70, 90, 100, and 125 ºC), which were kept constant for 16 hours on the rollers in motion. The cell was removed and left for 24 hours cooling at room temperature. Finally, flow curves were obtained at atmospheric pressure and temperatures of 25, 55, and 70 ºC following the procedure of section 4.3.2.1. The objective was to analyze the temperature's influence in long time intervals and how it modifies the drilling fluid's properties.

4.4.2 Scanning Calorimetry Tests with Micro-DCS

In order to validate possible molecular changes in the water-based drilling fluid with xanthan gum, DSC tests were developed, Differential scanning calorimetry is a thermoanalytical technique in which the difference in the amount of heat required to increase the temperature of a sample and reference is measured as a function of temperature. Both the sample and reference are maintained at nearly the same temperature throughout the experiment (PICÓ, 2012).

Endothermic samples will need more heat flux during analysis to increase the temperature at the same rate as the reference material. Otherwise, exothermic materials will require less heat flux to raise the temperature. The result of a DSC experiment is a curve of heat flux versus temperature or time. There are two different conventions: exothermic peaks upward and endothermic peaks downward (MORAES; SILVA; VIEIRA, 2020).

The transition temperature for most biopolymers is checked with DCS. Transition temperature depends on the molecular weight of the polymer and thermal history. DSC can also be used to study the thermal degradation of polymers using an approach such as Temperature/Time (PERCEC; PUGH, 1989).

The transition temperature of xanthan gum in the studied water-based drilling fluid was determined through tests with DCS. First, a validation of the measurement procedure used was carried out. The microcalorimetry tests consisted in homogenizing the sample for 15 minutes in a Hamilton Beach HMD200 mixer. Then, with a single-channel micropipette, 0.5 mg of the xanthan gum solution was placed into the cell used for the samples, leaving the reference cell empty. The test was configured to perform various intervals that consist of isotherms and temperature ramps. The methodology used for the measurements was Pelletier et al. (2001), which was validated in Appendix C, obtaining satisfactory repeatability of the test data. The same methodology was used for the drilling fluid sample, considering that the analysis range from 4 to 110 ºC with heating rate of 1 ºC.min^{-1} was used to analyze the temperature range and exothermic peak, where occurs the structural transition of the xanthan gum. And finally, all measurements were done in triplicate. In previous studies, the transition temperature can increase with the concentration of NaCl and xanthan gum.

4.5 CHAPTER SUMMARY

The chapter presented the drilling fluid used for rheological tests and the different equipment that allowed rheological characterization under HPHT conditions. The rheological experiments were defined describing the experimental methodology and the results obtained were verified.

In the next chapter, the results and analysis of the influence of temperature, pressure, and xanthan gum concentration on the drilling fluid's rheological characteristics are presented.

5 RESULTS AND DISCUSSION

This chapter presents the results of the different rheological tests with water-based drilling fluid with xanthan gum and limestone under high-pressure and high-temperature conditions.

The chapter is divided into three main sections. The first Section shows the results analyzing the effect of high-temperature on the drilling fluid through rheological tests, thermal aging tests, and microcalorimetry. The second Section presents the results of rheological tests on the effect of high-pressure at different temperatures and also shows the fit of the experimental data under HPHT conditions to the FMT model. Finally, the results of rheological tests with different concentrations of xanthan gum are presented.

5.1 EFFECTS OF TEMPERATURE

5.1.1 Flow Curve at Different Temperatures

The shear stress as a function of temperatures was measured according to the procedure described in Section 4.3.2.1. The temperature effect analysis is initiated with flow curves of the water-based drilling fluid with xanthan gum and limestone at temperatures of 4, 10, 25, 40, 55, 70, 90, 100, and 125 ºC at constant pressure.

The different shear rates were imposed for 1000 seconds, each reaching the stable-state of the shear stress. The criteria used is based on the moving average with 50 seconds intervals, with variations less or equal to 1% as shown in Equation 5.1.

$$\left[\frac{X_{i+50sec} - X_i}{X_{i+50sec}}\right] \cdot 100 \leq 1\%/range \cdot 1000 \tag{5.1}$$

where $X_{i+50sec}$ is the measured value of the shear stress filtered after 50 seconds, and X_i is the shear stress filtered at any time.

The tests were performed in duplicate. The experimental data of the flow curves at different temperatures are shown in Appendix D. As same as the average, standard deviation, and variance analysis. The statistical analysis results indicated no significant differences between the different values of shear stresses obtained in the different flow curves at the same temperature.

Experimental results are shown in Figure 5.1, where a shear-thinning behavior was evidenced for all temperatures. The Shear stress values decreased with increasing temperature, indicating that the viscosity values are reduced with temperature. The shear stress data lowered by approximately 10% between 4 to 25 ºC at almost all measured shear rates. The difference between the results obtained at 25 and 70 ºC was 51%. For temperatures of 90, 100, and 125 ºC, shear stress dropped drastically, approximately 82%, 90%, and 95% lower when compared to the value measured at 25 ºC. Experimental data were fitted to the power-law model. The fit obtained correlation coefficients R^2 of 0.99 in all temperatures. Other models, such as Herschel-Bulkley and Casson presented correlation coefficients R^2 smaller than 0.80. The results showed the effects of temperature on the water-based drilling fluid with xanthan gum. The results

agree with the ones found in the literature review. Echt e Plank (2019) indicated that temperature increases begin to precipitate the macromolecules of the drilling fluid, presenting modifications in the ionic bonds formed in the polymeric chains of the xanthan gum, which decreases the inter-molecular forces present in the colloidal suspension. Some authors such as Xie e Lecourtier (1992), Pelletier et al. (2001), Reinoso et al. (2019), Mao et al. (2019), observed that temperature raises generate possible energetic increases in chemical components as well as possible physical modifications of the structures of macromolecules of the xanthan gum, resulting in the reduction of the capacity of the fluid's rheological properties.

Figure 5.1 – Equilibrium flow curve fitted by the power-law model in the temperature range from 4 to 125 °C for water-based drilling fluid. The power-law model describes the apparent viscosity η as a proportional function to shear rate, where m is the consistency coefficient, $\dot{\gamma}$ the shear rate, and n the flow behavior index.

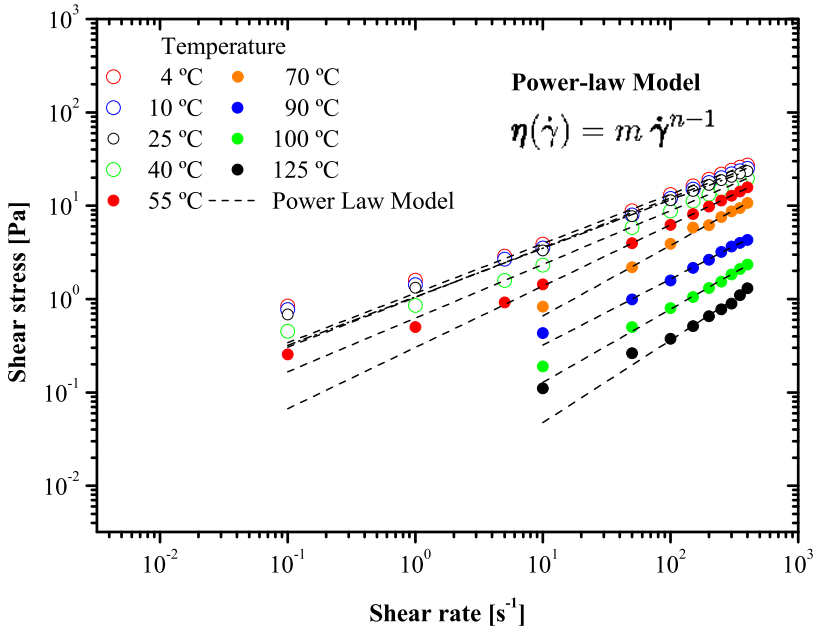

Source: Author (2021)

The comparison of fit parameters of the Herschel-Bulkley and power-law models are shown in Figure 5.2. The dynamic yield stress τ_0, consistency coefficient m, and flow behavior index n are plotted for different temperatures at constant pressure. It was observed that the consistency coefficients and flow index for both models between the temperatures of 10 to 70 ºC presented similarities in behavior due to the low yield stress of the fluid.

The power-law model was selected as the most suitable to fit the experimental data. The water-based drilling fluid's rheological behavior can be depicted through the fit parameters. The consistency coefficient represents changes in the viscosity of the fluid. Reinoso et al. (2019) used the consistency coefficient for representing the effect of decreasing shear stress with temperature. The results show that the values m decreased from 1.15 to 0.11 from 4 ºC to 70 ºC, reducing 90%. And the values above 70 ºC decreased sharply. The temperature effect is noticed due to the increase in the molecules' thermodynamic state, the collision rate and the thermal motion that gradually raises (MAO et al., 2019). That results in a

weakening in the hydrogen bonds of the water (MAO et al., 2019), and polymeric chains of the xanthan gum take a partial transition from ordered random broken helix conformation to disordered random coil conformation (XIE; LECOURTIER, 1992; PELLETIER et al., 2001).

Figure 5.2 – Parameters fitting power-law and Herschel-Bulkley model at different temperatures. The red lines show the Herschel-Bulkley model's parameters, including the black line that indicates dynamic yield stress, and the blue lines the Power-law model's parameters.

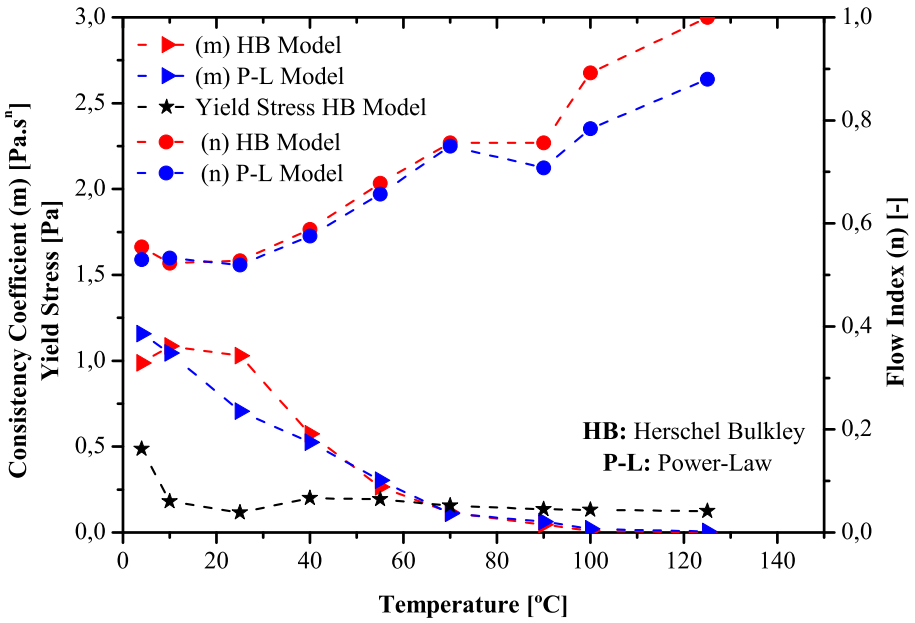

Source: Author (2021)

On the other hand, the flow behavior index presented a 70% growth with its values ranging from 0.53 to 0.75 between temperatures of 4 to 70 ºC, respectively, evidencing the reduction in the shear-thinning behavior. A characteristic phenomenon is observed at a temperature of 90 ºC, where the value of n falls from 0.75 to 0.70. Showing a decrease first and then a lower increase compared to the other temperatures. Indicating that above 70 ºC changes in the internal structures of the fluid are occurring.

The shear-thinning behavior of the solutions is attributed to the disruption of internal structures entanglements formed by the molecules when they are subjected to shear (OSAKI, 1987). The flow behavior index represents this characteristic. Nevertheless, changes in temperature and pressure also affect the fluid's internal structure, causing energetic increases between the molecules or leaving the structure more ductile. In the case of polymer solutions, increasing temperature causes the polymer to go through different structural transitions depending on the polymer's nature. For the xanthan gum case, polymeric chains undergo changes in conformation with increased temperature, depending on the concentration (dilute or semi-dilute) and the way of preparation. The xanthan gum conformation change was observed when the chains' backbone went from an ordered to a disordered state, causing values of n to rise. The temperature where the changes from order to the xanthan gum disorder begins is known as the transition temperature. According to Reinoso et al. (2019), the thermal transition region of xanthan gum solutions is

between 50 to 120 ºC.

In the first instance, it is concluded that the effect of temperature on the water-based drilling fluid reduces the values of shear stress. This effect has a strong influence on temperatures from 70 ºC. Due to changes in the structure of the macromolecules of xanthan gum or also changes in the dielectric parameters of the base fluid (water), as evidenced by several authors in other studies with water-based drilling fluids (AKPAN et al., 2019; REINOSO et al., 2019; MAO et al., 2019). Rising polymeric solutions' temperature increases the kinetic energy and promotes faster molecular movements, which disturb the network formed by the polymeric chains. It has been reported that the visco-elastic module of polymer solution formed by physical interactions decreases sharply around the melting point of junction zones formed by the polymeric chains, resulting in a more disordered structure (ZHANG; WANG; QIU, 2005).

5.1.2 Stress Amplitude Sweep Test at Different Temperatures

The effect of temperature can cause limitations during the drilling processes. Therefore, the analysis of the LVR is essential to know the fluid's behavior during these situations. Oscillatory stress amplitude sweeps tests were made at different temperatures to measure the linear visco-elastic region according to the procedure described in Section 4.3.1. The critical yield stress and critical strain values were obtained for certain oscillatory conditions. These tests were developed to obtain the static yield stress, once the flow curves one previously obtained, gives the dynamic yield stress values, which are values far from the static yield stress's real value. The results of the stress amplitude sweep oscillatory tests obtained are shown in Figure 5.3. The critical yield stress, the storage modulus G' within the LVR and critical strain were determined by the crossing of G' and G'' show a reduction with increasing temperature. The storage modulus decreased from 4.78 to 2.1 Pa between temperatures of 4 to 70 ºC. The evaporation limitations of the sample restrained precise measurements for temperatures higher than 70 ºC. Similarly, the critical strain falls from 0.27 to 0.09, and the critical static yield stress from 1.15 to 0.25 Pa between 4 and 70 ºC.

Xanthan gum is developed as one of the best thickening polymers due to its high intrinsic stiffness related to the helical conformation stabilized in the presence of excess salt (BRUNCHI et al., 2019). The rapid fall of the observed G' values was interpreted as evidence of a significant change in the solution's structural order due to the order-disorder transition of the xanthan gum molecules. For changed xanthan gum, the helix-coil transition is characterized when the temperature rise destabilizes the hydrogen bonds, which oppose the electrostatic repulsion at a given temperature T_m. The electrostatic repulsions cause an extension of the molecule and interchain interactions with temperature growth, depending on the polymer concentration and external salt concentration and composition. Some studies that carried out oscillatory tests with temperature rises showed a different behavior depending on the concentration of xanthan gum. For solutions with concentrations above the critical concentration the values of G' increase with rising temperature. A polymer concentration under the critical value in which xanthan gum solutions still exhibit typical semi-dilute solution behavior, rising the temperature decreases the G' values. The addition of electrolytes reduces the value of the visco-elastic module value (TAM; TIU, 1989; PELLETIER et al., 2001). The previous behavior is typical of poly-electrolytes and can be attributed to the resulting charge screening causing a decrease in hydrodynamic volume, which leads to a reduction the values of various rheological parameters. Above this critical concentration, the addition of electrolyte can induce an increase in rheological parameters' values due to inter-molecular associations, facilitated by the

Figure 5.3 – Stronger modulus G' on the LVR, critical yield stress and strain for different temperatures, oscillatory amplitude stress sweep tests from 0.01 to 100 Pa ensuring that it measures within the LVR; and frequency of 1 [Hz], at temperatures of 4, 10, 25, 40, 55, and 70 ºC.

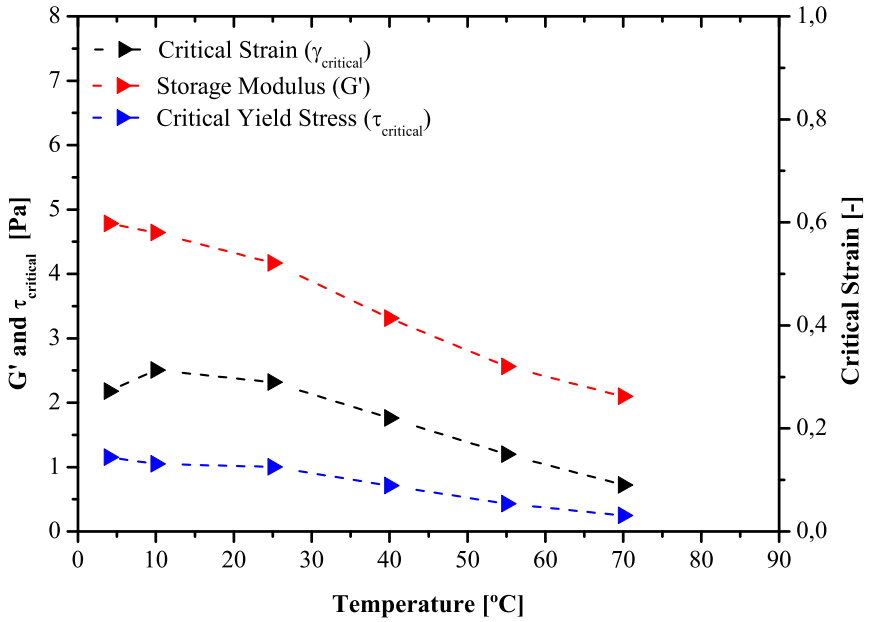

Source: Author (2021)

reduced electrostatic repulsion and order of the chains, leading to the development of a three-dimensional network demonstrated by Bercea e Morariu (2020). It is concluded that the tested water-based drilling fluid is a semi-dilute solution of xanthan gum, causing a diminution in rheological parameters with increasing temperature, which causes a weakening of the networks of the xanthan gum. Indicating that the ability to maintain cuttings in a Section with high-temperatures can cause operational problems.

5.1.3 Thermal Aging Tests

As described in Chapter 4, Section 4.4.1, the thermal aging tests were developed following the API's recommendations (13B-1, 2016) standards to verify the thermal stability and the effect of the thermal history in the water-based drilling fluid. The conditions of high temperatures encountered by the drilling fluid at the bottom of the hole are simulated through the aging of drilling fluid at 55, 70, 90, 100, and 125 ºC for 16 hours at a pressure of 6 bar. Flow curves were obtained to validate the possible degradation. First, the results of the different aged fluids with different test temperatures of 25, 55, and 70 ºC are shown. The data were fitted to the power-law model and finally, a comparison was made with non-aged fluid.

Figure 5.4 presents the resultant shear stress as a function of the shear rate of the four fluids that were aged under the same conditions at different temperatures and the non-aged fluid. Next, flow curves were obtained at 25 ºC, where it was observed that the fluids aged at temperatures of 55 and 70 ºC the imposed thermal history did not generate degradation or modification of the fluid, which produced

decreases in shear stress as shown in Figure 5.4 (a). For the aging temperatures of 100 ºC, a minor degradation was evidenced with a variation of 5% compared with non-aged fluids. Moreover, for the aged fluid at 125 ºC, it was found that thermal history at this temperature generated intense modifications possibly on its physicochemical properties and structure, presenting a 58% drop in its shear stress compared to the fluid aged at 55 ºC. On the other hand, the flow curves obtained at 55 and 70 ºC shown in Figures 5.4 (b) and (c) with the same aged fluids presented a reduction in their shear stress compared to the values of the flow curve at 25 ºC. For the fluids aged at 55 and 70 ºC the variations were insignificant at the flow curves at 25 and 55 ºC. The decrease in their shear stress was 30% when comparing the flow curves at 55 ºC to the ones at 25 ºC and 42% comparing the flow curves at 70 ºC to the ones at 25 ºC. On the other hand, the shear stress lowering of the fluid aged at 125 ºC was 35% when comparing the flow curves at 55 ºC to the ones at 25 ºC. Moreover, the shear stress values decreased 52% compared the flow curves at 70 ºC to the ones at 25 ºC.

Figure 5.4 – Comparison between flow curves of non-aged fluid and fluids dynamically aged for 16 hours based on the ANSI/API Recommended Practice 13B-1 procedure. For temperatures of 55, 70, 100, and 125 ºC with the fit of the power-law model, the tests were performed at (a) 25 ºC; (b) 55ºC; and (c) 100 ºC, both at atmospheric pressure.

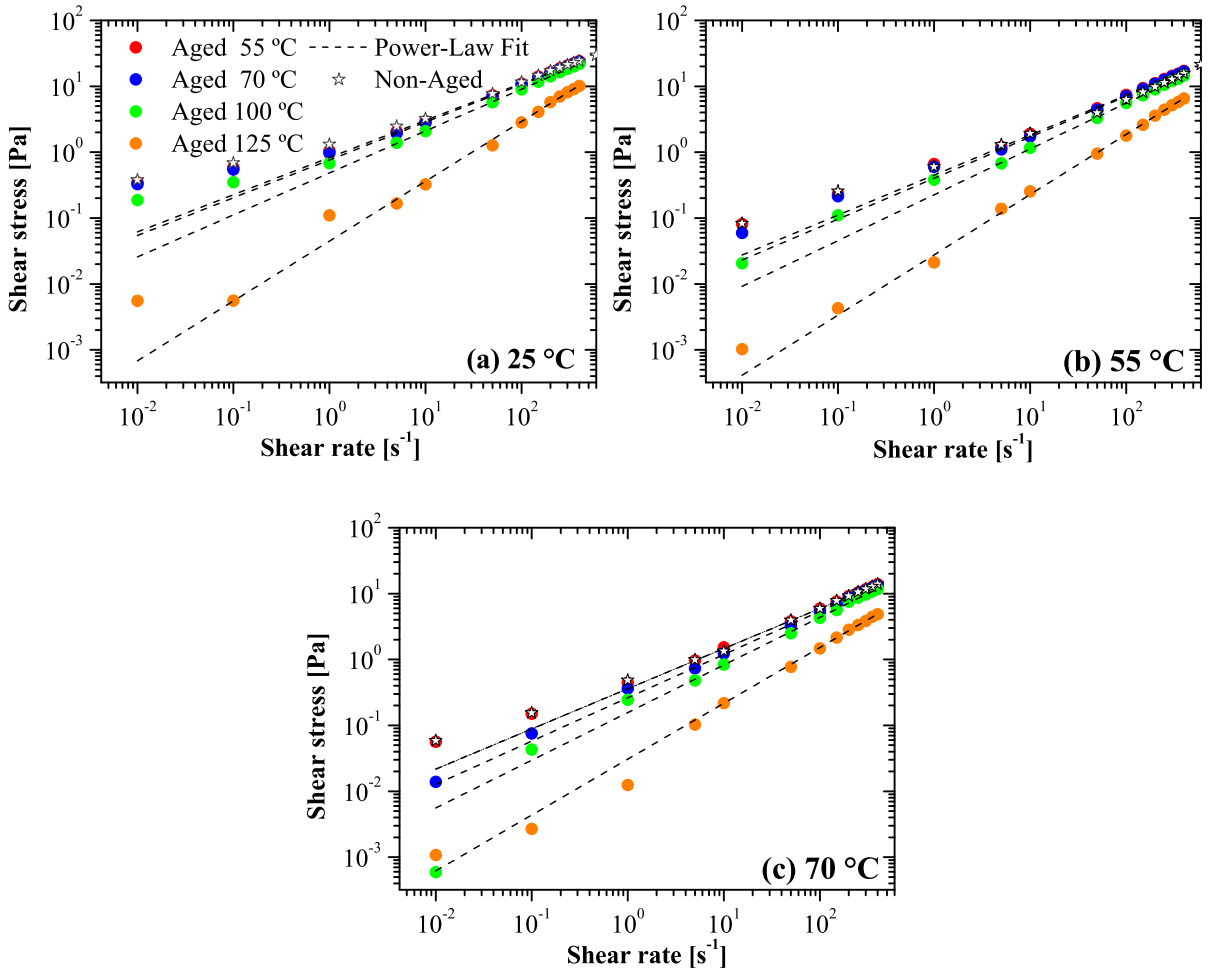

Source: Author (2021)

When comparing different aged fluids, one can notice that there is a temperature range where the effect of the thermal history generates intense irreversible degradation on the fluid. This was evidenced between temperatures of 100 and 125 ºC, where the polymeric chains of the xanthan gum did not return to the initial structural state when subjected to these temperatures for 16 hours. Besides, there may also be degradation of other additives that form the drilling fluid. Therefore, it is necessary to perform an analysis on the XRD and MEV to identify and verify if the chemical compound within the fluid is undergoing modifications due to the imposed thermal history. It is essential to keep in mind that the performance of these tests depends on external laboratories, which do not belongs to the structure of the laboratory of rheology (LabReo) directed by the research group (CERNN).

The previous results are of great interest for drilling fluid engineers. It is possible to verify for how long and for which temperature ranges the fluid is still stable. That aids the planning of the treatment or conditioning phase of the drilling fluid by adding other rheological modifiers that fit its properties or even know how to identify when the drilling fluid suffers degradation and make its final disposal following the current environmental regulations.

The data of the measurements carried out was fitted to the power-law model and its parameters are shown in Figure 5.5. A comparison of the model's fit parameters was performed based on the aging temperature, where the consistency coefficients and flow index are shown for the three temperatures in which the aged fluids were measured.

Figure 5.5 – Fit parameters Power-law model at 25, 55, and 70 ºC, for the aging temperatures of 55, 70, 100, and 125 ºC.

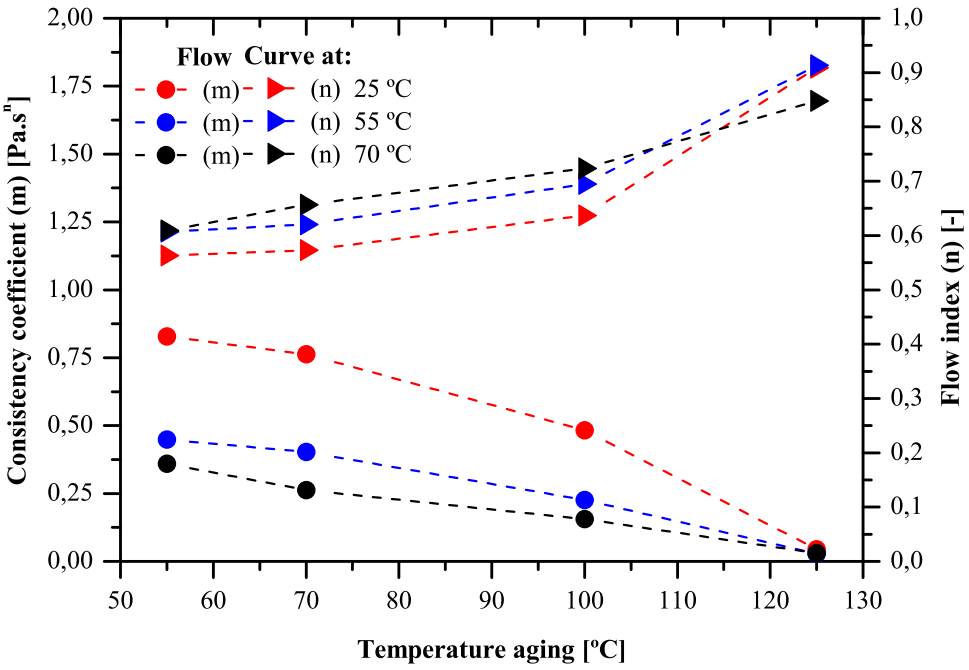

Source: Author (2021)

It was observed that the consistency coefficient decreases logarithmically with the rise in the aging temperature, as some works have reported (AMANI; AL-JUBOURI, 2012; HERMOSO; MARTÍNEZ-BOZA; GALLEGOS, 2014; MAO et al., 2019). The temperature at which the consistency coefficient is measured as previously observed varies from 0.82 to 0.04 $Pa.s^n$ for flow curves at 25 ºC, 0.44 to 0.02 $Pa.s^n$ for 55 ºC and 0.35 to 0.03 $Pa.s^n$ for 70 ºC. On the other hand, the flow index increased, indicating that the shear-thinning behavior declines as the temperature climbs. The growth of the flow behavior index values of flow curves at 25 ºC was from 0.56 to 0.90. At a temperature of 55 ºC increases was from 0.60 to 0.91 and at 70 ºC it was from 0.60 to 0.92.

Analyzing the effect of high temperature on the water-based drilling fluid, a temperature range was identified where the xanthan gum possibly undergoes a structural modification from an ordered to a disordered state. When the structure is cooled down it returns from its disordered to an ordered state. When fluid is subjected to a thermal history for 16 hours, the fluid undergoes a modification in its structure from an ordered to a disordered state. However, in this case, when a critical aging temperature is exceeded, the fluid does not return to its previous state. Figure 5.6 shows two fluids aged at temperatures of 90 and 125 ºC where the non-return process occurs within this range. It can be concluded that the transition temperature of degradation of the polymer was exceeded, generating irreversible modifications in its structure. This also suggests that physical, electrochemical, and chemical modifications occurred during the aging process, as mentioned by Alderman et al. (1988).

Figure 5.6 – Comparison between equilibrium flow curves of non-aged fluid and fluids dynamically aged for 16 hours based on the ANSI/API Recommended Practice 13B-1 procedure. For temperatures of 90 and 125 ºC with the power-law model's fit, the tests were performed (a) at 25 ºC; (b) at 55 °C, both at atmospheric pressure. The schematic represents the ordered and disordered states of crosslinked chains adapted from Bueno e Petri (2014).

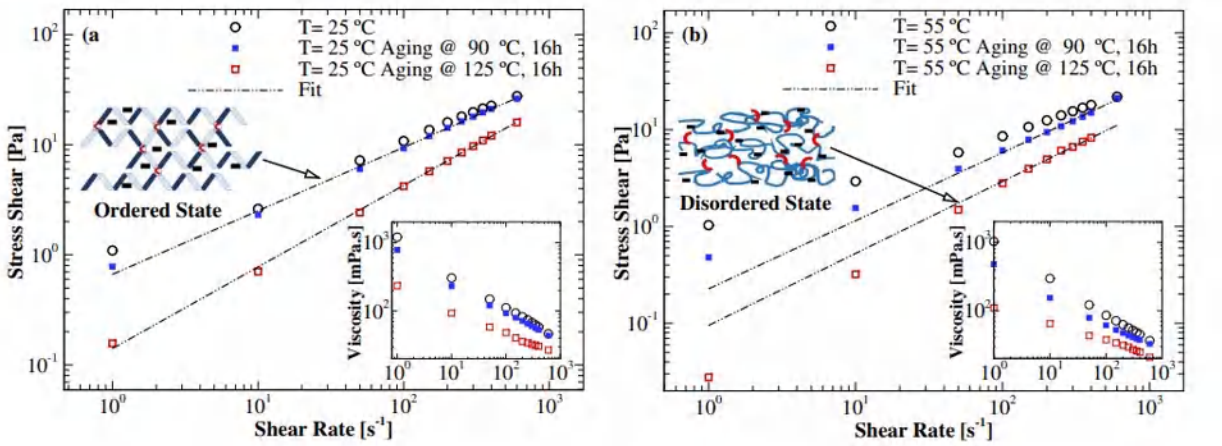

Source: Author (2021)

Figure 5.7 shows the crystallization of sodium chloride for the three fluids used in the thermal aging comparison. Fluids aged at 90 and 125 ºC are shown in Figure 5.7 (b) - (c), respectively. The samples were left for 3 days at 20 ºC and 50% of relative humidity when the liquid part's evaporation was evidenced. The crystallization of the electrolytes shows a higher supersaturation as the solvent evaporates due to the increase in the thermal history imposed, producing more crystals and reducing their size (QUILAQUEO;

AGUILERA, 2016). This indicates that the solubility of the salt in the suspension increased. Mao et al. (2019) highlighted that the electrolytes' solubility has significant effects on rheological properties, which is mentioned by Reinoso et al. (2019) in xanthan gum solutions with brine. Furthermore, Figure 5.7 shows that the pH values of the fluids rise with aging temperature. Therefore a lower ionization causes degradation of the rheological properties, as other physicochemical modifications of the fluid as evidenced by Akpan et al. (2019).

Figure 5.7 – Comparison of pH values for each of the fluids performed at 20 ± 0.5 ºC with a standard deviation of 0.02, and experiment visual of dry samples of aged drilling fluid, (a) non-aged; (b) the thermally aged at 90 ºC; (c) thermally aged at 125 ºC.

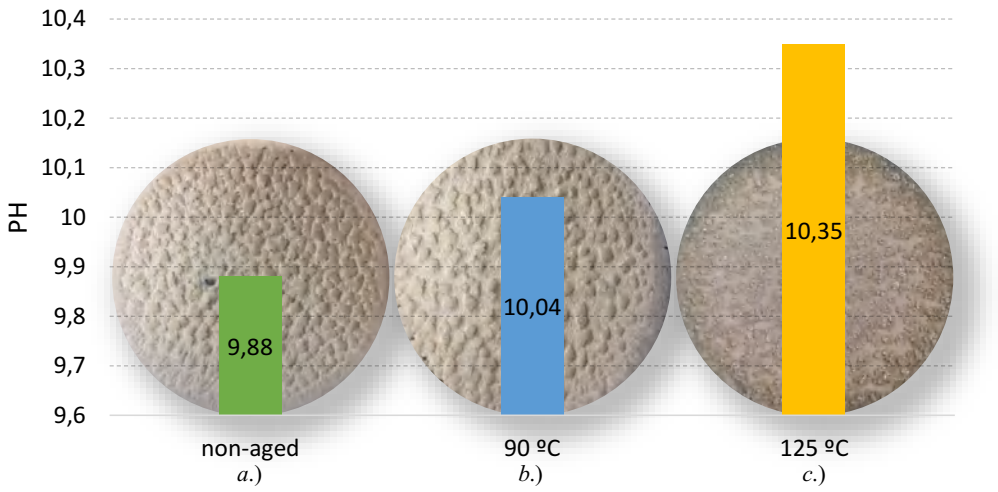

Source: Author (2021)

The imposition of thermal history leads to the degradation of the fluid. The degradation is observed through the rheological properties and visually through the particles' flocculation and sedimentation over time under static conditions. Figure 5.8 presents the separation between the liquid and solid phases over time for aging drilling fluids. For the image sequence of Figure 5.8 (a) - (b) is observed that phase separation speed is greater with increasing aging temperature.

The observations of the current work indicate that possible molecule interactions with temperature decrease the relative dielectric constant of water (SPRIK, 1991; FERNANDEZ et al., 1995; SURESH; NAIK, 2000) by decreasing the polarity of water and promoting thermally induced phase separation (TIPS) precipitating the macromolecules dissolved in the drilling fluid (MAO et al., 2019). Therefore, functions such as transport and suspension of cuttings are diminished with the aging of the water-based drilling fluid.

Figure 5.8 – The visual appearance of suspensions stabilized for samples of the aged water-based drilling fluid at (a) at 90 ºC for 77 minutes and (b) at 125 ºC for 30 minutes. In each figure, 6 steps are shown in sequence, guided by the blue arrow. Every step shows the drilling fluid when it is left at rest.

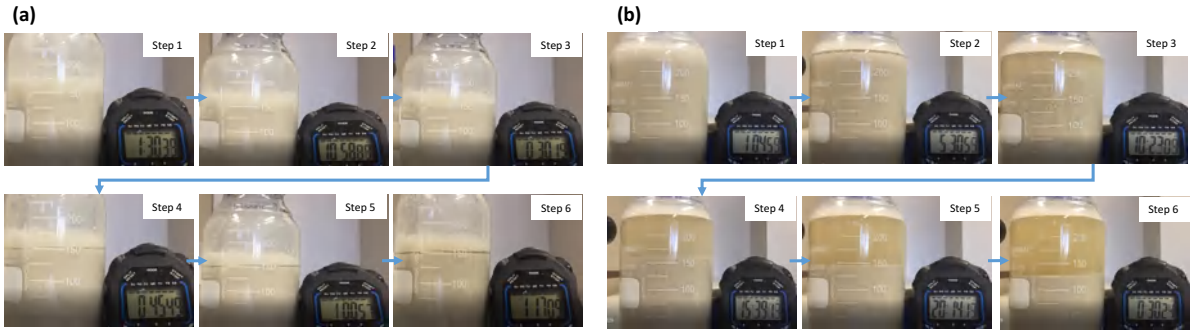

Source: Author (2021)

5.1.4 DSC Tests for Determination of Transition Temperature

Differential scanning microcalorimetry tests were performed according to the procedure described in Section 4.4.2 of chapter 4. The experimental results show that water-based drilling fluid with xanthan gum presents two exothermic peaks. According to Williams et al. (1991), those peaks correspond to an order-disorder conformational transition of the xanthan gum. Figure 5.9 shows a DSC heating curve of xanthan gum drilling fluid with 0.25% xanthan gum and 55 bl/bbl NaCl. The curve shows first a broad endothermic peak starting at 67.08 ºC and ending at 70.62 ºC. The midpoint transition temperature T_m, is 69.24 °C. The curve shows a second broad peak starting at 80.07 ºC and ending at 85.31 ºC. The midpoint transition temperature T_m, is 82.09 °C.

Therefore, it is observed that the transition from an ordered to a disordered state of xanthan gum beginning at 70 ºC and ending at 90 ºC results in a decrease in shear-thinning behavior as evidenced in the flow curves in Section 5.1.1, confirming the phenomenon. It is possible to rule out that other components suffer alteration at this temperature range, since the xanthan gum polymer chains' initial structure returns to their previous state after cooling. Moreover, it was observed that prolonged heating time above the degradation transition temperature observed in tests with aged drilling fluid caused viscosity losses and imbalance of the suspension, showing a degradation of the xanthan gum's polymeric chains.

The experiments' results coincide with the general effect of the thermal treatment on the xanthan gum solutions. Therefore, it can be summarized that the xanthan gum of the drilling fluid undergoes a dissociation of the double helix into single strands, as shown in Figure 5.10. The previous hypothesis can be verified using X-ray diffraction that can demonstrate the type of conformation and other dimensional parameters of the polymer chains as developed by Moorhouse, Walkinshaw e Arnott (1977), Milas et al. (1990), Gulrez et al. (2012). It is also possible to observe how the other additives are distributed in the drilling fluid.

In this study, similar results were observed when using xanthan gum solutions and NaCl brine. The ordered molecule of xanthan gum can undergo a conformational transition to a disordered flexible coil

Figure 5.9 – Order-disorder transition of water-based drilling fluid with xanthan gum (0.25% w/w) monitored by differential scanning calorimetry (scan rate 1 °C.min^{-1}).

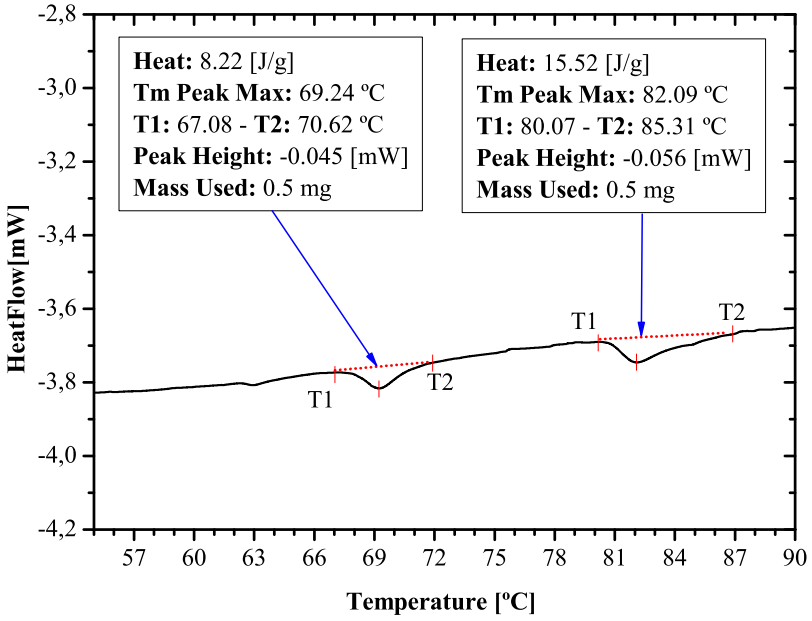

Source: Author (2021)

Figure 5.10 – Schematic illustration of structural and conformational changes in a commercial xanthan gum sample due to the effect of high-temperature.

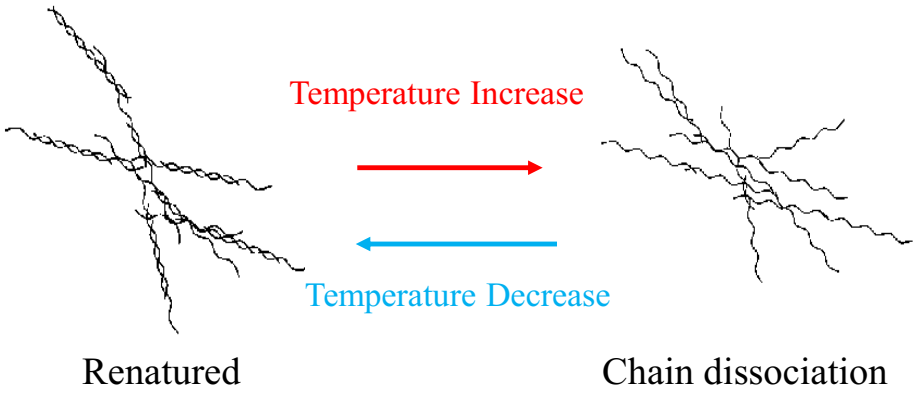

Source: Author (2021) and Adapted from Gulrez et al. (2012)

either by increasing the temperature above characteristic temperature (T_m) or by decreasing the salinity of the solution (CALLET; MILAS; RINAUDO, 1989; KAWAKAMI; NORISUYE, 1991). Transition temperature largely depends on the concentration of the polymer and external salt (RINAUDO, 2001). The disordered structure (denatured) is unanimously believed to be a random coil and can be obtained by raising the temperature above T_m. While prolonged heating at high-temperature results in degradation (NISHINARI et al., 1996).

Together with the results obtained in this study and those reported previously for xanthan gum solutions when subjected to high temperature, it is now possible to understand xanthan conformation as shown in the scheme presented in Figure 5.11. The diagram shows the representation of the conformation changes of xanthan gum that occur during thermal processes. Initially, the xanthan gum in the drilling fluid behaves as a semi-dilute solution, and its polymeric chains are in the form of a flexible double-helical in a renatured state (order). When the native (order) polymeric chain was subjected to a temperature rise by few minutes, it is rapidly cooled, presenting growth in hydrodynamic volume. When the drilling fluid is subjected to temperature increase during rheological measurements, a conformation change occurs into a denatured state (disorder) characterized by viscosity reduction on its hydrodynamic volume. This state can be reversible for temperatures lower than the transition temperature T_m. Another effect is also known and discussed in Section 5.1.3. When the xanthan gum in the drilling fluid is subjected to thermal aging for several hours, a degradation of the polymeric chains takes place, which means a further viscosity loss.

Figure 5.11 – Schematic representation summarizing the order-disorder conformation of xanthan in aqueous solution when a high-temperature and thermal aging are applied.

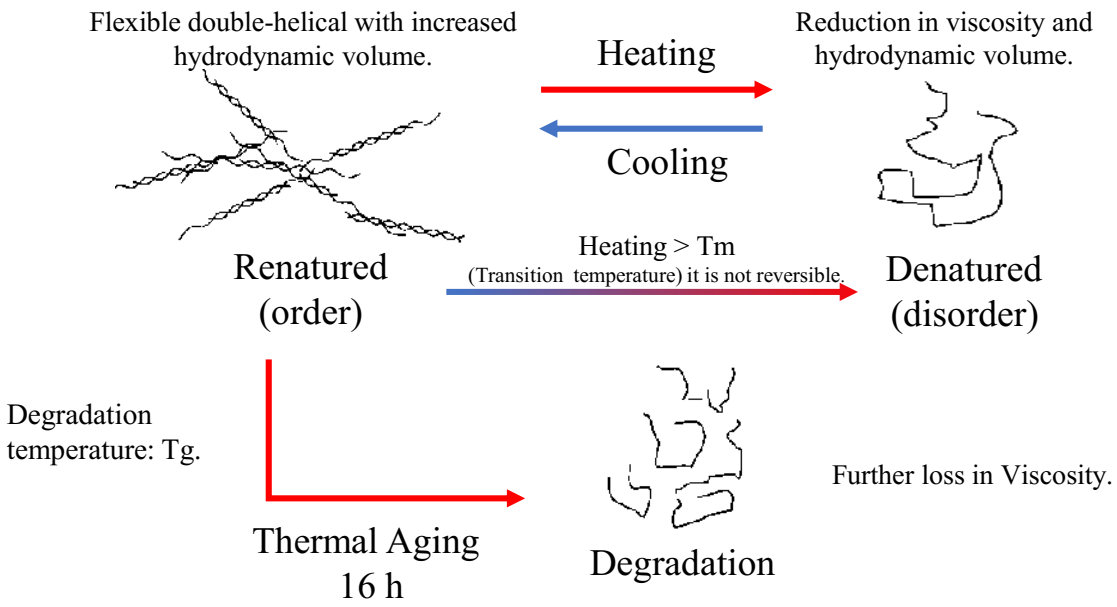

Source: Author (2021) and Adapted from Gulrez et al. (2012)

In terms of the fluid's rheological behavior, Figure 5.12 shows the conformation transition of the xanthan gum present in the drilling fluid, which causes a drop in the shear-thinning behavior of the drilling fluid, approaching it to a Newtonian behavior. The power-law model's flow behavior index indicates that for temperatures higher than 70 ºC, the fluid suffers a diminution in viscosity and Herschel-Bulkley model showed a reduction in the yield stress. It was also observed that thermal aging for 16 hours above 100 ºC induces degradation and destabilization of the drilling fluid.

Figure 5.12 – Schematic of changes of behavior rheological the drilling fluid with increased temperature.

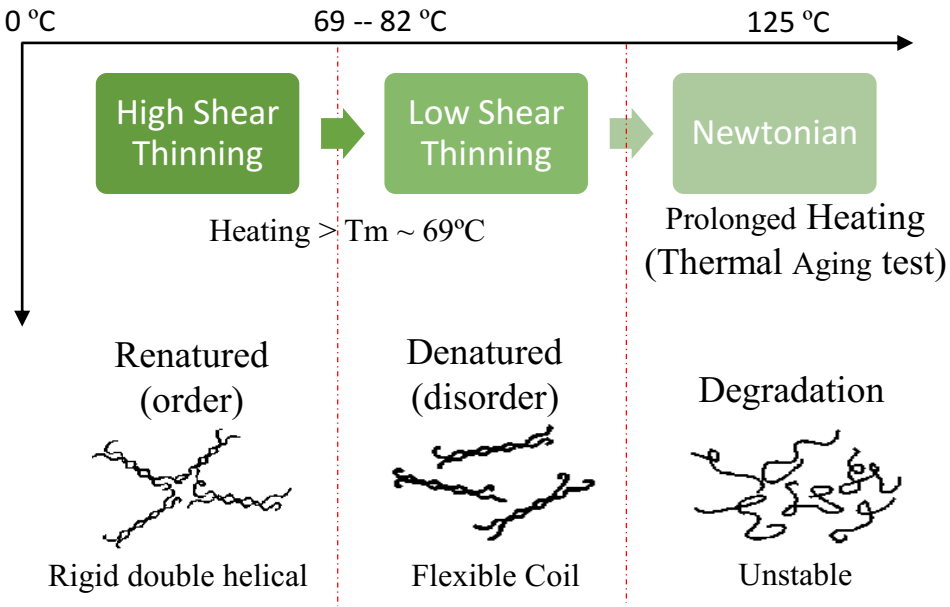

Source: Author (2021) and Adapted from Gulrez et al. (2012)

5.1.5 Synthesis of the Results of the Effect of Temperature

In Section 5.1 the experimental results obtained from the different tests with the objective of knowing the effect of temperature for a constant pressure condition were presented. The water-based drilling fluid results with xanthan gum and limestone for temperatures increases without being subjected to any heat treatment presents a limit due to structural modifications of the viscosifier used. The limit depends on several factors: the amount of salt in suspension and the concentration of the viscosifier. Therefore, the analyzed fluid has an operating range for its first use of up to 70 °C, providing the same rheological characteristics when the pressure does not present strong variations during the drilling operation.

On the other hand, with the imposition of thermals history or long operation hours, the fluid undergoes degradation for hole well temperatures higher than ± 120 °C. This happens due to the loss of the fluids' ability to restructure when being cooled again. In addition to that, it is possible that some of its components, apart from xanthan gum, also suffered degradation when exceeding 100 °C. This caused a destabilization of the suspension formed, causing other problems during operation such as blockage and settling of solids (gelation times) in less time. It was also observed that the transition temperature does not present a significant variation when the fluids are subjected to thermal aging for temperatures below 90 °C. While increasing ionic strength promotes a more ordered structure, increasing temperature causes the opposite effect. The most disordered xanthan gum structure obtained by the thermal conformational change was the one that had a weaker peak and a stronger trough, accompanied by a shift to smaller wavelengths (EREN; SANTOS; CAMPANELLA, 2015).

5.2 EFFECTS PRESSURE AND TEMPERATURE

5.2.1 Effect of High Pressure at Constant Temperature

Water-based drilling fluids have an advantage over oil-based drilling fluids emulsions at high pressures, once the later has greater compressibility. Due to its ideal characteristic of low compressibility in its liquid state, water provides stability against pressure changes. Water-based fluids retain this characteristic, but when in suspension with other chemical substances and solid particulate materials, pressure can cause changes in the structure.

In the present study, measurements at high pressure using drilling fluid with xanthan gum showed degradation of the polymeric chains due to the effects of high-pressure homogenization, which is an operational phenomenon of the instrument that consists of making xanthan gum solutions flow through contractions of tiny cavities. Figure 5.13 (a) observed that the renatured xanthan is degraded into smaller molecules but retains its double helical. An illustration of the effect that occurred during the drilling fluid preparation for rheological measurements and after measurements is provided in Figure 5.13 (b). It is observed that the fluid is in the 3 cm diameter storage tank when imposing the pressure makes the fluid flow through a contraction to reach a tube with a diameter of 3 mm. After that it is expanded inside the pressure cell that has a diameter of 3 cm and collides with geometry. After the pressure test, the pressure is reduced by opening the valve. The fluid suffers the same effect in the opposite direction, which causes the fluid to degrade, as reported by Gulrez et al. (2012), who conducted behavioral studies of xanthan gum's structural conformation solutions in different industrial processes.

Figure 5.13 – Effect of high pressure on semi-diluted xanthan gum in the water-based drilling fluid, (a) schematic illustration of structural and conformational changes; (b) Representation of the physical process inside the pressure cell, where the yellow circles represent the xanthan gum molecules passing through the storage tank, the pipeline, and reaching the gap between the geometry and the pressurization cell.

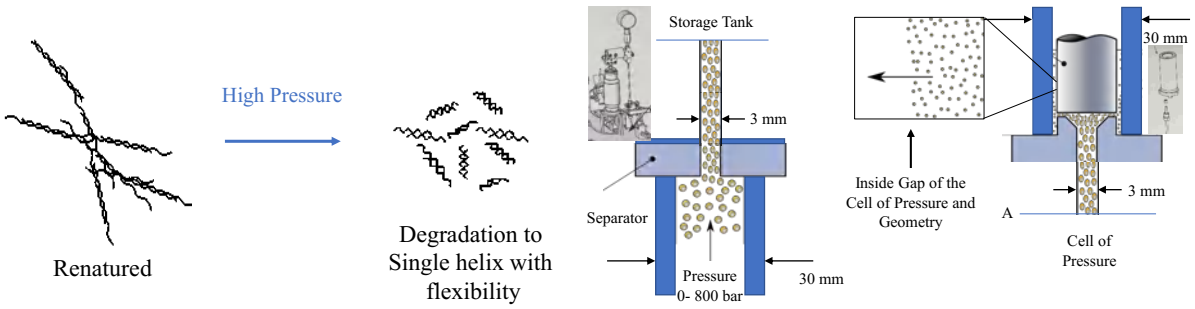

Source: Author (2021) and Adapted from Gulrez et al. (2012)

It was observed that for each cycle of homogenization at high pressure, the consistency coefficient decreased as presented by Tipvarakarnkoon e Senge (2010). Therefore, all the tests were used new fluid without the possibility of reusing the same fluid. During the test's repeatability, it was observed that the variation from one test to another under the same conditions was less than 8%.

As explained in Section 4.3.2.1, the high temperature generated structural modifications on the fluid, mainly in the xanthan gum. Intending to identify the fluid's modifications when it is subjected

to high pressure, maintaining an ambient temperature of 25 °C, oscillatory tests were carried out at the pressures of 10, 100, 400, 600, and 800 bar. During the analysis of oscillatory test results using the pressure cell, it is essential to keep in mind that because of the inaccuracy related to the delay effect at the measurements (the magnetic coupling technology that controls the movement of geometry within the cell) qualitative and not quantitative analyzes were performed.

Figure 5.14 (a) shows the storage modulus G' as a function of the stress amplitude for the different pressures at 25 °C. The rising pressure causes an increase in the fluids restructure, incrementing the linear visco-elasticity region (LVR) and the G' values. For pressures of 10, 100, and 400 bar the changes in storage modulus are smaller, and between the pressures 600 and 800 bar the increase were slightly higher. It was observed that despite the water being a low compressible liquid, the other components within the suspension at these pressures begin to reduce their space between the molecules, as demonstrated by Milas et al. (1990). The linear viscoelastic region was within a 1% strain over the angular frequency range of 0.3-80 rad/s^{-1}.

Figure 5.14 – Storage modulus as a function of (a) the stress amplitude; (b) Strain stress ; (c) Phase angle for oscillatory stress sweep tests from 0.01 to 100 Pa and frequency of 1 Hz obtained in atmospheric pressure and 10, 100, 400, 600 and 800 bar at a constant temperature of 25 °C.

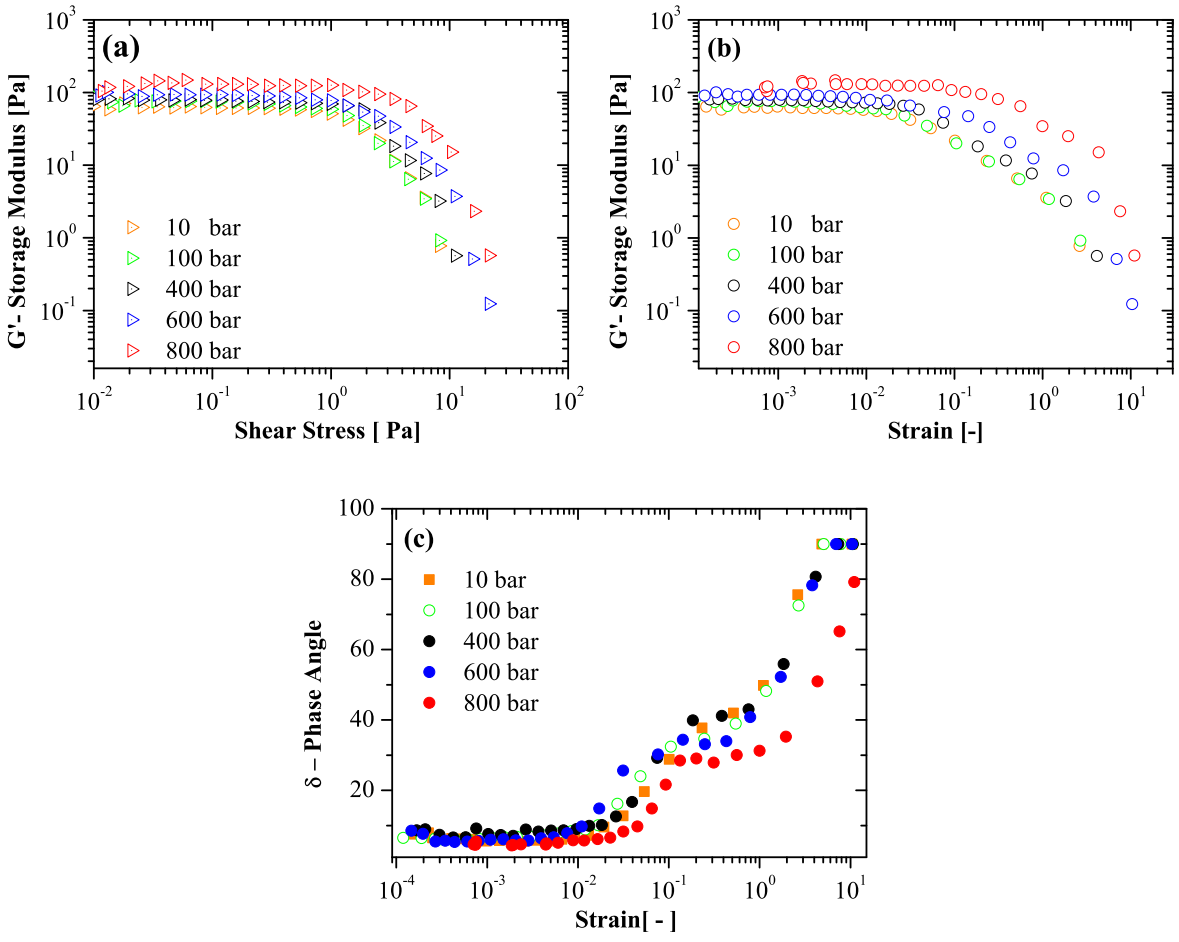

Source: Author (2021)

When observing Figure 5.14 (b), the storage modulus as a function of strain for each of the measured pressures, it is evident that the pressure provides the drilling fluid a predominantly elastic characteristic, increasing the strain with rising pressure, which gives greater capacity of suspension of cuttings. Figure 5.14 (c) shows the phase angle as a function of the strain, where it is observed that the fluid presents an elastic behavior for low strain. Followed by overcoming the critical strain, the material begins to flow as viscous flow, increasing the phase angle from 6-9 ° to 90 ° in all cases.

Figure 5.15 shows the crossover values between the storage and the loss modulus, where values of critical static yield stress, critical strain, and values of G' on LVR were determined. All these values contain inaccuracies, as previously mentioned. But the trend of its behavior shows that the pressure climbs static yield stress of the drilling fluid and its critical deformation point also increases. Besides, the LVR also increases as previously analyzed.

Figure 5.15 – The storage modulus G' in the LVER, critical yield stress, and the strain obtained in atmospheric pressure and 10, 100, 400, 600, and 800 bar at a constant temperature of 25 °C.

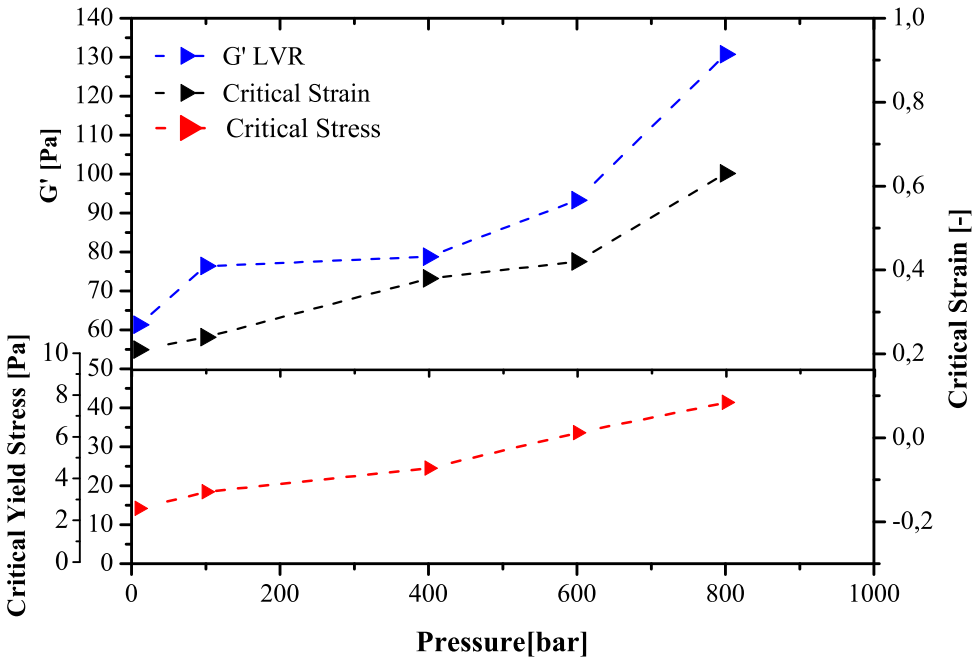

Source: Author (2021)

In the literature, many works deal with temperature changes in solutions and drilling fluids with xanthan gum. Most of them specify that the effects of pressure are not dominant due to the water's incompressibility. Mainly on water-based drilling fluids where used the depths exceed 1500 bar in offshore operation, the fluid structures' effects favor pressure control avoiding problems such as kick and blowouts.

Lagoueyte e Paquin (1998) demonstrated that the decrease in xanthan gum's molecular weight occurs due to mechanical forces during the high-pressure homogenization process. Gulrez et al. (2012) observed that molecular weight drop provided sufficient energy input to cause degradation of molecules to a great extent. Therefore, the treatment might break some of the molecules and shrink the molar

mass, but not all of them, giving place to an increase in polydispersity as in the case of pectin's valve homogenization.

5.2.2 Flow Curve at Different Pressure and Temperature

In the previous section, the drilling fluid structure was evaluated at high pressure, maintaining a constant temperature of 25 °C. In order to know the effect of pressure and temperature combined on the behavior of the fluid, flow curves are shown for temperatures of 25, 55 and 100 °C pressures of 10, 100, 400, 600, and 800 bar. The flow curves are shown in Figures 5.16 and the data was fitted to the power-law model. An equilibrium condition on the shear stress data was determined to indicate that the fluid is in a steady-state, when the shear stress values present variations of less than 5%. The data was subjected to statistical analysis.

Figure 5.16 – Flow curve fitted by the power-law model in the pressure range from 10 to 800 bar at temperatures (a) 25 °C; (b) 55 °C; and (c) 100 °C, for water-based drilling fluid. The power-law model describes the apparent viscosity η as a proportional function to shear rate, where m is the consistency coefficient, $\dot{\gamma}$ the shear rate, and n the flow behavior index.

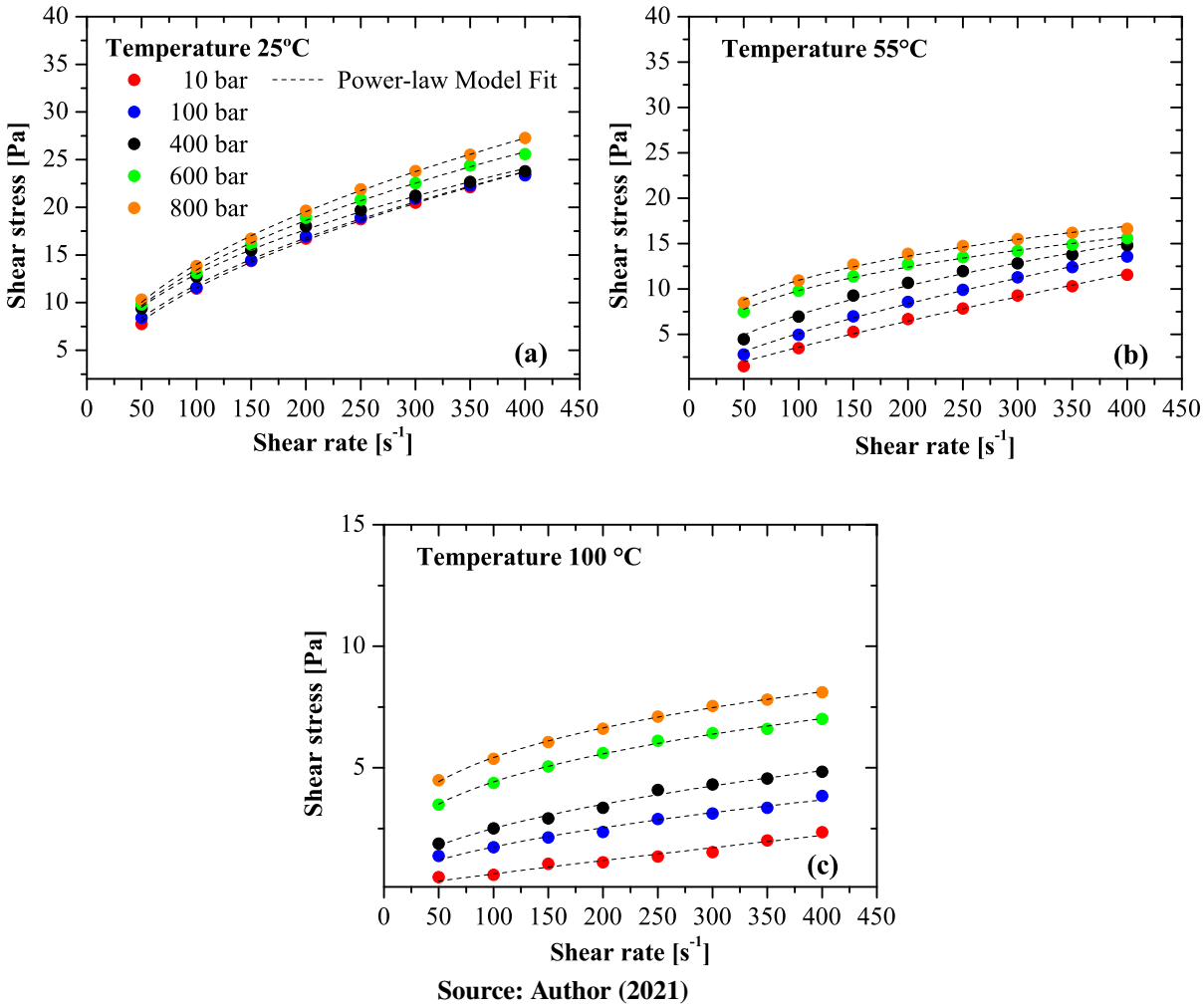

Source: Author (2021)

Figure 5.16 (a) shows the flow curve for the temperature of 25 °C. The effects of pressure on

the shear stress begin to grow progressively for high shear rates, the shear stress values were 8% for each new imposed pressure value, especially in 400 s^{-1}. On the other hand, for low shear rates, the increase was lower 3% for the pressures of 400, 600, and 800 bar. When the temperature is increased, the effects described above begin to have adverse effects on shear stress. The influence of pressure was less significant when the temperature was kept constant, but it is evident that the effect of temperature is more dominant, as observed when it is increased to 55 and 100 °C and the same pressures. Figure 5.16 (b) shows the flow curves for 55 °C, one can see that the fluid still shows a shear-thinning behavior. However, as the temperature increases, the shear stress decreased by 50 % considering the values of the measurement at 25 °C, the effects of temperature begin to be observed more and more dominates. At 100 °C, Figure 5.16 (c), it is evidenced that the fluid has already passed through the transition temperature where the conformation of the xanthan gum polymer chains changes for a disordered state.

The experimental data was fitted to power-law and Herschel-Bulkley models, and their parameters are shown as function of pressure in Figure 5.17. That allows one observing the predominance of temperature effect on the combined effects of temperature and pressure.

Figure 5.17 – Parameters fits of power-law and Herschel-Bulkley models as a function of pressure. The dashed lines indicate the trend of the models' parameters as a function of the pressure rise, for temperature (a) 25 ºC; (b) 55 ºC; (c) 100 ºC.

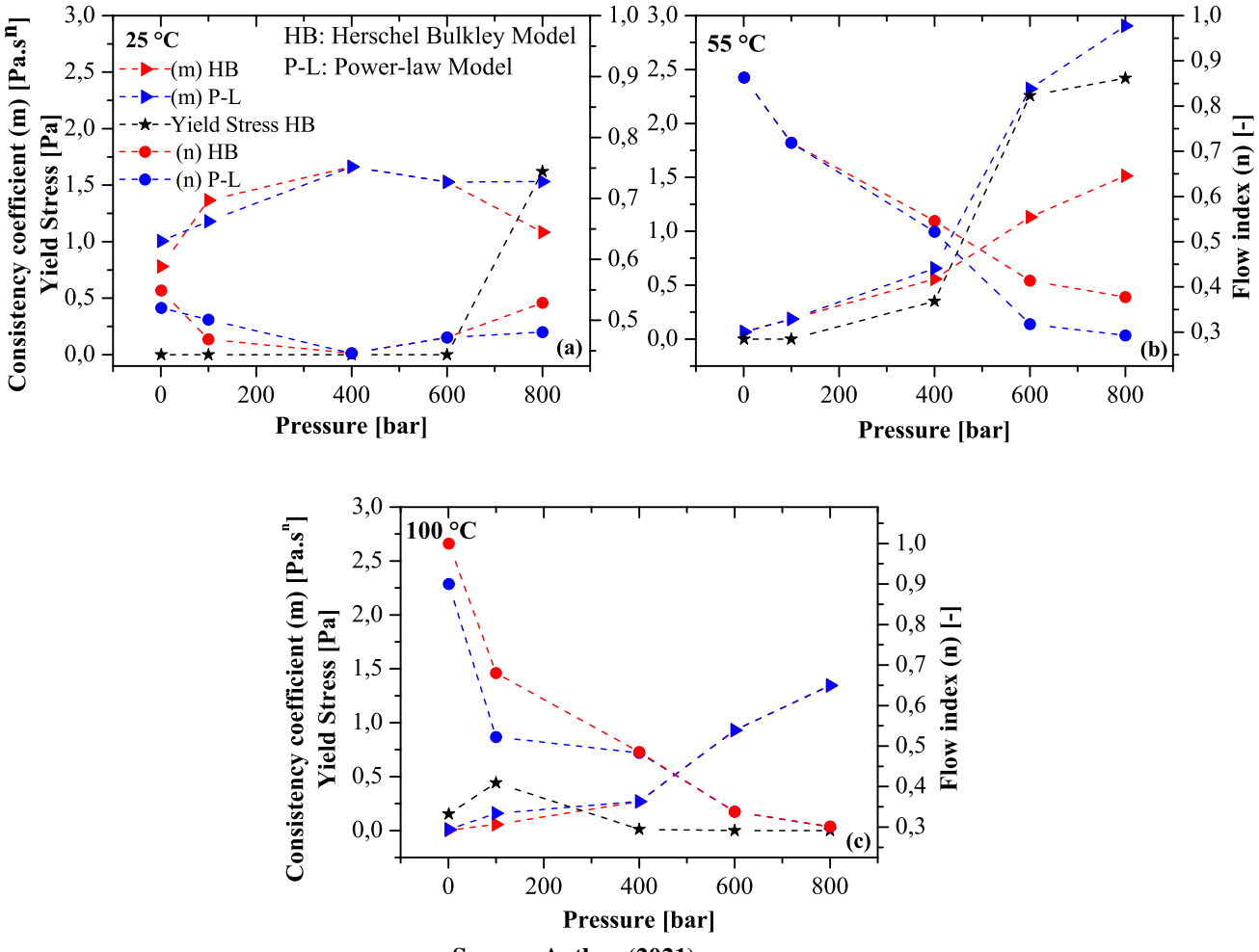

Source: Author (2021)

Figure 5.17 (a) shows the fit parameters of the power-law and Herschel-Bulkley models. The consistency coefficient rises with pressure, and the flow behavior index decreases in the pressure values from 10 to 400 bar. Above that value, the flow behavior index falls and remains constant. Both models present the same behavior based on the fact that the fits were made from the lowest measured shear rate. It was evidenced that the dynamic yield stress of the Herschel-Bulkley model was minimal. As the temperature in the fluid grows, it shows an increasing trend on all pressure values at the consistency coefficient. An even higher proportion at that consistency coefficient was registered for pressure values above 400 bar. The flow behavior index had an opposite behavior, decreasing more over 400 bar presenting the same behavior shown in Figure 5.17 (b). Figure 5.17 (c) shown that the climbs in the consistency coefficient was not higher than 1.5 when the pressure was increased to 800 bar. That indicates that the fluid was compacted and presented a disordered state of the polymeric chains, which decrease the ability to gain viscosity. The flow behavior index decreased from 0.98 to approximately 0.3, showing that the pressure strengthens the fluid structure despite being in a state of simple linear chains.

Finally, shear stress as a function of pressure is shown in Figure 5.18. Shear rates of 50, 100, 200, 300, and 400 s^{-1} were plotted for 25, 55, and 100 °C. In order to observe the shear stress growth with pressure rise, at 25 °C, the effects of pressure are more evident, resulting in a shear stress increase between 2.5 and 5 Pa. As the temperature increases to 55 and 100 °C, shear stress varies between 1.5 and 2.5 Pa, indicating that the effects of pressure more than 800 bar are not significant with pressure rises.

Therefore, it is possible to conclude that the water-based drilling fluid subjected to pressure and temperature variations presents stronger variations due to the effect of temperature. The results show that the pressure only generates increases of 16,01% shear stress on pressure variation from 10 to 800 bar. The increase happens because most of the fluid is composed by liquid water, which has very low compressibility. In terms of operation, this fluid would present greater stability in pressure variations during drilling and an instantaneous well control mechanism independent of temperature. The pressure directly affects the apparent viscosity of xanthan gum. Various researchers have reported a significant decrease in apparent viscosity during heat treatment (AUTIO; MYLLYMÄKI; MÄLKKI, 1987). However, considering pressure, the apparent viscosity behaved differently. High-pressure causes the denaturation of xanthan gum at non-denaturing temperatures with a different mechanism than the heat treatment. The structural modifications of xanthan gum by high pressure are strongly influenced by the pressure level, the treatment temperature, and the ionic strength (GULREZ et al., 2012).

Mechanical modification of bio-polymers is similar and has the same objectives as mechanical degradation of synthetic polymers. The only input is a mechanical force at a macroscopic level. Permanent loss of viscosity was the common indicator of structural modifications as polymer degradation. For instance, high pressure of xanthan gum was reported as a more complicated mechanism than a regular polymer degradation under mechanical forces (LANEUVILLE; TURGEON; PAQUIN, 2013).

Figure 5.18 – Behavior of the shear stress as a function of pressure at a shear rate of 50, 100, 200, 300, and 400 s^{-1}, for pressures of 10, 100, 400, 600, and 800 bar at temperatures of (a) 25 ºC; (b) 55 ºC; (c) 100 ºC.

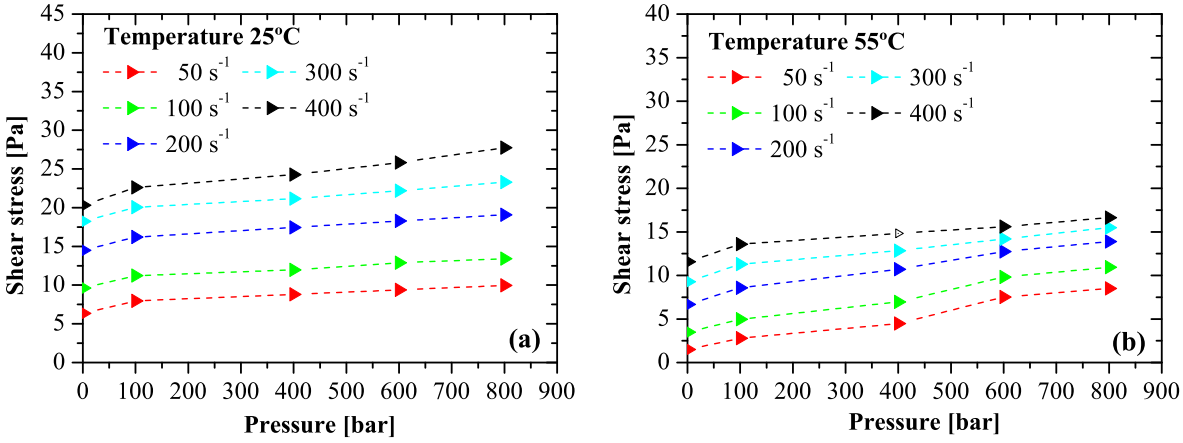

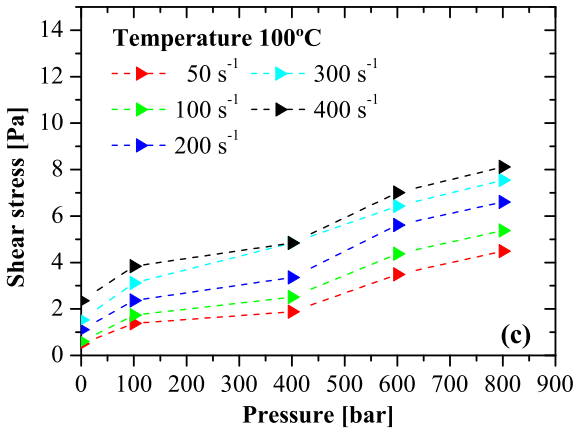

Source: Author (2021)

5.2.3 Fitting of Viscosity Dependence as a Function of Pressure, Temperature and Shear Rate with MTF Model

In Chapter 3, a literature review about different models used for the viscosity modeling in drilling fluid was carried out. There are models developed from experimental data over the years, attempting to describe the phenomenon's dependent variables. Theoretical models are based on free volume and polymer theories. On both, almost all parameters have physical meanings. These models get close to the behavior recorded by many non-Newtonian fluids. In addition to the shear rate's dependence, the viscosity is highly dependent on temperature and pressure as also many other variables. Several equations independently describe the effects of temperature and pressure on viscosity, as shown in detail in Section 3.3. The equations were tested through the data obtained in the rheological tests for different temperatures at constant pressure and different pressures and temperatures.

Initially, independent modeling of each effect was carried out, followed by fitting of the combined effects of pressure and temperature. The WLF model presented in Equation 3.3 was used to fit the temperature effect, which presented the best correlation coefficient concerning other models. The WLF

model used the power-law model's consistency coefficient as the apparent viscosity of the fluid as a function of temperature.

$$\boldsymbol{\eta}(\dot{\gamma}, T) = \left[1.15 \cdot \ 10^{-\left(\frac{136.54\ (T-4)}{12306 + (T-4)}\right)}\right] \cdot \dot{\boldsymbol{\gamma}}^{n-1} \tag{5.2}$$

The temperature effects were fitted with the WLF model, using the reference temperature of 4 °C, studies such as Hermoso, Martínez-Boza e Gallegos (2014), Hermoso, Martínez-Boza e Gallegos (2017), demonstrated that there is no rule for the selection of the reference temperature. Therefore, the reference temperature that provided the best fit was selected. The correlation coefficient (R^2) for reference temperature of 4 °C was 0.96 provided the best fit. The correlation obtained is shown in Equation 5.2.

In Figure 5.19, the consistency coefficient is shown as a function of temperature. For temperatures from 4 to 55 °C the model was fitted appropriately. For temperatures higher than 70 °C, it was noticed that the model data fitted was less than experimental data, due to fact of xanthan gum starting its conformation process from ordered to a disordered state, as explained in Section 5.1.1.

Figure 5.19 – Fitting of the predicted values of the power-law model's consistency coefficient as a function of temperature through a non-linear regression of the WLF model proposed by Williams et al. (1991).

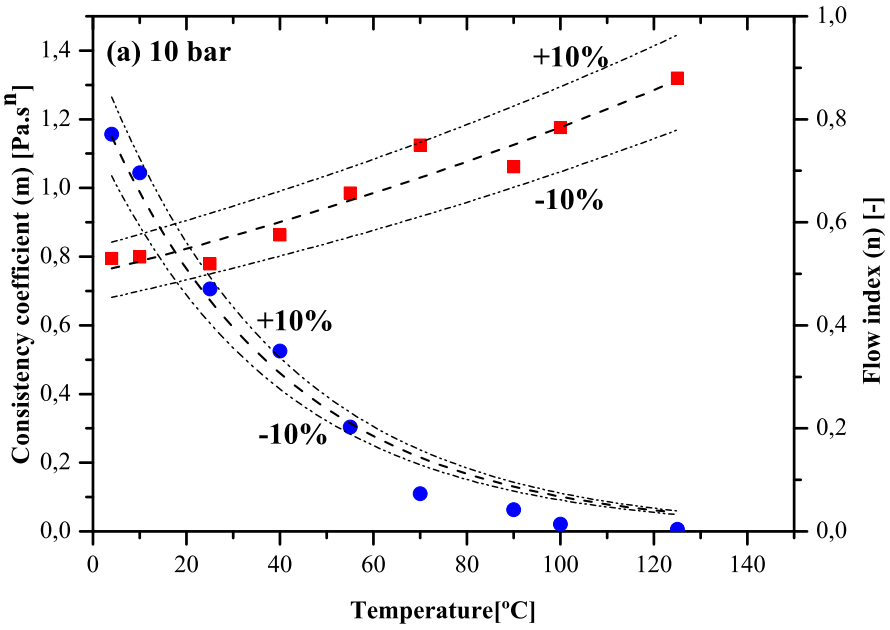

Source: Author (2021)

The flow behavior index was also fitted to see the influence on the structure. Equation 5.3

presented a correlation coefficient (R^2) of 0.90. In both figures, the error limits are shown $\pm$ 10%.

$$\boldsymbol{\eta}(\dot{\gamma}, P) = 0.97 + 0.003 \cdot \left(\frac{EXP(-0.006 \cdot P) - 1}{-0.006} \right) \cdot \dot{\boldsymbol{\gamma}}^{n-1} \tag{5.3}$$

Figure 5.20 shows the consistency coefficient as a function of the pressure fitting the data to the modification Barus' model, where the reference pressure was 1 bar. The error of $\pm$ 10% was plotted together to observe how far they are from the model. With an increase in pressure and its consistency coefficient a gain on the structure's rigidity was observed between 10 and 400 bar. Above that value, the rigidity of the structure remained practically constant.

Figure 5.20 – Fitting of the predicted values of the power-law model's consistency coefficient as a function of pressure through a non-linear regression.

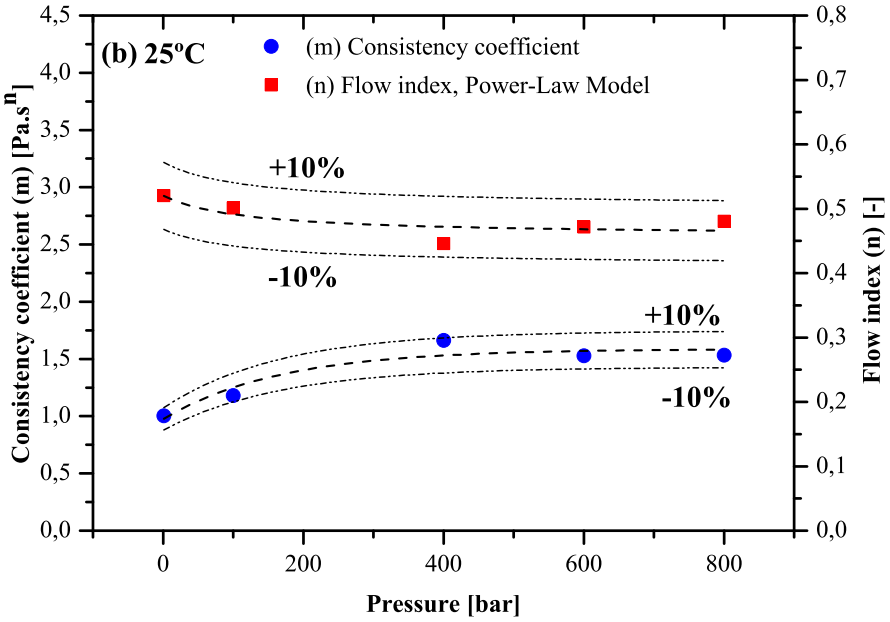

Source: Author (2021)

Apparent viscosity has been considered as an essential quality control parameter to industrial process. The experimental viscosity data is shown as a function of the shear rate for temperature and pressure variations. The flow curves were obtained at 25, 55, and 100 ºC. The measured pressures were 10, 100, 400, 600, and 800 bar for each of the temperature values as shown in Figure 5.21. The results show that the pressure effect on the apparent viscosity is not significant. Shear stress values presented a difference of 2 to 8% between 10 to 800 bar when measured at 25 ºC. On the other hand, the difference presented for low shear rates between 100 s^{-1} and 50 s^{-1} might be due to the obtained data was measured below the minimum recommended torque. Therefore the reliability for low shear rates is lower than for high shear rates. It is observed when the temperature goes from 55 to 100 ºC where the variations of the shear stress values were 41 %, it shows the strong influence of exceeding the transition temperature of xanthan gum. Meanwhile, the increases of pressure from 10 to 800 bar when passing through the transition

temperature, it showed that the viscosity doubled for each of the pressures. It was observed that the effect of temperature decreased the viscosity, regardless of the pressure increase.

Figure 5.21 – Experimental viscosity curves for (a) 25 ºC and pressure of 10, 100, 400, 600 and 800 bar; (b) 55 ºC, and ; (c) 100 ºC.

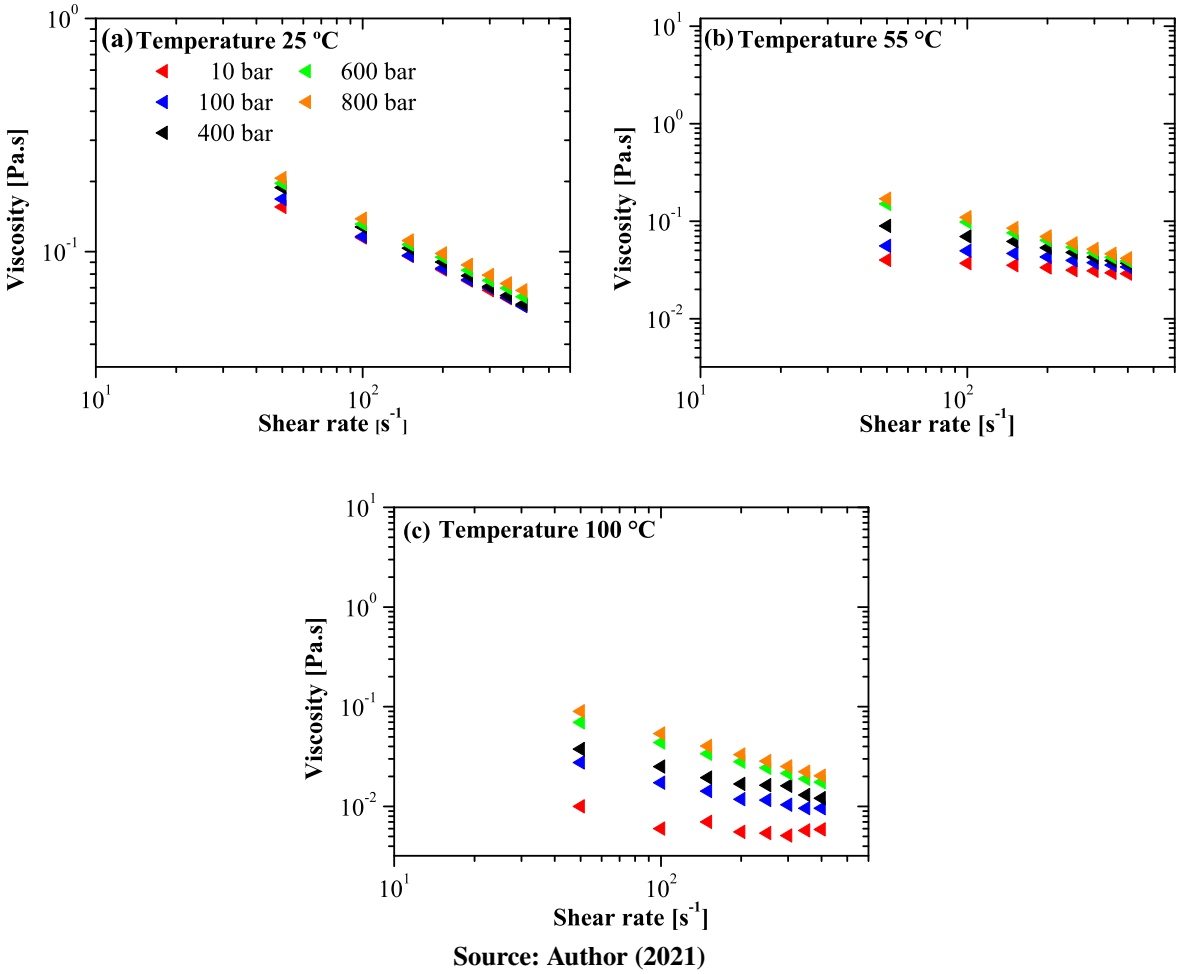

Source: Author (2021)

Models based on molecular theories have the advantage of predicting the evolution of the rheological properties based on the temperature-pressure evolution of some physical properties, such as expansivity and compressibility in the case of the FMT model. The FMT model was fitted to the experimental viscosity data, which fits the viscosity, pressure, and temperature concerning molecular parameters.

The viscosity measurement can be used to determine some parameters of the model such as k_e, k_e^*, k_ϕ, k_ϕ^*, and α. The fit was developed with the set of Equations 3.7 - 3.10 of Chapter 3. Due to the lack of experimental PVT data, some values such as the fractional free volume f_0 were taken from PVT studies found in the literature for drilling fluids. The considerations for the data fitting are listed in Table 5.1, where B'' is a constant typically taken to be 0.50, reference temperature of 55 ºC, the pressure of 1 bar, reference viscosity 0.031 Pa.s were obtained of present work. The fractional free volume at the reference temperature must be obtained through PVT tests because there is no equipment to perform this

Table 5.1 – Reference values of the different FMT model parameters for the fitting of the viscosity on HPHT conditions.

Reference values for fit FMT model.	
f_0	0.1
B''	0.5
T_{ref}	55 °C
η_{ref}	0.031 Pa.s
P_{ref}	1 bar

Source: Author (2021)

type of measurement, the fractional free volume value was taken from the drilling fluid studies of Eren, Santos e Campanella (2015), Hermoso, Martínez-Boza e Gallegos (2017).

It is helpful to use a reference temperature within the fluid's normal behavior, not exceeding the transition temperature. To fit the higher temperature values, it is necessary to implement other models that include the transition temperature to fit the xanthan gum's disordered behavior.

Figure 5.22 shows the viscosity fitting as a function of pressure at 25, 55, and 100 ºC for water-based drilling fluid with xanthan gum. The viscosity experimental data with temperature and pressure was fitted for the shear rates of 300, 150, and 50 s^{-1}.

The fit values of the bulk modulus occupied volume, empirical constants of bulk modulus, and expansion coefficient free-volume are shown in Table 5.2, for each shear rate, with their respective value of standard deviation and correlation coefficient. The fit parameters of the FMT model present physical significance, which are based on the molecular theories of polymers, especially the free volume theory.

Table 5.2 – Values of the various parameters of the FMT model for the water-based drilling fluid studied.

Parameters			
Shear Rate [s^{-1}]	300	150	50
k_e [-]	14	76	85
k_e^* [bar]	59700	39500	32000
k_ϕ [-]	37	45	45
k_ϕ^* [bar]	74600	89000	89000
α [bar]	0.000416	0,000475	0,000741
Residual sum of squares	0,105	0,098	0,017
Standard deviation	0.085	0.055	0.015
R^2	0.99	0.98	0.89
% AARD (Absolute Average Relative Deviation)	3,84	6,14	8,04

Source: Author (2021)

Figure 5.22 – Viscosity curve as a function of pressure, with the fitting of the FMT model for pressures 0 to 1000 bar and temperatures of 25, 55, and 100 ºC, at the shear rates of (a) 300 s^{-1}; (b) 150 s^{-1}; and (c) 50 s^{-1}.

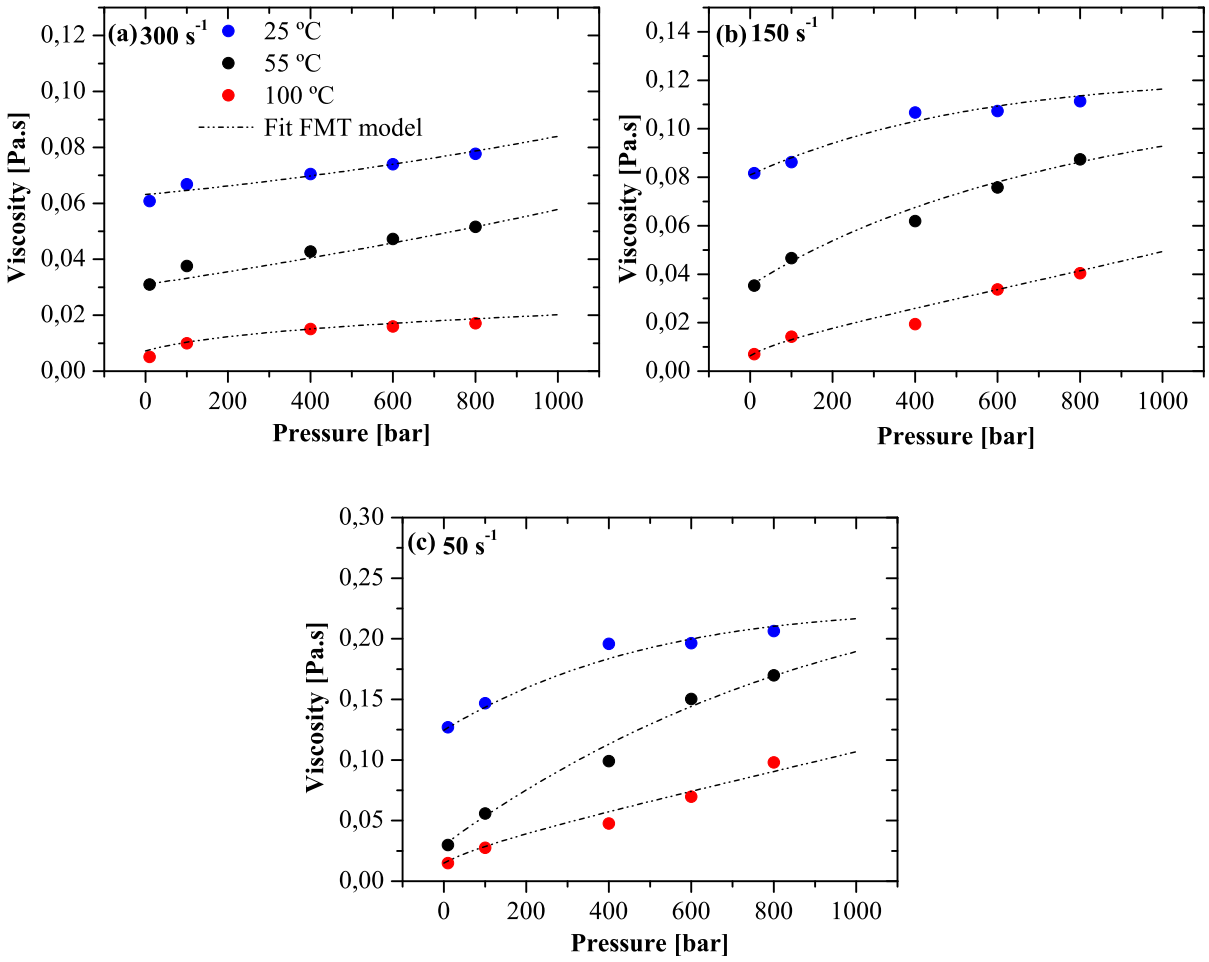

Source: Author (2021)

The free volume is associated with the space between molecules in a sample. The free volume of a liquid is the volume in excess of the random close-packed volume, which may be present as holes or irregular voids. The free volume provides the fluidity and controls the viscosity of a fluid which is summarized in the Doolittle equation (DOOLITTLE, 1951). The free volume increases with the temperature but decreases with the pressure. The volume of liquids can be divided into two different parts: the free volume and the occupied volume. It was observed that as the shear rate decreases, the bulk modulus k_{ϕ}^{*} increases. The occupied volume bulk module refers to is a measure of how resistant to compression that substance is. The ratio of the change in pressure to the fractional volume compression is called the bulk modulus of the material. For a fluid, only the bulk modulus is meaningful.

The water has a bulk modulus of 2.2. GPa, compared to the fitted modulus which is 7.46, 8.9, and 8.9 GPa for the shear rates of 300, 150, 50 s^{-1}, respectively, for the water-based drilling fluid with xanthan gum, which shows that when stops shearing the fluid, the compressive strength increases in the liquid, causing it to be more tenacious. This happens because the molecules' repulsive forces decrease,

decreasing their spacing between them (GILMAN, 1969). On the other hand, the bulk module of the entire volume decreases with the decrease in the shear rate, which represents that the free volume between the molecules decreases, and the interaction rate also decreases.

The expansivity of the free volume increase with decreased with shear rate. When a polymeric material is pressurized, and simultaneously exposed to an external mechanical excitation (strain or stress), not only the local movement of molecules (Brownian motion) is constrained, but also their relative motion is hindered. Consequently, molecular rearrangements enforced by external loading are slowed down, which on the macroscale is observed as a slowdown in creep and/or relaxation process. At the same time, by pressurization we increase the amount of internal energy, which on macroscale results in an increase of material temperature Under high pressures, polymers become brittle and sensitive to cracks formation, Due to the decreased volume, molecules are less free to move relative to each other, which on the macroscale is exhibited in time dependency of their mechanical properties.

Hence, pressure significantly changes time-dependent material behavior; at sufficiently large pressures, polymers may behave completely elastically. Different materials exhibit different sensitivities to pressure, yet there is no interrelation between the material chemical structure and its pressure dependence. And finally, A temperature change causes a change in the average kinetic energy of polymeric molecules, while a change in pressure does not change the energy state of the molecules but limits the available space for local molecular movements (AULOVA et al., 2020).

It was observed that pressure fitting presents an exponential increase on the three fitted shear rates. However, the trend for temperature increase is more linear. Nevertheless, it provides a good fit for the experimental data. On the other hand, Figure 5.23 shows the values of the evolution of the viscosity-temperature for pressure values of 100, 400, and 800 bar and for three values of shear rates of (300, 150, and 50 s^{-1}).

It was observed that at the temperature fitting, the viscosity values measured before the transition temperature fit well to the simulated model. In contrast, for higher temperatures, it presents very high standard deviations of the order of 0.56, as evidenced by the measurements made at 100 ºC showing that the model does not fit properly. The model fit the experimental results in the whole range of temperature and pressure tested fairly well (average error less than 5%). Nevertheless, based on the average absolute relative deviation and relative deviation percentage, each model behaves differently depending on the sample.

Figure 5.23 – Viscosity curve as a function of temperature, with the fitting of the FMT model for temperature 4 to 140 ºC and pressure of 100, 400, and 800 bar, at the shear rates of (a) 300 s^{-1}; (b) 150 s^{-1}; and (c) 50 s^{-1}.

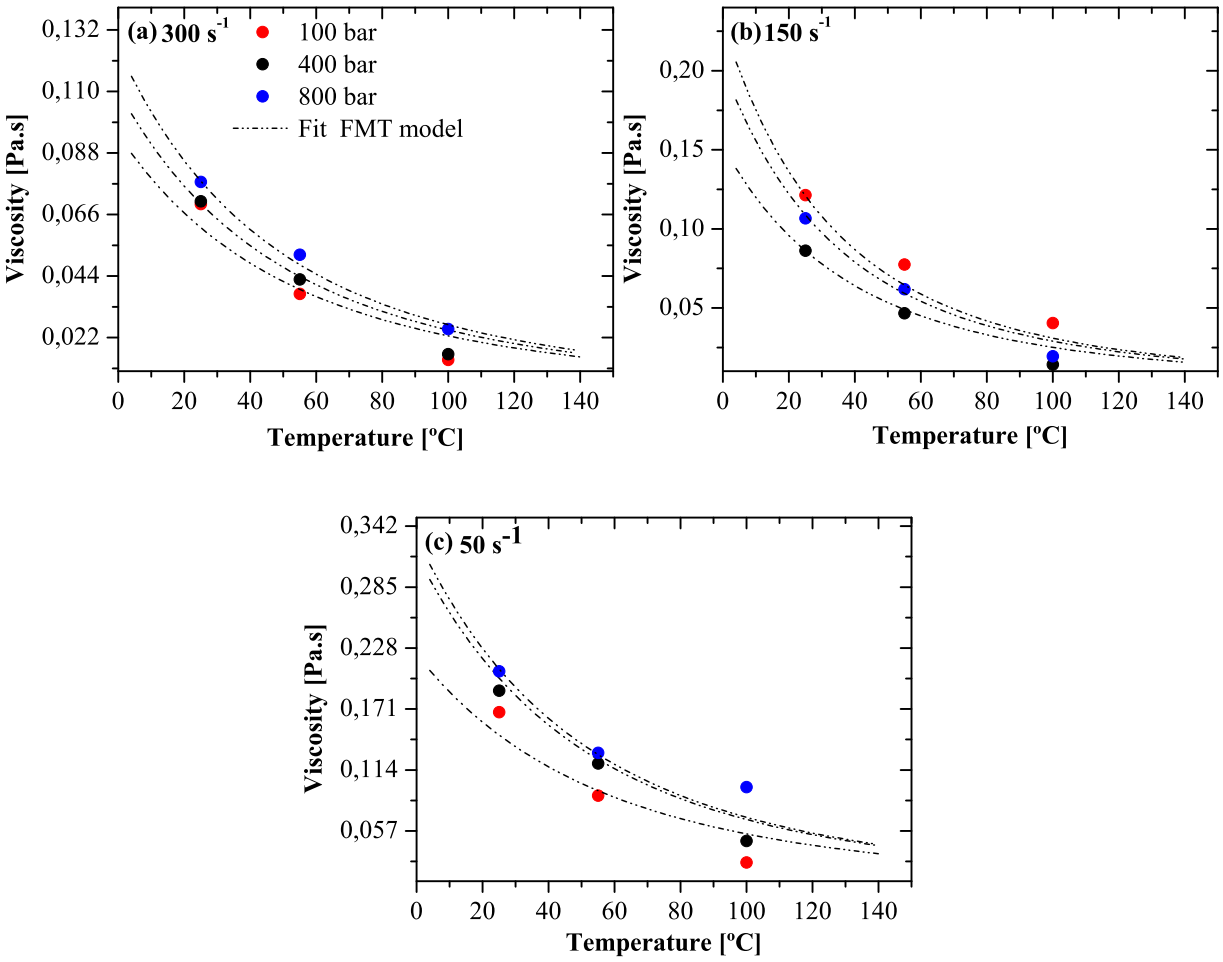

Source: Author (2021)

5.3 RHEOLOGICAL ANALYSIS OF DIFFERENT CONCENTRATIONS OF XANTHAN GUM

As there is a need for drilling fluid stability under high salinity conditions, the xanthan gum was evaluated as a clay/polymer suspension component. Some studies on xanthan gum solutions have shown to be stable in the presence of a high concentration of NaCl, within the pH range 6-10. However, the stability in the presence of calcium (Limestone) depends on the xanthan gum sample's nature. Therefore, a minimum xanthan gum concentration is required to stabilize the suspension.

A colloid suspension is not thermodynamically stable; coagulation or flocculation may take place. Nowadays there are two general ways through which colloid stability can be controlled by electrostatic and polymeric stabilization. In electrostatic stabilization, the stability is provided by the electrical double layers' mutual repulsion, which overcomes the van der Waal's attraction. In other words, increasing the ionic strength significantly diminishes the thickness of the double layers, and the electrostatic repulsion then becomes insufficient to outweigh the Van Der Waal's attractions (OLPHEN, 1991). In polymeric

stabilization, stability may be provided by either steric or depletion stabilization. Steric stabilization of colloidal particles is imparted by macro-molecules attached (e.g. by grafting or physical adsorption) to the particles' surfaces. Depletion stabilization is imparted by macro-molecules that are free in the dispersion medium. But both kinds of stabilization are originated from the excluded volume of polymer chains.

The stability and changes in the water-based drilling fluid rheology with xanthan gum and limestone were analyzed through the three drilling fluids with contractions of 0.5, 1, and 2% xanthan gum. The suspension was prepared with drilling fluid used to analyze the effects of high pressure and temperature previously presented and that from now on, it will be called (standard fluid). It was homogenized for 10 minutes at room temperature, then 0.286, 0.57, and 1.142 grams were added in 200 ml of drilling fluid, mixing it for 4 hours at room temperature and after that the clay suspension was left for hydration saturation for 24 hours.

Xanthan gum is used as a thickener in many industries, stabilizing the suspensions and the emulsions at paper mill and textile industries (KATZBAUER, 1998). Therefore, xanthan gum concentration's effects must be analyzed to know the rheological changes that increase the drilling fluid concentration used in this dissertation. Time sweep oscillatory tests were performed to determine the thixotropy growth and gel times of the fluid at room temperature and determine the drilling fluid stability. Shear stress amplitude sweep oscillatory tests were then performed to determine the linear viscoelastic region increase and observe the fluid's yield stress increase. Another test performed was the start-up flow, this is important to determine important overshoot stresses for drilling operation processes. Finally, a temperature analysis was performed to observe the effect of the transition temperature.

5.3.1 Effect of Xanthan Gum Concentration on the Stability Drilling Fluid

Initially, time sweep oscillatory tests were carried out as described in Section 4.3.1, for the three different xanthan gum concentrations in the drilling fluid at 25 ºC and atmospheric pressure. These measurements were carried out with a TA rheometer, allowing to perform the tests in parallel with the high pressure and temperature tests developed at Anton Paar rheometer.

Figure 5.24 shows the influence of xanthan gum concentration on the stability of water-based drilling fluid. The storage modulus and the phase angle are presented as a function of time. Comparing the standard fluid to the three concentrations of xanthan gum, one can observe that the suspension stability was enhanced when xanthan gum concentration was increased. The results coincides shown by studies carried out by Xie e Lecourtier (1992), Ahmed e Ramaswamy (2004), Bercea e Morariu (2020). Furthermore, it was noticed that the thixotropy of the fluid grows with increasing xanthan gum concentration.

The fluids with concentrations of 0.25 and 0.5% of xanthan gum presented a maximum storage modulus of 7.3 and 9.01 Pa, which remained constant for 500 seconds. This indicates that the material was restructured and remained stable during this time. Then flocculation effects that destabilized the suspension were observed through the phase angle and both fluids increased their phase angle from 23.9 to 32º.

The concentrations of 1 and 2% xanthan gum show that the storage modulus rose to 15.1 and 19.05 Pa, respectively. Besides, a considerable growth of the thixotropy of drilling fluid was observed when the xanthan gum concentration reached 2%, the increase in thixotropy is observed when the measured

Figure 5.24 – Time sweep oscillatory test for concentrations 0.25, 0.5, 1, and 2% xanthan gum in water-based drilling fluid at 25 ºC and atmospheric pressure.

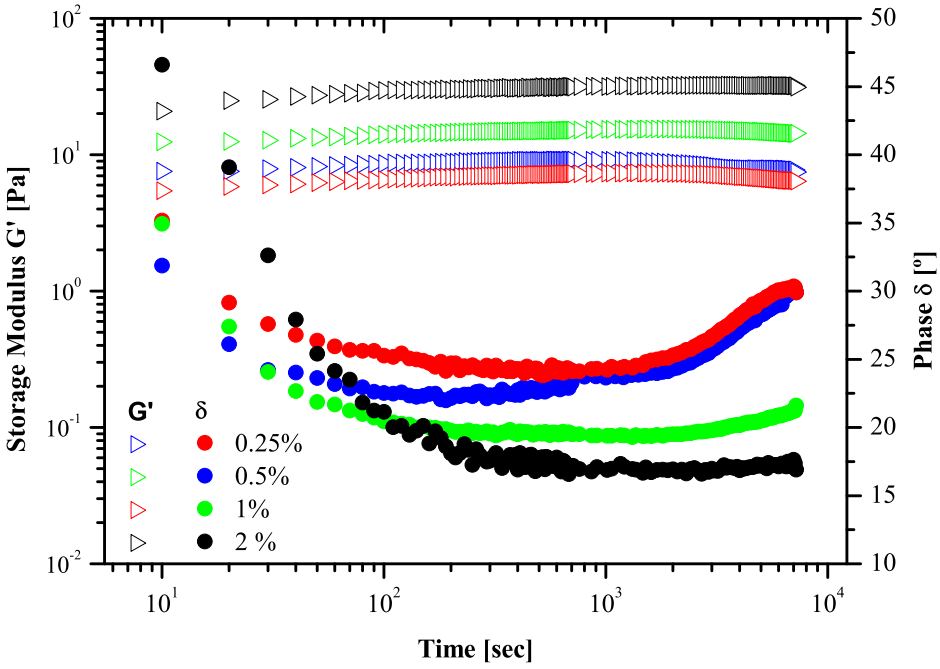

Source: Author (2021)

phase angle reaches a high value and begins to stabilize at a constant value over time. The time it takes for the phase angle to stabilize is known as gelation time. As a consequence, the gelation time of the drilling fluid rose from 200 to 800 seconds. On the other hand, an increased xanthan gum concentration provided greater stability in the suspension; once the phase angle remains constant at 17º until the end of the test. For a 1% of xanthan gum concentration, the phase angle values begin to rise from 19.5 to 21.6º after 2500 seconds of test with growth rate of 0.71º per hour. For those drilling fluids with 0.25 and 0.5% concentration, the phase angle values increased with a growth rate $\pm$ 2.38º per hour. In conclusion, the growth of the bio-polymer concentration increases the stability of the drilling fluid, as well as the gelation time, maintaining a stronger structure for a longer time, which represents a great help during operating stops.

5.3.2 Yield Stress Increase Due to Concentration

The rising on the water-based drilling fluid concentration can result in the yield stress increases of the fluid. (URLACHER; NOBLE, 1997) reported that xanthan gum concentration increment yield stress and consistent coefficient magnitude, as it was observed in the results obtained.

Therefore, stress amplitude sweep oscillatory tests were performed to determine the yield stress critical values, which are traditionally associated with the yield point (FERNANDES et al., 2017), and also to find out the critical strain determined by the crossing of the loss and storage modulus as a function of the shear stress amplitude.

Figure 5.25 shows the critical stress and critical strain as a function of the concentration of xanthan gum; it was observed that the rise in xanthan gum increments the fluid's yield stress of the fluid from 2.91 to 11.23 between concentrations of 0.25 and 2%, respectively, which means $\pm$ 4 times the value of the measured at the standard fluid. On the other hand, the critical strain is associated with the structural collapse that takes place when the yield stress is overcome (ANDRADE et al., 2016), increasing from 0.73 to 0.95. It could be concluded that the concentration growth intensifies the viscoelastic characteristics of the fluid due to the increase of the polymer chains of xanthan gum in suspension.

Figure 5.25 – Stress amplitude sweep for concentrations 0.25, 0.5, 1, and 2% Xanthan gum in water-based drilling fluid at 25 ºC and atmospheric pressure.

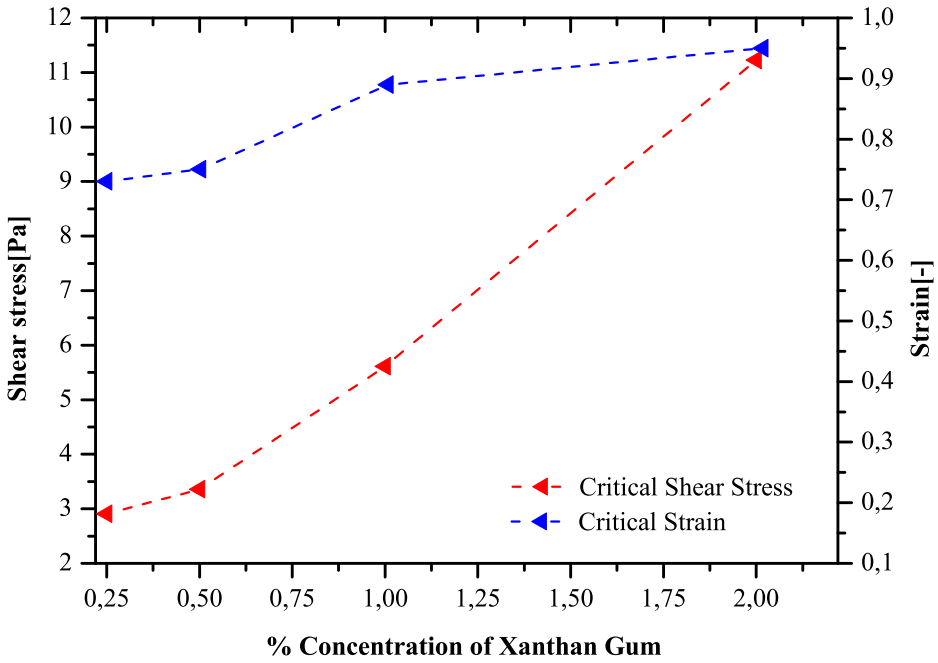

Source: Author (2021)

5.3.3 Start-up for Different Concentrations

Flow start-up tests were carried out to observe the influence of an aging time of 600 seconds for the 0.25, 0.5, 1, and 2% of xanthan gum concentration. Section 4.3.3 defines the procedure for executing the flow start-up for shear rates of 1, 5, 10, and 50 s^{-1} at the temperature of 25 °C at atmospheric pressure.

Figure 5.26 presents the shear stress as a function of the strain for the flow start-up experiments. It was observed that the peak stress rises with increasing concentration, indicating that the forces between the polymer chains increased, forming a more solid and compact structure.

The shear stress was measured to verify the transition from the predominantly elastic to the viscous behavior. According to Fernandes et al. (2017) for materials with yield stress and thixotropy, as in the case of drilling fluids, the shear stress response for the strain rate tests is primarily linear, which indicates a predominantly elastic behavior. Subsequently, the shear stress reaches the overshoot stress,

Figure 5.26 – Shear stress as a function of strain for the flow start-up shear rate tests performed after 600 seconds aging times. Shear rates controlled at 5, 10, and 50 s^{-1}, for different concentrations of (a) 0.25%; (b) 0.5%; (c) 1%; and (d) 2% xanthan gum at 25 ºC and atmospheric pressure.

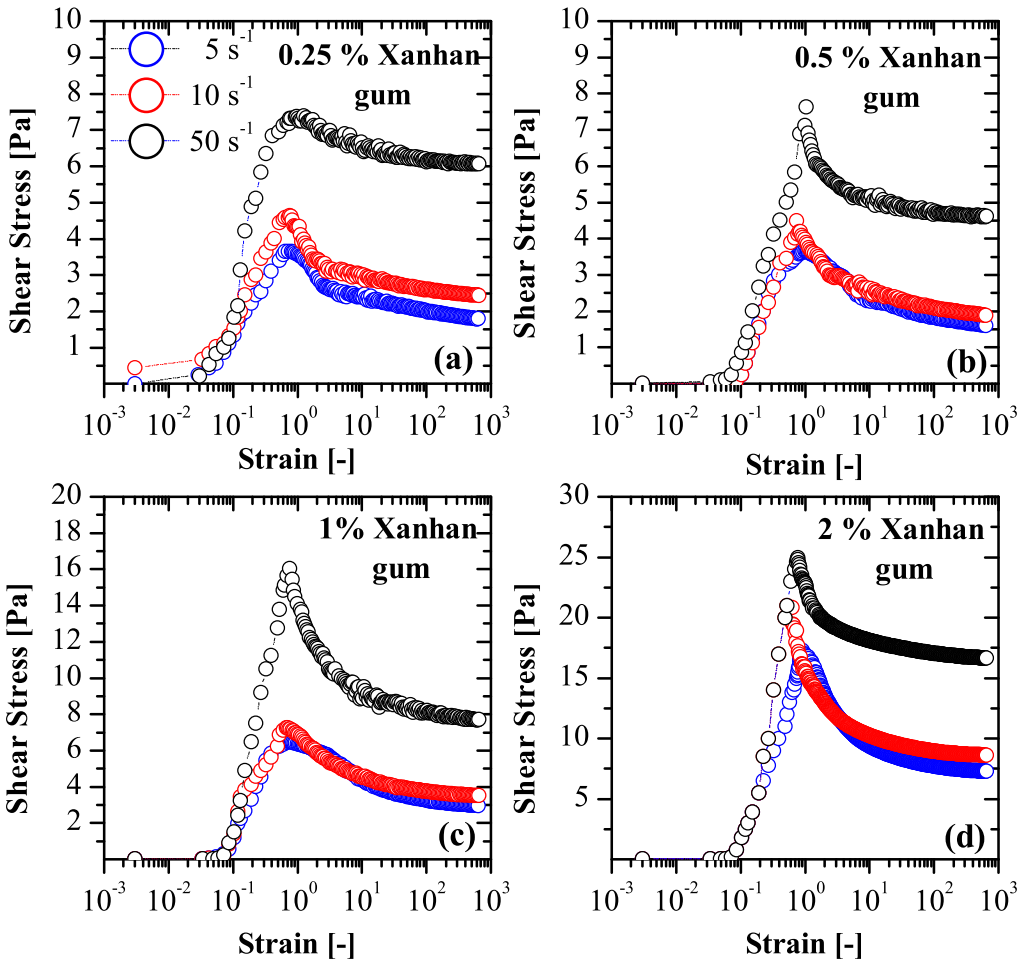

Source: Author (2021)

which is usually associated with the material structure's breakdown. After reaching the peak, the shear stress tends to a constant value, showing the predominantly viscous behavior, as observed at the 2% concentration drilling fluid. Hence, the high value of yield stress and thixotropy were evident on the linear response before overcoming the limit strain.

Figure 5.27 shows the overshoot stress increase as function of the xanthan gum concentration for the three measured shear rates. It was noted that as the concentration of xanthan gum rises, the overshoot stress climbs as-well. The results also show that the increase of xanthan gum concentration has several mechanical implications, during some industrial processes, which means that significant increases in power systems can cause overexertion in the different mechanical parts of industrial equipment.

Figure 5.27 – Overshoot stress for the flow start-up experiments at 5, 10, and 50 s^{-1} as a function of the concentration xanthan gum on water-based drilling fluid.

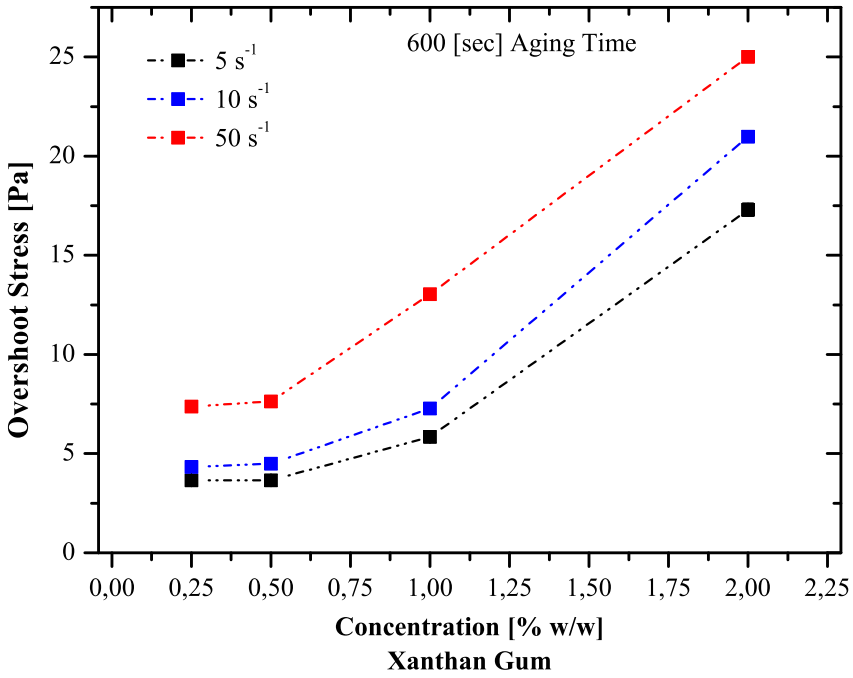

Source: Author (2021)

On the other hand, overshoot stress excess can be identified as a characteristic transition point between the predominantly elastic and predominantly viscous regions and is also associated with the material's elastic limit. The source of stress excess depends on the nature of the material tested and was carefully reviewed by Bonn et al. (2017). For polymer solutions, it relies on disentanglement of the structure of the material that had been previously responding elastically (WANG; WANG, 2009). On the other hand, colloidal systems relate to the maximum structural anisotropy point.

5.3.4 Effect of Temperature on Different Concentrations

The xanthan gum concentration is represented as an essential factor of the formulation of the drilling fluid. Therefore, the need to know the effects of temperature with increasing xanthan gum concentration made it possible to see the advantages during operations at high-pressure and high-temperature conditions. Once the effects attributed to the concentration increase of the drilling fluid at a constant temperature of 25 °C were known, it was shown that the pressure changes on water-based drilling fluids with xanthan gum have smaller variations in terms of viscosity when xanthan gum concentration increases. That indicate that the effects of temperature and mainly the transition temperature are fundamental to determine the fluid behavior.

Figure 5.28 shows the flow curves for 25, 55, and 100 °C at atmospheric pressure, for the 3 different concentrations compared to the standard fluid. The experimental data was fitted to the power-law and Herschel-Bulkley models to compare the consistency coefficient and flow behavior index. The

equilibrium condition was established when it is accepted that the permanent regime was reached when the last points obtained in each Section show a difference of less than 1% on the supply tension.

Figure 5.28 – Equilibrium flow curve at concentrations 0.25, 0.5, 1, and 2% of xanthan gum, fitted by the Power-law model on the temperature of 25, 55, and 100 °C for water-based drilling fluid. The power-law model describes the apparent viscosity η as a proportional function to shear rate, where m is the consistency coefficient, $\dot{\gamma}$ the shear rate, and n the flow behavior index.

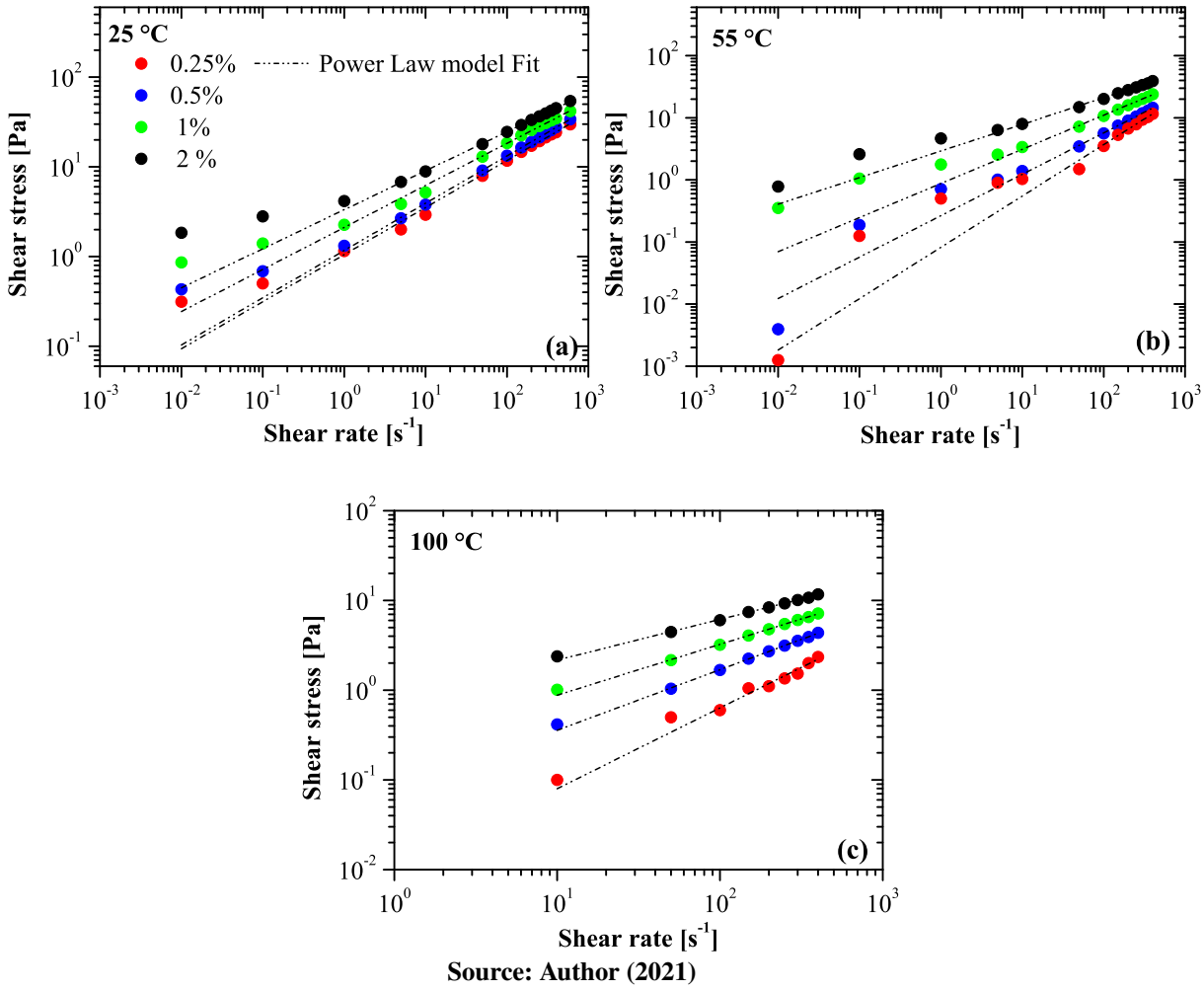

Source: Author (2021)

The flow curves shown in Figure 5.28 (a) shows that the shear stress increased with xanthan gum concentration. For a shear rate of 400 s^{-1} the increases were 11.9%, 29.8%, and 46.1% for the concentrations of 0.5, 1, and 2% xanthan gum, respectively. The results demonstrates that the effect of concentration on the shear stress on suspensions with xanthan gum is described through an exponential or power behavior (SPEERS; TUNG, 1986). Also, the values of dynamic yield stress increased to values of 1.32, 2.25, and 4.16 Pa. This effect happens due to the fact concentration changes are highly dependent on the size of the polymer chains and the magnitude of yield stress growths, as reported by Speers e Tung (1986), Ahmed e Ramaswamy (2004).

Figure 5.28 (b) shows flow curves at 55 °C for three xanthan gum concentration values. The gain of shear stress was 20.5%, 51,6%, and 70,3% for the concentrations of 0.5, 1, and 2% xanthan gum respectively. In contrast the effect of temperature dropped the shear stress by 34.6%, concerning the flow

curve at 25 °C for the concentration of 2%. For the temperature of 100 °C the xanthan gum's transition temperature was exceeded, causing a large shear stress decrease. In Figure 5.28 (c) the shear stress diminution was strong for the concentration of 0.25% because its transition temperature was exceeded. As the xanthan gum concentration rose to 0.5, 1, and 2%, compared to the standard fluid, the shear stress increased by 45.3, 67.3, and 79.9%, respectively, indicating that possibly the transition temperature of these concentrations shifted for higher temperatures.

Several researchers, such as Abdelrahim, Ramaswamy and Voort (1995), Marcotte, Hoshahili e Ramaswamy (2001) have used the combined effect of temperature and concentration on consistency coefficient/apparent viscosity to describe the xanthan gum's flow behavior suspensions. The consistency coefficient and flow behavior index values showed exponential and linear behavior, respectively, when they were fitted to the xanthan gum concentration variation as shown by (XUEWU et al., 1996). Figure 5.29 shows the fit made with error bands of $\pm$ 5 for 25 °C and $\pm$ 10% for other temperatures. Equations 5.4 show the fit parameters obtained implemented in the power-law model to obtain the behavior of the apparent viscosity as a function of the shear rate and the xanthan gum concentration for constant temperatures. The fits showed a correlation coefficient R^2 of 0.94, 0.96, and 0.97 for consistency coefficient for temperatures of 25, 55, and 100 °C; for the index of flow behavior were 0.85, 0.82, and 0.85 at the same temperatures, respectively.

$$\boldsymbol{\eta}(\dot{\gamma}, C_{XG}) = 0.978 \cdot EXP(0.619 \cdot C_{XG}) \cdot \dot{\boldsymbol{\gamma}}^{(0{,}53-0{,}05 \cdot C_{XG})} \qquad \text{at 25 °C} \tag{5.4}$$

$$\boldsymbol{\eta}(\dot{\gamma}, C_{XG}) = 0.187 \cdot EXP(1.281 \cdot C_{XG}) \cdot \dot{\boldsymbol{\gamma}}^{(0{,}80-0{,}20 \cdot C_{XG})} \qquad \text{at 55 °C} \tag{5.5}$$

$$\boldsymbol{\eta}(\dot{\gamma}, C_{XG}) = 0.044 \cdot EXP(1.426 \cdot C_{XG}) \cdot \dot{\boldsymbol{\gamma}}^{(0{,}85-0{,}22 \cdot C_{XG})} \qquad \text{at 100 °C} \tag{5.6}$$

where C_{XG} is xanthan gum concentration and $\dot{\gamma}$ is shear rate.

Figure 5.29 shows the fit parameters of the power-law model as a function of temperature. In Figure 5.29 (a) it is possible to observe that the consistency coefficient increased when rising in the concentration of xanthan gum from 1.05 to 3.32. This fact shows that the transport capacity of the fluid was increment. The flow behavior index remained constant at 0.52 between 0.25 and 0.5 % of xanthan gum. But at 1 and 2 % concentration the index decreased to 0.46 and 0.43, respectively, indicating a structural gain of the drilling fluid with the increase of the xanthan gum concentration. Figure 5.29 (b) shows that the consistency coefficient values lowered to values of 0.08, 0.26, 0.87, and 2.41 at the temperature of 25 ºC respectively, to each xanthan gum concentration values. On the other hand, the flow index rose to 0.82 at the 0.5 % concentration of xanthan gum. As the concentration climbs, the structure strengthens, returning to values of 0.54 and 0.42 in 1 and 2% concentrations, respectively. Raising the temperature to 100 ºC. Figure 5.29 (c) the consistency coefficient diminishes sharply, so that for 2% xanthan gum, its value was 0.76, and its flow index, on the other hand, maintained its values of 0.45.

The result showed the consistency coefficient gains with increasing concentration, while the temperature significantly decreases the consistency coefficient as previously reported by Abdelrahim, Ramaswamy and Voort (1995), KRUMEL e SARKAR (1975), Marcotte, Hoshahili e Ramaswamy (2001), Rao, Walter e Cooley (1981), where xanthan gum solutions and brine were used in results obtained. Many

Figure 5.29 – Fitting parameters Power-law model at 0.25, 0.5, 1, and 2% of xanthan gum and temperatures (a) 25 ºC; (b) 55 ºC; and (c) 100 ºC.

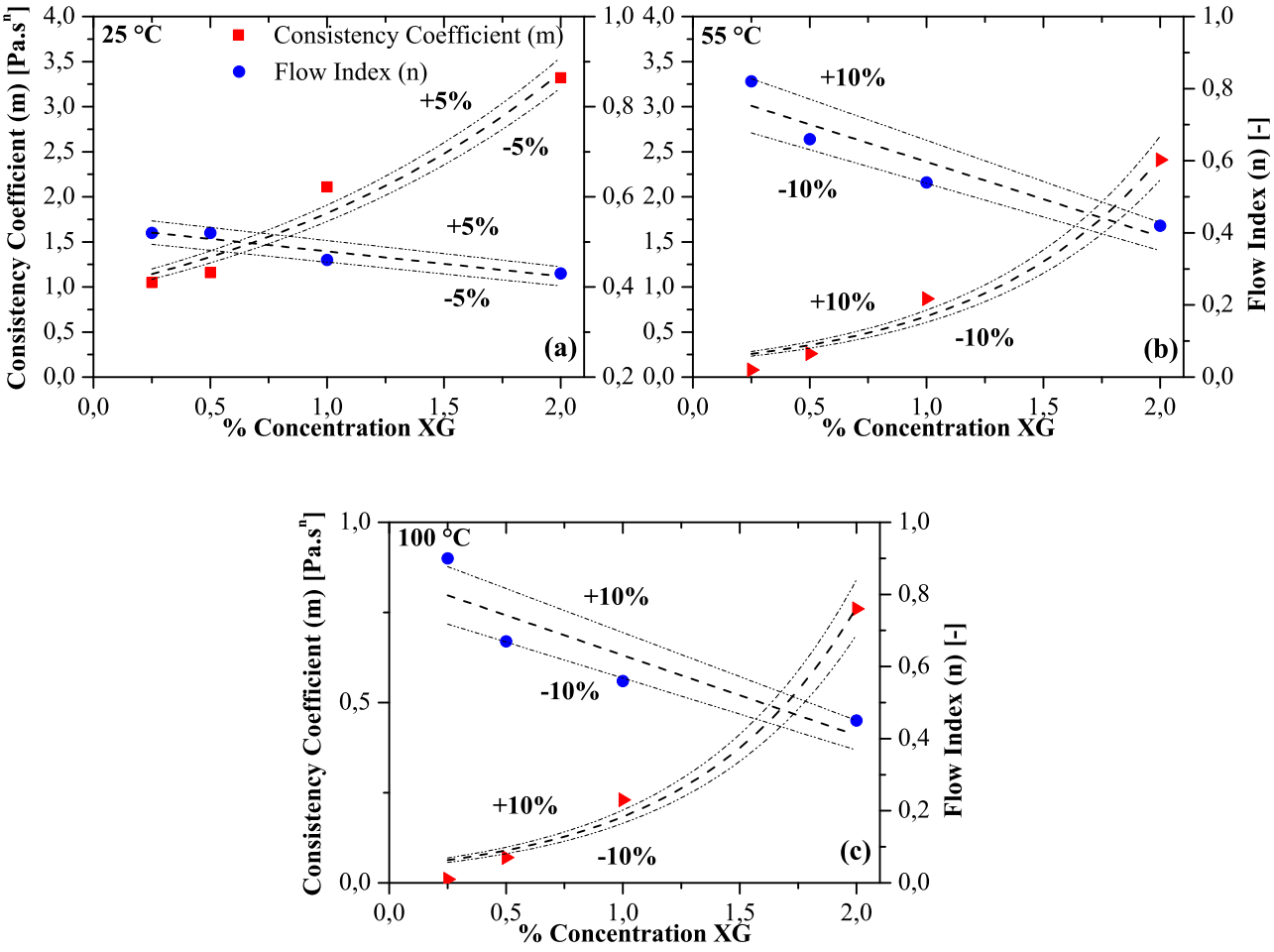

Source: Author (2021)

authors concluded that the viscosity increases significantly as the concentration of xanthan gum rises. The behavior is attributed to the polymer's intermolecular interaction and the entanglement that increments the dimensions and the molecular weight of the effective macro-molecules.

The effect of temperature and xanthan gum concentration was fitted to a model based on the WLF model for the effect of temperature and exponential behaviors of the consistency coefficient for the concentration effect. Equation 5.7 shows the fitted parameters for 3 temperatures and 4 concentrations of xanthan gum.

$$\boldsymbol{\eta}(\dot{\gamma}, T, C_{XG}) = 1.09 \cdot exp(0.828 \cdot C_{XG}) \cdot \ 10^{-\left(\frac{116.54\ (T-4)}{8543.54 + (T-4)}\right)} \cdot \dot{\boldsymbol{\gamma}}^{(0.58+0.05 \cdot C_{XG})} \tag{5.7}$$

Figure 5.30 shows the viscosity for different concentrations as a function of the shear rate. One can notice that the viscosity increases exponentially with rising concentration, which can generate problems during operational stops, as seen above. Figure 5.30 (a) shows that the viscosity of the drilling

fluid with a concentration of 2% xanthan gum increased by 86.05% for the shear rate of 0.01 s^{-1} when compared to the fluid with a concentration of 0.25% when the temperature is 25 °C. As previously observed, the increase in concentration generates an exponential increase in viscosity, maintaining the shear-thinning behavior. For a temperature of 25 °C, it is observed that zero shear viscosity increased with increasing concentration. When the temperature increases to 55 °C as shown in Figure 5.30 (b), the viscosity values fall by 92 %, 56.6% and 55.8% for the concentrations of 0.5, 1 and 2% xanthan gum. It is observed that the effect is less for concentrations greater than 1% of xanthan gum. Finally, for the temperature of 100 °C the viscosity drops sharply for all concentrations of xanthan gum, the drilling fluid exhibits less shear-thinning behavior as shown in Figure 5.30 (c), which implies little capacity to keep cuttings in suspension.

Figure 5.30 – Experimental viscosity curves for (a) 25 ºC; (b) 55 ºC, and ; (c) 100 ºC at 0.25, 0.5, 1 and 2% concentrations xanthan gum on water-based drilling fluid.

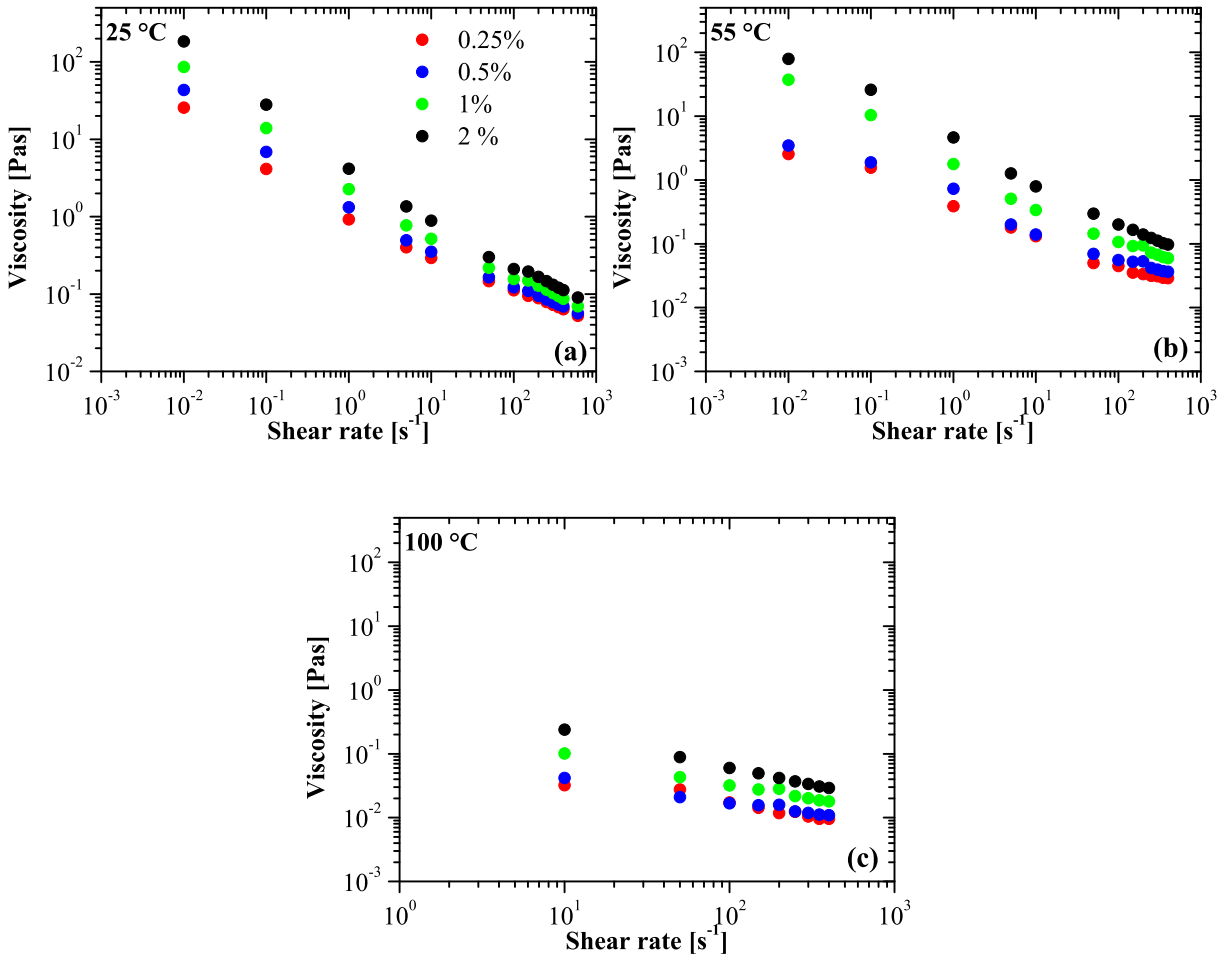

Source: Author (2021)

Another factor that influences the decrease of xanthan gum's viscosity is the salt concentration, which was not analyzed in this study. Considering what was demonstrated by Garcıa-Ochoa et al. (2000), on low polymer concentration, the viscosity falls slightly when a small amount of salt is added to the solution. Above a critical concentration, the addition of electrolytes can induce rheological parameters'

value increase due to intermolecular associations, facilitated by the reduced electrostatic repulsion and ordering of the chains, leading to the development of a three-dimensional network.

5.4 RESULTS CONSOLIDATION

This chapter presented the test results obtained using a water-based drilling fluid with xanthan gum and limestone provided by PETROBRAS S.A. Flow curve experiments with constant shear rates, oscillatory stress sweep, time sweep, flow start-up, dynamic thermal aging tests and microcalorimetry temperature scans tests were performed. They were executed in order to validate the effects of temperature at 4, 10, 25, 40, 55, 70, 90, 100 and 125 °C, the pressure at 10, 100, 400, 600 and 800 bar and concentration of xanthan gum at 0.25, 0.5, 1 and 2%. Also, the experimental data was fitted to rheological models with shear rate variation (Power-law and Herschel-Bulkley model) and theoretical models based on free volume with temperature and pressure variation (WLF and FMT model).

It was observed that the effect of temperature on the water-based drilling fluid with xanthan gum for temperatures below 55 °C presented thermal stability with minimal shear stress value variations. At higher temperature, the encountered effects were more significant on higher temperatures due to the fluid exceeding the xanthan gum's transition temperature, which causes a change in the conformation of the polymer chains. The temperature of the drilling fluid causes a decrease in the linear visco-elasticity region in the fluid. The connections between its particles diminish and the material begins to separate the phases over time. As the material is broken up to a viscous response, it exhibited shear-thinning behavior at all temperatures, and the temperatures decreased the shear stress values. This was attributed to the dis-entanglement and alignment of the xanthan gum polymer chains along the flow direction. Also, the drilling fluid transport capacity dropped because the polymeric chains were disorganized and this way weakened the structure of the fluid. It was also observed that the conformation of the polymeric chains of the xanthan gum is reversible when the fluid is cooled. Dynamic thermal aging tests showed that the drilling fluid supports thermal loads for 16 hours without undergoing modifications on its viscosity values when the temperature does not exceed 90 °C. For higher temperatures, during 16 hours of exposure, the fluid undergoes thermal degradation without reversible effect, causing a total destabilization of the drilling fluid. In addition, through the flow curves, it was observed that the transition temperature of xanthan gum diminished when the fluid was subjected to thermal aging.

The effect of pressure showed that the fluid structure in the linear visco-elastic region gained stiffness with increasing pressure. Regarding the temperature and pressure variations on the drilling fluids analysis, the experimental data showed that the individual effects of temperature continue to cause energy increases on the molecules and modifications on the different structures and bonds. On the other hand, the pressure acts as a stabilizer, reducing the possible spaces between the fluid structures. The pressure increment of the shear stress values was greater with increasing temperature. The increments can be understood as an increase in the polymer chains' free volume within the suspension when increasing temperature, especially when the xanthan gum exceeds the transition temperature. Subsequently, when high pressure is imposed, the individual chains are compacted one on top of the other, increasing their rigidity.

In order to find a model that adequately adjusts to variations of temperature, pressure and shear rate, the experimental results were adjusted to models such as WLF, Barus and FMT. The WLF model presented a good fit for the experimental data up to the fluid's transition temperature. In the case of the Barus model, the experimental values fitted very well to the pressure variations. Finally, the FMT model's use based on free volume theory and commonly used to model polymers, presented an adequate fit for the three shear rates used for the comparison. For this fit to be more precise PVT measurements are necessary.

On the other hand, as the concentration of xanthan gum increased, a fluid with greater thixotropy was shown, and an improved stability of the fluid at room temperature. The critical yield stress and strain roses. The structure gained an elastic response since the connections between the polymer and the fluid suspended particles were increased. Analyzing the flow start-up tests carried out for the four different concentrations of xanthan gum, it was observed that the overshoot stress climbed strongly with increasing concentration. This occurred due to the unraveling of the material structure that was previously responding elastically as reviewed by Bonn et al. (2017) for polymer suspensions. It should be noted that the overshoot stress value is directly related to the thixotropic and viscoelastic behavior of the material before yielding. Therefore, a greater energy power is required to start-up the flow. Finally, increasing the concentration of xanthan gum leads to viscosity gain. This effect has been attributed to intermolecular interaction or entanglement that grows the effective macromolecule dimensions and molecular weight. The incremented viscosity of the xanthan gum can increase the residual resistance factor and improve the sweep efficiency, as reported previously. As the concentration rises, the polysaccharides chains move closer together, resulting in their mutual entanglement. In entanglement, domain viscosity grows exponentially. The temperature affected the apparent viscosity of xanthan gum inversely. As the temperature climbs, the average speed of molecules in liquids increases, so the time they spend in contact with their nearest neighbor decreases. Thus, as temperature increments, the average intermolecular forces drop. As the temperature of the, the solvent viscosity lowers, but the xanthan gum's degree of hydrolysis rises. As the degree of hydrolysis increases, the viscosity of xanthan gum grows due to the electrostatic repulsion between the negative charges on the polymer chain. The effects of decreasing the fluid viscosity continue with increasing temperature, but the proportion of decreasing viscosity is lower with rising concentration. Therefore, it can be assumed that the transition temperature of xanthan gum climbs with rising concentration. Besides, it was possible to observe that more energy is required for xanthan gum molecules to change from an ordered to a disordered structure.

6 CONCLUSIONS

The knowledge of the behavior of the drilling fluids rheological properties is of great interest for the oil and gas industry. It allows the companies to plan and execute more efficient, economic, and safe drilling projects. The high demand for HPHT wells, globally and mainly in Brazilian pre-salt, has brought enormous challenges for the oil and gas industry. One of the main challenges is designing a proper drilling fluid to withstand the high-pressure and high-temperature conditions.

As final conclusions, during the development of the methodology for the measurements of drilling fluid with xantham gum under HPHT conditions , problems of evaporation and sedimentation were found, and those problems were augmented with temperature. They were eliminated using moistened pieces of cotton and pre-shearing before measuring low shear rates. On the other hand, the pressure cell generated degradation on the fluid chains due to the high-pressure homogenization process, which was avoided by placing directly the fluid inside the pressure cell, avoiding direct filling from the storage tank.

Regarding the effects of temperature, the following conclusions were obtained:

- The flow curves showed a decrease in shear stress with increasing temperature but maintaining their shear-thinning behavior.
- The data obtained for drilling fluid aged dynamically was compared with standard fluids data. It was noticed that the values of the shear stress for aged fluids remained almost constant up to the aging temperature of 100 °C, without losing their rheological characteristics.
- The drilling fluid's transition temperature was about 70 to 90 °C , which produces a decay of the viscosity values. However, in case the fluid is cooled, it returns to its initial characteristics.

In the rheological analysis performed on the drilling fluid, the combined effects of temperature and pressure were determined the following conclusions:

- The effects of pressure at a constant temperature caused a slight increase of the viscosity, and a significant restructuring in their elastic phase, obtaining higher yield stress values.
- The measurements with combined pressure and temperature showed, that temperature has a greater predominance than the effect of pressure.
- The effects of pressure generated slight variations of shear stress for the combined analysis, but also the fluid showed good stability with pressure changes, while the degradation of the fluid predominated under temperature changes
- Finally, the rheological behavior with each variable (pressure and temperature) was obtained, fitting their behavior through the non-linear fit, the models presented a good correlation coefficient in all cases.

On the analysis of the drilling fluid's behavior with the concentration increase of the xanthan gum viscosifier, it was concluded that:

- The fluid incremented the thixotropy and its structural stability. Data obtained showed an increase in the yield stress and the critical strain, due to the concentration of the polymeric chains.
- Also it was observed that with increasing concentration, the overshoot in the start-up tests increased dramatically, indicating that will leads to higher power consumption in the pumps to flow start-up.
- Finally, when analyzing the effect of temperature with the xanthan gum concentration gain, it was observed that it presents more thermal stability with rising concentration because the fluid needs more energy for the conformation transition of xanthan gum to occur.

This experimental study demonstrated that it is possible to obtain relevant information on the effects of temperature and pressure on water-based drilling fluid with xanthan gum. The previous information allows operators to identify critical points of the drilling fluid under operating conditions, as well as to formulate drilling fluid with greater capacity and operating stability under HPHT conditions. It was also possible to use a pressure cell for oscillatory tests, obtaining the fluid's structural changes for increases in temperature and pressure in a qualitatively way.

6.1 DISCUSSIONS

The experimental data obtained indicate that water-based drilling fluids with xanthan and limestone on HPHT applications have some disadvantages, mainly under high temperatures. However, if placed on an offshore application area with high salt content in the rocky soils, it can behave more adequately. As observed in the literature, a growth of the salts content in xanthan gum solutions increments the fluid properties' capacity of the properties of the fluid to increase its transition temperature. It was also observed that the use of higher concentrations of xanthan gum improved its properties against the negative effect of temperature. It is possible to say that by exploring a little more the mixture of quantities of these two components, an improvement of the use of this drilling fluid for HPHT applications can be applied, finding a possible balance of components.

By analyzing individually and combined the effects of the components of the drilling fluids, a better understanding of the possible phenomena that occur in a macromolecular way under HPHT conditions was done, resulting in a better drilling fluid formulation. The results suggests that the xanthan gum concentration increase allows greater range of temperature and pressure during operation. This would imply a higher consumption of the power of the pumps. However, this cost would be lower than the cost of the formulation of a higher quantity of water-based drilling fluid or the use of oil-based fluid, which represents even higher costs due to the required final disposal.

6.2 LIMITATIONS

The analysis of visco-elastoplastic and thixotropic fluids such as drilling fluids is a difficult task. Fitting them to experimental models that consider variations in temperature, pressure and shear rate in a

single correlation is difficult due to their wide variation. On the other hand, the pressure cell rheometer's sensitivity limitations, due to its magnetic coupling, made it impossible to measure lower shear rates where yield stress is observed in the flow curves. This restriction represented a limitation to characterize drilling fluid under flow start-up conditions and dynamic conditions. Another limitation was found in the use of DCS to find conformational transition changes of xanthan gum with increasing concentration and pressurization of DCS, which was not yet in use.

6.3 SUGGESTIONS FOR FUTURE RESEARCH

For water-based drilling fluids with xanthan gum under high-pressure and high-temperature conditions, the following topics could be investigated in more detail in future researches:

- Carry out a detailed flow start-up study with different aging times for aged fluids that suffered thermal degradation and different xanthan gum concentrations.
- Perform water-based drilling fluid tests with xanthan gum, increasing the salt concentration in the fluid to simulate salts' dissolution condition present in the rocks during drilling.
- Determine dynamic modules through high-pressure oscillatory tests for different concentrations of xanthan gum.
- Perform oscillatory frequency tests to superposition viscosity with temperature.
- Carry out PVT tests to determine the water-based drilling fluid's free volume parameters to make a more precise fit with the Andrade-Barus, FMT and Yasutomi models, as they decrease the apparent viscosity in the function of pressure and temperature.
- Perform XRD (X-ray diffraction) and MEV (scanning electron microscope) tests for the physical-chemical analysis of the components of the drilling fluid and verify of the type of conformation of the polymeric chains of the xanthan gum present in the drilling fluid before and after thermal aging.
- Determine the amount of solid content in the different water-based drilling fluid compositions (xanthan gum concentration, NaCl concentration, Temperatures, pressure).

Finally, a general suggestion is to analyze the behavior of drilling fluid with a mixture of bentonite and xanthan gum as viscosifiers under high-pressure and high-temperature conditions.

BIBLIOGRAPHY

13B-1, R. A. **13B-1 Recommended practice standard procedure for field testing water-based drilling fluids**. 5nd. ed. Washington DC, USA: American Petroleum Institute (API), 2016.

ABDELRAHIM, K.; RAMASWAMY, H.; VOORT, F. Van de. Rheological properties of starch solutions under aseptic processing temperatures. **Food Research International**, Elsevier, v. 28, n. 5, p. 473–480, 1995.

ABEND, S.; LAGALY, G. **Sol-gel transitions of sodium montmorillonite dispersions.** Institute of Inorganic Chemistry, University of Kiel, Olshausenstr. 40-60, D-24098 Kiel, Germany, 2000.

AHMED, J.; RAMASWAMY, H. Effect of high-hydrostatic pressure and concentration on rheological characteristics of xanthan gum. **Food Hydrocolloids**, Elsevier, v. 18, n. 3, p. 367–373, 2004.

AHMED, M. A.; HEGAB, O. A.; SABRY, A. Early detection enhancement of the kick and near-balance drilling using mud logging warning sign. **Egyptian Journal of Basic and Applied Sciences**, Taylor & Francis, v. 3, n. 1, p. 85–93, 2016.

AKPAN, E. U. et al. **Water-based drilling fluids for high temperature and dispersible shale formation applications**. Tese (Doutorado) — University of Salford, 2019.

AL-MARHOUN, M.; RAHMAN, S. Optimizing the properties of water-based polymer drilling fluids for penetrating formations with electrolyte influx. **Erdol Erdgas**, p. 318–323, 1988.

ALCÁZAR-VARA, L. A.; CORTÉS-MONROY, I. R. Drilling fluids for deepwater fields: an overview. **In SPE Annual Technical Conference and Exhibition. Society of Petroleum Engineers**, BoD–Books on Demand, v. 71, 2018.

ALDERMAN, N.; GAVIGNET, A.; GUILLOT, D.; MAITLAND, G. et al. High-temperature, high-pressure rheology of water-based muds. **In SPE Annual Technical Conference and Exhibition. Society of Petroleum Engineers**, 1988.

ALI, M. S.; AL-MARHOUN, M. A. et al. The effect of high temp., high pressure and aging on water-base drilling fluids. **In SPE Annual Technical Conference and Exhibition. Society of Petroleum Engineers**, 1990.

AMANI, M.; AL-JUBOURI, M. The effect of high pressures and high temperatures on the properties of water-based drilling fluids. **Energy Science and Technology**, Citeseer, v. 4, n. 1, p. 27–33, 2012.

AMANI, M.; AL-JUBOURI, M. J. et al. An experimental investigation of the effects of ultra-high pressures and temperatures on the rheological properties of water-based drilling fluids. **In SPE Annual Technical Conference and Exhibition. Society of Petroleum Engineers**, 2012.

ANDRADE, D. E.; FERNANDES, R. R.; SANTOS, T. G.; CECCON, E. V.; CRUZ, A. C. da; FRANCO, A. T.; NEGRÃO, C. O. Curve-fitting equation for prediction of the start-up stress overshoot of an oil-based drilling fluid. **Journal of Petroleum Science and Engineering**, Elsevier, v. 146, p. 902–908, 2016.

ANDRADE, E. D. C. The viscosity of liquids. **Nature**, Nature Publishing Group, v. 125, n. 3148, p. 309–310, 1930.

ANNE-ARCHARD, D.; MAROUCHE, M.; BOISSON, H.-C. Hydrodynamics and metzner – otto correlation in stirred vessels for yield stress fluids. **Chemical Engineering Journal**, Elsevier, v. 125, n. 1, p. 15–24, 2006.

ANNIS, M. R. et al. High-temperature flow properties of water-based drilling fluids. **Journal of Petroleum Technology**, Society of Petroleum Engineers, v. 19, n. 08, p. 1–074, 1967.

ANOOP, K.; SADR, R.; YRAC, R.; AMANI, M. Rheology of a colloidal suspension of carbon nanotube particles in a water-based drilling fluid. **Powder Technology**, Elsevier, v. 342, p. 585–593, 2019.

ARABLOO, M.; SHAHRI, M. P.; ZAMANI, M. Characterization of colloidal gas aphron-fluids produced from a new plant-based surfactant. **Journal of Dispersion Science and Technology**, Taylor & Francis, v. 34, n. 5, p. 669–678, 2013.

ARAMENDIZ, J.; IMQAM, A.; FAKHER, S. M. et al. Design and evaluation of a water-based drilling fluid formulation using sio and graphene oxide nanoparticles for unconventional shales. **International Petroleum Technology Conference**, 2019.

AULOVA, A.; OSELI, A.; BEK, M.; PRODAN, T.; EMRI, I. Effect of pressure on material properties of polymers. **Springer**, 2020.

AUTIO, K.; MYLLYMÄKI, O.; MÄLKKI, Y. Flow properties of solutions of oat β-glucans. **Journal of Food Science**, Wiley Online Library, v. 52, n. 5, p. 1364–1366, 1987.

BALED, H. O.; TAPRIYAL, D.; GAMWO, I. K.; BAMGBADE, B. A.; MCHUGH, M. A.; ENICK, R. M. Viscosity measurements of two potential deepwater viscosity standard reference fluids at high temperature and high pressure. **Journal of Chemical & Engineering Data**, ACS Publications, v. 61, n. 8, p. 2712–2719, 2016.

BARNES, H. A. The yield stress – a review or '$\pi\alpha\nu\tau\alpha\ \rho\varepsilon\iota$'- everything flows? **Journal of Non-Newtonian Fluid Mechanics**, Elsevier, v. 81, n. 1-2, p. 133–178, 1999.

BARNES, H. A. **A handbook of elementary rheology.** University of Wales, Institute of Non-Newtonian Fluid Mechanics Aberystwyth, 2000.

BARRETT, M. L. Drilling mud: a 20th century history. **Petroleum History Institute**, 2011.

BARUS, C. Isothermals, isopiestics and isometrics relative to viscosity. **American Journal of Science** (1880-1910), American Periodicals Series II, v. 45, n. 266, p. 87, 1893.

BERCEA, M.; MORARIU, S. Real-time monitoring the order-disorder conformational transition of xanthan gum. **Journal of Molecular Liquids**, Elsevier, v. 309, p. 113168, 2020.

BIRD, R. B.; CURTISS, C. F.; ARMSTRONG, R. C.; HASSAGER, O. **Dynamics of polymeric liquids, volume 2: kinetic theory**. Wiley, 1987.

BLAND, R.; WAUGHMAN, R.; TOMKINS, P.; HALLIDAY, W.; PESSIER, R.; ISBELL, M. et al. Water-based alternatives to oil-based muds: do they actually exist? **Society of Petroleum Engineers**, 2002.

BONN, D.; DENN, M. M.; BERTHIER, L.; DIVOUX, T.; MANNEVILLE, S. Yield stress materials in soft condensed matter. **Reviews of Modern Physics**, APS, v. 89, n. 3, p. 035005, 2017.

BREIT, D. **Existence theory for generalized Newtonian fluids**. Academic Press, 2017.

BRIDGMAN, P. W. The viscosity of liquids under pressure. **Proceedings of the national academy of sciences of the United States of America**, National Academy of Sciences, v. 11, n. 10, p. 603, 1925.

BRISCOE, B.; LUCKHAM, P.; REN, S. The properties of drilling muds at high pressures and high temperatures. **Philosophical Transactions of the Royal Society of London**. Series A: Physical and Engineering Sciences, The Royal Society London, v. 348, n. 1687, p. 179–207, 1994.

BROOKEY, T. et al. " micro-bubbles": new aphron drill-in fluid technique reduces formation damage in horizontal wells. **In SPE Annual Technical Conference and Exhibition. Society of Petroleum Engineers** , 1998.

BRUNCHI, C.-E.; AVADANEI, M.; BERCEA, M.; MORARIU, S. Chain conformation of xanthan in solution as influenced by temperature and salt addition. **Journal of Molecular Liquids**, Elsevier, v. 287, p. 111008, 2019.

BUENO, V. B.; PETRI, D. F. S. Xanthan hydrogel films: Molecular conformation, charge density and protein carriers. **Carbohydrate Polymers**, v. 101, p. 897–904, 2014.

CAENN HCH DARLEY, G. R. G. R. **Composition and properties of drilling and completion fluid**, 1th editions. Gulf Professional Publishing, 2017.

CAENN, R.; CHILLINGAR, G. V. Drilling fluids: state of the art. **Journal of Petroleum Science and Engineering**, Elsevier, v. 14, n. 3-4, p. 221–230, 1996.

CALLET, F.; MILAS, M.; RINAUDO, M. On the role of thermal treatments on the properties of xanthan solutions. **Carbohydrate Polymers**, Elsevier, v. 11, n. 2, p. 127–137, 1989.

CAMESANO, T. A.; WILKINSON, K. J. Single molecule study of xanthan conformation using atomic force microscopy. **Biomacromolecules**, ACS Publications, v. 2, n. 4, p. 1184–1191, 2001.

CARLSEN, L. A.; NYGAARD, G.; NIKOLAOU, M. Evaluation of control methods for drilling operations with unexpected gas influx. **Journal of Process Control**, Elsevier, v. 23, n. 3, p. 306–316, 2013.

CASTELLS, X. E. **Tratamiento y valorización energética de residuos**. Ediciones Díaz de Santos, 2012.

CHERU, A. J. **Kick detection using downhole weight measurements.** Thesis (Master's degree) — Norwegian University of Science and Technology, 2017.

CHESSER, B. G.; ENRIGHT, D. P. et al. High-temperature stabilization of drilling fluids with a low-molecular-weight copolymer. **Journal of Petroleum Technology**, Society of Petroleum Engineers, v. 32, n. 06, p. 950–956, 1980.

CHHABRA, R. P.**Non-Newtonian fluids: an introduction.** Springer, 2010.

CHHABRA, R. P.; RICHARDSON, J. F. **Non-Newtonian flow and applied rheology: engineering applications**. Butterworth-Heinemann, 2011.

CHILINGARIAN, G. V.; VORABUTR, P. **Drilling and drilling fluids**. Elsevier Science Pub. Co., Inc., New York, NY, 1983.

COUSSOT, P.; GAULARD, F. Gravity flow instability of viscoplastic materials: the ketchup drip. **Physical Review E.**, APS, v. 72, n. 3, p. 031409, 2005.

COUSSOT, P.; NGUYEN, Q. D.; HUYNH, H.; BONN, D. Viscosity bifurcation in thixotropic, yielding fluids. **Journal of Rheology**, The Society of Rheology, v. 46, n. 3, p. 573–589, 2002.

CRUZ, F. D.; CHEVOIR, F.; BONN, D.; COUSSOT, P. Viscosity bifurcation in granular materials, foams, and emulsions. **Physical Review E.**, APS, v. 66, n. 5, p. 051305, 2002.

D3418, S. A. D3418-12. **Standard test method for transition temperatures and enthalpies of fusion and crystallization of polymers by differential scanning calorimetry**, ASTM International, 2012.

DARBY, R. Viscoelastic fluids. **An introduction to their properties and behavior**, Marcel Dekker, 1976.

DARLEY, H. C.; GRAY, G. R. **Composition and properties of drilling and completion fluids**. Gulf Professional Publishing, 1988.

DEALY, J. M. **Rheometers for molten plastics: a practical guide to testing and property measurement**; 1982.

DESHPANDE, A. P. Oscillatory shear rheology for probing nonlinear viscoelasticity of complex fluids: Large amplitude oscillatory shear. In: **Rheology of complex fluids**. Springer, 2010. p. 87–110.

DESHPANDE ABHIJIT P., K. J. M. K. S. E. **Rheology of complex fluids**. Springer Nature Logo, 2010.

DIVOUX, T.; GRENARD, V.; MANNEVILLE, S. Rheological hysteresis in soft glassy materials. **Physical Review Letters**, APS, v. 110, n. 1, p. 018304, 2013.

DONG, G.; CHEN, P. A review of the evaluation methods and control technologies for trapped annular pressure in deepwater oil and gas wells. **Journal of Natural Gas Science and Engineering**, Elsevier, v. 37, p. 85–105, 2017.

DOOLITTLE, A. K. Studies in newtonian flow. ii. the dependence of the viscosity of liquids on free-space. **Journal of Applied Physics**, American Institute of Physics, v. 22, n. 12, p. 1471–1475, 1951.

ECHT, T.; PLANK, J. An improved test protocol for high temperature carrying capacity of drilling fluids exemplified on a sepiolite mud. **Journal of Natural Gas Science and Engineering**, Elsevier, v. 70, p. 102964, 2019.

ELKATATNY, S.; KAMAL, M. S.; ALAKBARI, F.; MAHMOUD, M. Optimizing the rheological properties of water-based drilling fluid using clays and nanoparticles for drilling horizontal and multi-lateral wells. **Applied Rheology**, De Gruyter, v. 28, n. 4, 2018.

EREN, N. M.; SANTOS, P. H.; CAMPANELLA, O. Mechanically modified xanthan gum: Rheology and polydispersity aspects. **Carbohydrate polymers**, Elsevier, v. 134, p. 475–484, 2015.

FERNANDES, R. R.; ANDRADE, D. E.; FRANCO, A. T.; NEGRÃO, C. O. The yielding and the linear-to-nonlinear viscoelastic transition of an elastoviscoplastic material. **Journal of Rheology**, Society of Rheology, v. 61, n. 5, p. 893–903, 2017.

FERNANDEZ, D. P.; MULEV, Y.; GOODWIN, A.; SENGERS, J. L. A database for the static dielectric constant of water and steam. **Journal of Physical and Chemical Reference Data**, American Institute of Physics for the National Institute of Standards and Technology, v. 24, n. 1, p. 33–70, 1995.

FERRY, J. D. **Viscoelastic properties of polymers**. John Wiley & Sons, 1980.

FILLERS, R.; TSCHOEGL, N. The effect of pressure on the mechanical properties of polymers. **Transactions of the Society of Rheology**, SOR, v. 21, n. 1, p. 51–100, 1977.

FOSTER, W. R.; SAVINS, J.; WAITE, J. Lattice expansion and rheological behavior relationships in water-montmorillonite systems. **Clays and Clay Minerals**, Springer, v. 3, n. 1, p. 296–316, 1954.

GARCIA-OCHOA, F.; SANTOS, V.; CASAS, J.; GÓMEZ, E. Xanthan gum: production, recovery, and properties. **Biotechnology Advances**, Elsevier, v. 18, n. 7, p. 549–579, 2000.

GILMAN, J. J. **Micromechanics of flow in solids**. McGraw-Hill, 1969.

GOKDEMIR, M. G.; ERKEKOL, S.; DOGAN, H. A. Investigation of high pressure effect on drilling fluid rheology. **In ASME 2017 36th International Conference on Ocean, Offshore and Arctic Engineering**. American Society of Mechanical Engineers Digital Collection. 2017.

GRAY, G.; NEZNAYKO, M.; GILKESON, P. et al. Some factors affecting the solidification of lime-treated muds at high temperatures. **American Petroleum Institute**, 1952.

GULREZ, S. K.; AL-ASSAF, S.; FANG, Y.; PHILLIPS, G. O.; GUNNING, A. P. Revisiting the conformation of xanthan and the effect of industrially relevant treatments. **Carbohydrate polymers**, Elsevier, v. 90, n. 3, p. 1235–1243, 2012.

GUVEN, N.; PANFIL, D.; CARNEY, L. et al. Comparative rheology of water-based drilling fluids with various clays. **In SPE Annual Technical Conference and Exhibition. Society of Petroleum Engineers** , 1988.

HAMED, S. B.; BELHADRI, M. Rheological properties of biopolymers drilling fluids. **Journal of Petroleum Science and Engineering**, Elsevier, v. 67, n. 3-4, p. 84–90, 2009.

HERMOSO, J.; JOFORE, B. D.; MARTÍNEZ-BOZA, F.; GALLEGOS, C. High pressure mixing rheology of drilling fluids. **Industrial & Engineering Chemistry Research**, ACS Publications, v. 51, n. 44, p. 14399–14407, 2014.

HERMOSO, J.; MARTÍNEZ-BOZA, F.; GALLEGOS, C. Combined effect of pressure and temperature on the viscous behaviour of all-oil drilling fluids. **Oil & Gas Science and Technology–Revue d'IFP Energies nouvelles**, Technip, v. 69, n. 7, p. 1283–1296, 2014.

HERMOSO, J.; MARTÍNEZ-BOZA, F. J.; GALLEGOS, C. Modeling pressure-viscosity behavior of oil-based drilling fluids. **Oil & Gas Science and Technology–Revue d'IFP Energies nouvelles**, EDP Sciences, v. 72, n. 4, p. 18, 2017.

HERZHAFT, B.; ROUSSEAU, L.; NEAU, L.; MOAN, M.; BOSSARD, F. et al. Influence of temperature and clays/emulsion microstructure on oil-based mud low shear rate rheology. **In SPE Annual Technical Conference and Exhibition. Society of Petroleum Engineers** , 2002.

HILLE, M. et al. Vinylsulfonate/vinylamide copolymers in drilling fluids for deep, high-temperature wells. **In SPE Annual Technical Conference and Exhibition. Society of Petroleum Engineers** , 1985.

HILLER, K. et al. Rheological measurements on clay suspensions and drilling fluids at high temperatures and pressures. **Journal of Petroleum Technology**, Society of Petroleum Engineers, v. 15, n. 07, p. 779–788, 1963.

HOLZWARTH, G.; PRESTRIDGE, E. Multistranded helix in xanthan polysaccharide. **Science**, American Association for the Advancement of Science, v. 197, n. 4305, p. 757–759, 1977.

HOUWEN, S. C. R. O.; T GEEHAN, S. F. Rheology of oil-based. **61st Annual Technical Conference and Exhibition of the Society of Petroleum Engineers held**, v. 1, n. 12, p.125–125, 1986.

HUYNH, H.; ROUSSEL, N.; COUSSOT, P. Aging and free surface flow of a thixotropic fluid. **Physics of Fluids**, American Institute of Physics, v. 17, n. 3, p. 033101, 2005.

IADC. **Directional drilling stand-alone chapter of the IADC drilling manual**, 12th editions. International Association of Drilling Contractors, 2014.

IBEH, C. S. Investigation on the effects of ultra-high pressure and temperature on the rheological properties of oil-based drilling fluids. **Unpublished MSc Project Report**, Texas A&M University, USA, 2007.

JAIN, R.; MAHTO, V.; SHARMA, V. Evaluation of polyacrylamide-grafted-polyethylene glycol/silica nanocomposite as potential additive in water based drilling mud for reactive shale formation. **Journal of Natural Gas Science and Engineering**, Elsevier, v. 26, p. 526–537, 2015.

JR, W. M.; BENNETT, R.; BLAND, R. et al. The effect of temperature and pressure on the viscosity of oil-base muds. **Journal of Petroleum Technology**, Society of Petroleum Engineers, v. 27, n. 07, p. 884–886, 1975.

KATZBAUER, B. Properties and applications of xanthan gum. **Polymer Degradation and Stability**, Elsevier, v. 59, n. 1-3, p. 81–84, 1998.

KAWAKAMI, K.; NORISUYE, T. Second virial coefficient for charged rods: sodium xanthan in aqueous sodium chloride. **Macromolecules**, ACS Publications, v. 24, n. 17, p. 4898–4903, 1991.

KELESSIDIS, V. Sustainable drilling for oil and gas: challenging drilling environments de-mand new formulations of bentonite based drilling fluids. **In 3rd International Conference on Sustainable Development Indicators in the Minerals Industry**, Milos island, Greece in june 2007.

KELESSIDIS, V.; DALAMARINIS, P. Monitoring drilling bit parameters allows optimization of drilling rates. **In International Multidisciplinary Scientific GeoConference: SGEM, 1, 605**, 2009.

KRUMEL, K.; SARKAR, N. Rheology of gums important in formulation-flow properties of natural and synthetic hydrocolloids. **Food Technology**, Inst Food Technologists Suites, v. 29, n. 4, p. 36, 1975.

KURU, E.; BJORNDALEN, N.; JOSSY, E.; ALVAREZ, J. et al. Reducing formation damage with microbubble-based drilling fluid: Understanding the blocking ability. **Journal of Canadian Petroleum Technology**, Petroleum Society of Canada, v. 47, n. 11, 2008.

LAGOUEYTE, N.; PAQUIN, P. Effects of microfluidization on the functional properties of xanthan gum. **Food Hydrocolloids**, Elsevier, v. 12, n. 3, p. 365–371, 1998.

LAMB, J. Viscoelasticity and lubrication: a review of liquid properties. **Journal of Rheology**, The Society of Rheology, v. 22, n. 4, p. 317–347, 1978.

LANEUVILLE, S. I.; TURGEON, S. L.; PAQUIN, P. Changes in the physical properties of xanthan gum induced by a dynamic high-pressure treatment. **Carbohydrate polymers**, Elsevier, v. 92, n. 2, p. 2327–2336, 2013.

LAPASIN, R.; PRICL, S. **Rheology of industrial polysaccharides; theory and applications**. Chapman & Hall, 1995.

MAGLIONE, R.; GALLINO, G.; ROBOTTI, G.; ROMAGNOLI, R.; ROMMETVEIT, R. et al. A drilling well as viscometer: studying the effects of well pressure and temperature on the rheology of the drilling fluids. **In SPE Annual Technical Conference and Exhibition. Society of Petroleum Engineers** , 1996.

MAO, H.; YANG, Y.; ZHANG, H.; ZHANG, J.; HUANG, Y. A critical review of the possible effects of physical and chemical properties of subcritical water on the performance of water-based drilling fluids designed for ultra-high temperature and ultra-high pressure drilling applications. **Journal of Petroleum Science and Engineering**, Elsevier, p. 106795, 2019.

MARCOTTE, M.; HOSHAHILI, A. R. T.; RAMASWAMY, H. Rheological properties of selected hydrocolloids as a function of concentration and temperature. **Food Research International**, Elsevier, v. 34, n. 8, p. 695–703, 2001.

MARTÍN-ALFONSO, M. J.; MARTÍNEZ-BOZA, F. J.; NAVARRO, F. J.; FERNÁNDEZ, M.; GALLEGOS, C. Pressure-temperature-viscosity relationship for heavy petroleum fractions. **Fuel**, Elsevier, v. 86, n. 1-2, p. 227–233, 2007.

MENDES, P. R. de S.; THOMPSON, R. L. Time-dependent yield stress materials. **Current Opinion in Colloid & Interface Science**, Elsevier, 2019.

MEWIS, J.; WAGNER, N. J. Thixotropy. **Advances in Colloid and Interface Science**, Elsevier, v. 147, p. 214–227, 2009.

MEZGER, T. G. **Applied rheology: with Joe flow on rheology road**. Anton Paar, 2015.

MILAS, M.; RINAUDO, M.; KNIPPER, M.; SCHUPPISER, J. L. Flow and viscoelastic properties of xanthan gum solutions. **Macromolecules**, ACS Publications, v. 23, n. 9, p. 2506–2511, 1990.

MITCHELL, M. Complex systems: Network thinking. **Artificial Intelligence**, Elsevier, v. 170, n. 18, p. 1194–1212, 2006.

MITCHELL, R.; MISKA, S. et al. **Fundamentals of drilling engineering**. Society of Petroleum Engineers, 2011.

MOHIDEEN, A. A. M.; SAHEED, M. S. M.; MOHAMED, N. M. Multiwalled carbon nanotubes and graphene oxide as nano-additives in water-based drilling fluid for enhanced fluid-loss-control & gel strength. **In AIP Conference Proceedings** (Vol. 2151, No. 1, p. 020001), AIP Publishing LLC, v. 2151, n. 1, p. 020001, 2019.

MOONAN, W.; TSCHOEGL, N. The effect of pressure on the mechanical properties of polymers. iv. measurements in torsion. **Journal of Polymer Science: Polymer Physics Edition**, Wiley Online Library, v. 23, n. 4, p. 623–651, 1985.

MOORHOUSE, R.; WALKINSHAW, M.; ARNOTT, S.**Xanthan gumâ– molecular conformation and interactions**. ACS Publications, 1977.

MORAES, M. A. D.; SILVA, C. F. D.; VIEIRA, R. S. **Biopolymer Membranes and Films: Health, Food, Environment, and Energy Applications**. Elsevier, 2020.

MORRISON, F. A. et al.**Understanding rheology**. Topics in Chemical Engineering, 2001.

MOURA, M. R. V. de; MORENO, R. B. Z. L. Concentration, brine salinity and temperature effects on xanthan gum solutions rheology. **Applied Rheology**, De Gruyter, v. 29, n. 1, p. 69–79, 2019.

NEFF, J. M. Composition, environmental fates, and biological effect of water-based drilling muds and cuttings discharged to the marine environment: a synthesis and annotated bibliography, **In Report Prepared for the Petroleum Environmental Research Forum (PERF)**. Washington DC, 2005.

NISHINARI, K.; WATASE, M.; RINAUDO, M.; MILAS, M. Characterization and properties of gellan-κ-carrageenan mixed gels. **Food Hydrocolloids**, Elsevier, v. 10, n. 3, p. 277–283, 1996.

OGAWA, K.; YUI, T. **Polysaccharides: structural diversity and functional versatility-X–ray diffraction study of polysaccharides**. Marcel Dekker, New York, 1998.

OLIVEIRA, R. C. T. **Long-range description of rheological properties of a high-pressure high-temperature oil-based drilling fluid**. Thesis (Doctorate) — Texas A & M University, 2016.

OLPHEN, H. V. **An introduction to clay colloid chemistry, for clay technologists, geologists, and soil scientists**. New York Wiley, 1963.

OLPHEN, H. V. **Clay colloid chemistry: for clay technologists, geologists, and soil scientists**. Krieger, 1991.

OORT, E. van; HALE, A. H.; MODY, F.; ROY, S. et al. Transport in shales and the design of improved water-based shale drilling fluids. **SPE Drilling & Completion**, Society of Petroleum Engineers, v. 11, n. 03, p. 137–146, 1996.

OSAKI, K. **Molecular conformation and dynamics of macromolecules in condensed systems**. Elsevier: Amsterdam, p. 185–201, 1987.

OSSWALD T., . R. N. **Polymer rheology**. Carl Hanser, München, 2015.

OSTWALD, W. Ueber die geschwindigkeitsfunktion der viskosität disperser systeme. **Kolloid-Zeitschrift**, Springer, v. 36, n. 3, p. 157–167, 1925.

PANASETI, P.; DAMIANOU, Y.; GEORGIOU, G. C.; HOUSIADAS, K. D. Pressure-driven flow of a herschel-bulkley fluid with pressure-dependent rheological parameters. **Physics of Fluids**, AIP Publishing LLC, v. 30, n. 3, p. 030701, 2018.

PELLETIER, E.; VIEBKE, C.; MEADOWS, J.; WILLIAMS, P. A rheological study of the order–disorder conformational transition of xanthan gum. **Biopolymers: Original Research on Biomolecules**, Wiley Online Library, v. 59, n. 5, p. 339–346, 2001.

PERCEC, V.; PUGH, C. **Comprehensive Polymer Science and Supplements**. Elsevier: Oxford, UK, 1989.

PIBER, M.; PROHASKA, M.; HUBLIK, G.; THONHAUSER, G. et al. Time-dependent behavior of drilling fluids under cyclic temperature and pressure loads. **In SPE Annual Technical Conference and Exhibition. Society of Petroleum Engineers** , 2006.

PICÓ, Y. **Chemical analysis of food: Techniques and applications**. Academic Press, 2012.

QUILAQUEO, M.; AGUILERA, J. M. Crystallization of nacl by fast evaporation of water in droplets of nacl solutions. **Food Research International**, v. 84, p. 143–149, 2016.

RAO, M.; WALTER, R.; COOLEY, H. Effect of heat treatment on the flow properties of aqueous guar gum and sodium carboxymethylcellulose (cmc) solutions. **Journal of Food Science**, Wiley Online Library, v. 46, n. 3, p. 896–899, 1981.

RAPP, B. E. **Microfluidics: modeling, mechanics and mathematics**. William Andrew, 2016.

RAVI, A. **Experimental assessment of water-based drilling fluids in high pressure and high temperature conditions**. Thesis (Doctorate) — Texas A & M University, 2012.

REINOSO, D.; MARTIN-ALFONSO, M.; LUCKHAM, P.; MARTINEZ-BOZA, F. Rheological characterisation of xanthan gum in brine solutions at high temperature. **Carbohydrate Polymers**, Elsevier, v. 203, p. 103–109, 2019.

RINAUDO, M. Relation between the molecular structure of some polysaccharides and original properties in sol and gel states. **Food Hydrocolloids**, Elsevier, v. 15, n. 4-6, p. 433–440, 2001.

ROCHEFORT, W. E.; MIDDLEMAN, S. Rheology of xanthan gum: salt, temperature, and strain effects in oscillatory and steady shear experiments. **Journal of Rheology**, The Society of Rheology, v. 31, n. 4, p. 337–369, 1987.

ROMMETVEIT, R.; BJORKEVOLL, K. et al. Temperature and pressure effects on drilling fluid rheology and ecd in very deep wells. **In SPE Annual Technical Conference and Exhibition. Society of Petroleum Engineers** , 1997.

ROSALAM, S.; ENGLAND, R. Review of xanthan gum production from unmodified starches by xanthomonas comprestris sp. **Enzyme and Microbial Technology**, Elsevier, v. 39, n. 2, p. 197–207, 2006.

ROSE, M. A. The environmental impacts of offshore oil drilling. **Technology and Engineering Teacher**, International Technology Education Association, v. 68, n. 5, p. 27, 2009.

ROSSI, S.; LUCKHAM, P.; ZHU, S.; BRISCOE, B. et al. High-pressure/high-temperature rheology of na^{+}montmorillonite clay suspensions. **SPE International Symposium on Oilfield Chemistry**, Society of Petroleum Engineers, 1999.

ROYER, J. R.; DESIMONE, J. M.; KHAN, S. A. High-pressure rheology and viscoelastic scaling predictions of polymer melts containing liquid and supercritical carbon dioxide. **Journal of Polymer Science Part B: Polymer Physics**, Wiley Online Library, v. 39, n. 23, p. 3055–3066, 2001.

SALIMI, S.; SADEGHY, K.; KHARANDISH, M. **Rheological behaviour of polymer-extended water-based drilling muds at high pressures and temperatures**. University of Tehran, Iran, p. 1–6, 2000.

SEYMOUR, K.; MACANDREW, R. et al. The design, drilling, and testing of a deviated high-temperature, high-pressure exploration well in the north sea. **Offshore Technology Conference**, 1993.

SOHM, R.; TADROS, T. F. Viscoelastic properties of sodium montmorillonite (gelwhite h) suspensions. **Journal of Colloid and Interface Science**, Elsevier, v. 132, n. 1, p. 62–71, 1989.

SONG, K.-W.; KIM, Y.-S.; CHANG, G.-S. Rheology of concentrated xanthan gum solutions: steady shear flow behavior. **Fibers and Polymers**, Springer, v. 7, n. 2, p. 129–138, 2006.

SPEERS, R.; TUNG, M. Concentration and temperature dependence of flow behavior of xanthan gum dispersions. **Journal of Food Science**, Wiley Online Library, v. 51, n. 1, p. 96–98, 1986.

SPRIK, M. Hydrogen bonding and the static dielectric constant in liquid water. **The Journal of Chemical Physics**, American Institute of Physics, v. 95, n. 9, p. 6762–6769, 1991.

SRINI-VASAN, S.; GATLIN, C. et al. The effect of temperature on the flow properties of clay-water drilling muds. **Journal of Petroleum Technology**, Society of Petroleum Engineers, v. 10, n. 12, p. 59–60, 1958.

SUN, W.; CHEN, J.; LI, Z. et al. Comparison of rheological models in high shear rate range and experimental relationship between penetration rate and high shear viscosities. **Society of Petroleum Engineers**, 1986.

SURESH, S.; NAIK, V. Hydrogen bond thermodynamic properties of water from dielectric constant data. **The Journal of Chemical Physics**, American Institute of Physics, v. 113, n. 21, p. 9727–9732, 2000.

TAM, K.; TIU, C. Steady and dynamic shear properties of aqueous polymer solutions. **Journal of Rheology**, The Society of Rheology, v. 33, n. 2, p. 257–280, 1989.

TELESFORO, S.; ANTONIO, H. **Rheological behavior of an OBM sample of the GOM under xHPHT conditions**. Thesis (Doctorate) — Texas A & M University, 2017.

TIPVARAKARNKOON, T.; SENGE, B. **Effect of high pressure treatment on rheological properties of xanthan/guar mixtures**. Department of Food Rheology, Technology University Berlin, Berlin, Germany, 2010.

TSCHOEGL, N. W.; KNAUSS, W. G.; EMRI, I. The effect of temperature and pressure on the mechanical properties of thermo-and/or piezorheologically simple polymeric materials in thermodynamic equilibrium–a critical review. **Mechanics of Time-Dependent Materials**, Springer, v. 6, n. 1, p. 53–99, 2002.

TSCHOEGL, N. W.; KNAUSS, W. G.; EMRI, I. Poisson's ratio in linear viscoelasticity–a critical review. **Mechanics of Time-Dependent Materials**, Springer, v. 6, n. 1, p. 3–51, 2002.

URLACHER, B.; NOBLE, O. Xanthan gum. In: **Thickening and Gelling Agents for Food**. Springer, 1997. p. 284–311.

VAJARGAH, A. K.; OORT, E. van. Early kick detection and well control decision-making for managed pressure drilling automation. **Journal of Natural Gas Science and Engineering**, Elsevier, v. 27, p. 354–366, 2015.

WANG, Y.; WANG, S.-Q. Exploring stress overshoot phenomenon upon startup deformation of entangled linear polymeric liquids. **Journal of Rheology**, The Society of Rheology, v. 53, n. 6, p. 1389–1401, 2009.

WILLIAM, J. K. M.; PONMANI, S.; SAMUEL, R.; NAGARAJAN, R.; SANGWAI, J. S. Effect of cuo and zno nanofluids in xanthan gum on thermal, electrical and high pressure rheology of water-based drilling fluids. **Journal of Petroleum Science and Engineering**, Elsevier, v. 117, p. 15–27, 2014.

WILLIAMS, M. L.; LANDEL, R. F.; FERRY, J. D. The temperature dependence of relaxation mechanisms in amorphous polymers and other glass-forming liquids. **Journal of the American Chemical Society**, ACS Publications, v. 77, n. 14, p. 3701–3707, 1955.

WILLIAMS, P.; DAY, D.; LANGDON, M.; PHILLIPS, G.; NISHINARI, K. Synergistic interaction of xanthan gum with glucomannans and galactomannans. **Food Hydrocolloids**, Elsevier, v. 4, n. 6, p. 489–493, 1991.

XIE, W.; LECOURTIER, J. Xanthan behaviour in water-based drilling fluids. **Polymer Degradation and Stability**, Elsevier, v. 38, n. 2, p. 155–164, 1992.

XU, L.; ZHAO, L.; XU, M. B.; XU, J.; WANG, X. **Lab investigations into high temperature high pressure rheology of water-based drilling fluid**. Trans Tech Publ, v. 418, p. 191–195, 2013.

XUEWU, Z.; XIN, L.; DEXIANG, G.; WEI, Z.; TONG, X.; YONGHONG, M. Rheological models for xanthan gum. **Journal of Food Engineering**, Elsevier, v. 27, n. 2, p. 203–209, 1996.

ZHANG, R.; WANG, R.-h.; QIU, Z.-s. Temperature/pressure relationships of yield stress and plastic viscosity for foamed drilling fluids. **Oilfield Chemistry**, v. 22, n. 1, p. 6–12, 2005.

ZHOU, Y.; SHAH, S. N. Rheological properties and frictional pressure loss of drilling, completion, and stimulation fluids in coiled tubing. **Journal Fluids Eng.**, v. 126, n. 2, p. 153–161, 2004.

APPENDIX A - RHEOMETRY AND GEOMETRY VERIFICATION TESTS

This appendix shows the tests' verification under atmospheric pressure and high-pressure conditions to understand some variations observed in rheological measurements depending on the type of rheometer and type of geometry.

A.1 Atmosphere Pressure Measurement

By comparing the flow curve measurements between rheometers and the two types of geometries available in LabReo laboratory, it was possible to identify the differences between each piece of equipment and each geometry, allowing to define a suitable geometry for measurements of water-based drilling fluid and to demonstrate the few differences between the Anton Paar MCR 702TD, Haake Mars III, and TA Instruments DHR-3 rheometer.

The geometries used with Anton Paar MCR 702TD were showed in section 4.2.1, for Haake Mars III were used serrated plate-plate geometry of 35 mm with a gap of 1 mm and Mooney-Ewart coaxial cylinder of 25 mm inner diameter with a radius ratio of 1.089 with a bottom gap of 4 mm as shown in Figure A.1 (a)-(b). For TA Instruments DHR-3 were used serrated plate-plate geometry of 40 mm with a gap of 1 mm and a Smart-Swap coaxial cylinder of 28 mm inner diameter with a radius ratio of 1.084 bottom a gap of 4 mm as shown in Figure A.1 (c)-(d). Tests with different xanthan gum concentrations were carried out in parallel on the TA Instrument rheometer when high-pressure tests were performed with the Anton Paar rheometer.

Table A.1 shows the shear stress with their respective standard deviation between the measurements made at 25 ºC. To achieve a better degree of comparison, the torque and angular velocity data measured by the rheometers were used.

Table A.1 – Experimental measurements of shear stress with the geometries of parallel plates (PP) and concentric cylinders (CC) with the rheometers Anton Paar MCR 702TD, Haake Mars III, and TA Instrument DHR 3.

Shear Rate $[s^{-1}]$	**TA instrument DHR 3**		**Haake Mars III**		**Anton Paar MCR 702TD**	
	CC	PP	CC	PP	CC	PP
	Shear Stress[Pa]					
400	$22.52^{\pm 0.20}$	$23.18^{\pm 1.22}$	$22.39^{\pm 1.13}$	$22.99^{\pm 2.84}$	$22.62^{\pm 0.16}$	$23.28^{\pm 1.52}$
350	$21.22^{\pm 0.61}$	$20.90^{\pm 1.04}$	$21.14^{\pm 0.96}$	$20.88^{\pm 2.08}$	$21.32^{\pm 0.26}$	$20.93^{\pm 1.45}$
300	$19.70^{\pm 0.09}$	$19.04^{\pm 0.22}$	$19.60^{\pm 0.93}$	$18.96^{\pm 1.83}$	$19.74^{\pm 0.13}$	$19.13^{\pm 1.42}$
250	$17.90^{\pm 0.16}$	$17.02^{\pm 0.59}$	$17.84^{\pm 0.88}$	$16.94^{\pm 1.54}$	$17.99^{\pm 0.56}$	$17.13^{\pm 1.39}$
200	$15.92^{\pm 0.31}$	$14.95^{\pm 0.67}$	$15.79^{\pm 0.79}$	$14.61^{\pm 1.30}$	$15.96^{\pm 0.11}$	$14.97^{\pm 0.96}$
150	$13.55^{\pm 0.11}$	$12.48^{\pm 0.32}$	$13.43^{\pm 0.69}$	$12.44^{\pm 0.93}$	$13.62^{\pm 0.09}$	$12.54^{\pm 0.72}$
100	$10.72^{\pm 0.18}$	$9.69^{\pm 0.16}$	$10.63^{\pm 0.58}$	$9.57^{\pm 0.70}$	$10.79^{\pm 0.07}$	$9.74^{\pm 0.46}$
50	$7.25^{\pm 0.86}$	$6.26^{\pm 0.56}$	$7.06^{\pm 0.45}$	$6.25^{\pm 0.47}$	$7.20^{\pm 0.66}$	$6.39^{\pm 0.12}$
10	$2.83^{\pm 1.21}$	$2.47^{\pm 0.34}$	$2.81^{\pm 0.16}$	$2.43^{\pm 0.94}$	$2.61^{\pm 0.01}$	$2.52^{\pm 0.05}$
1	$1.24^{\pm 2.11}$	$1.08^{\pm 0.91}$	$0.96^{\pm 0.03}$	$0.86^{\pm 0.18}$	$1.09^{\pm 1.11}$	$0.88^{\pm 0.01}$

Source: Author (2021)

Figure A.1 – (a) Serrated plate-plate for Haake Mars III; (b) Mooney-Ewart coaxial cylinder for Haake Mars III; (c) Serrated plate-plate for TA Instrument DHR-3; (d) Smart-Swap coaxial cylinder for TA Instrument DHR-3.

(a) (b) (c) (d)

Source: Author (2021).

It was observed that the differences regarding the comparison of the serrated plate-plate geometries concerning the concentric cylinders were mainly due to two factors. First, secondary flows were observed for a shear rate of 400 s^{-1}, where the shear stress was increased. And second, migration of the sample to the surroundings was observed, due to the fluid's low surface tension, which causes a decrease in the measured torque. On the other hand, the cylinders' measurements show a difference due to sliding along the smooth walls of the geometry of the Haake Mars III, and TA instruments DHR 3 rheometer.

When the temperature rises to 55 °C, the sample's migration effect grows, and other effects such as thermal inertia and evaporation occur, causing a drop in shear stress in greater quantity. Figure A.2 shows a before and after of an experiment was carried out at 55 °C. The picture is evidence sample's migration, causing a decrease in the measurement radius and the sample's dehydration at the geometry edges.

It is important to note that the Haake Mars III and TA Instruments DHR 3 rheometer use a Peltier system for temperature control, below bottom geometry, minimizing the effects of thermal inertia. When they are compared with the Anton Paar MCR 702TD rheometer, its Peltier system is located on the convection chamber walls.

Finally, when comparing the geometries of plates-plates and coaxial cylinders, it can be observed

Figure A.2 – Reduction of the sample at the edges of the plate-plate geometry for the test at 55 ºC, (a) before Haake Mars III, (b) after Haake Mars III, (c) before Anton Paar MCR 702TD and (d) after Anton Paar MCR 702TD.

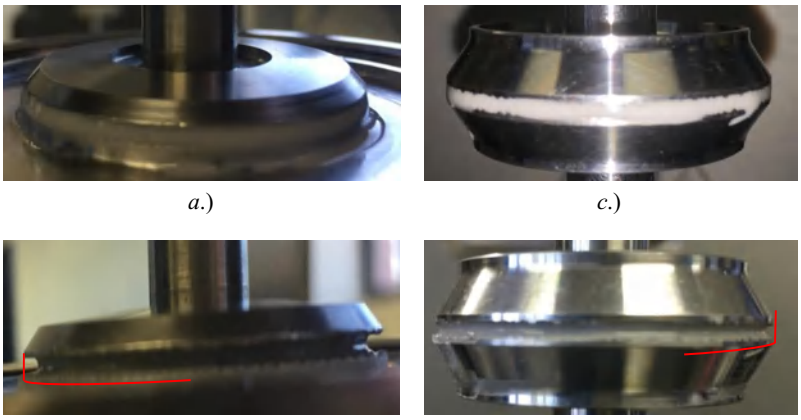

a.) *c*.)

b.) *d*.)

Source: Author (2021)

that, due to the fluid's low viscosity, the coaxial cylinders' geometry allows keeping the fluid confined without loss of mass to the environment, resulting in better results. Concentric cylinders were the most stable geometry for water-based drilling fluid measurements since they allow data acquisition at high temperatures while maintaining the measurements' precision.

Furthermore, the measurements show that regardless of the selected rheometer, the acquired data shows little difference. The factor with the greatest variation was the type of sensor. Therefore, the Anton Paar MCR 702TD and the TA instrument DHR 3 rheometer show a slight difference because Anton Paar's coaxial cylinder geometry's surface is sandblasted surface, which reduces the sliding effect of the sample with geometry.

A.2 High-Pressure Measurement

The 28H and 26S geometries available for the pressure cell were verified to determine the measurements' variations due to having different surface shapes, as seen in section 4.2.2. Figure A.3 shows us a flow curve for pressures of 10, 100, 400, 600, and 800 bar, measured in both geometries. The difference in each of the shear rates was minimal.

The results indicate that both the 28H and 26S geometry can be used for the range of shear rates tested without presenting secondary flow effects between the 28H helicoidal section or possible slip on the smooth 26S surface. On the other hand, it was performed a comparison of a shear rate ramp test and a flow curve with constant shear rates per 1000 seconds each. The tests were carried out at 10 and 600 bar pressure at a temperature of 25 ºC, where little difference was obtained in both tests.

Figure A.4 shows that no hysteresis area was observed between the up-ramp and the down-ramp in both pressures in the shear rate ramps, indicating the little thixotropy, as observed in section 5.3.1.

Figure A.3 – Comparison of measurements with the 26S and 28H geometrical smooth and helical measures with the pressure cell.

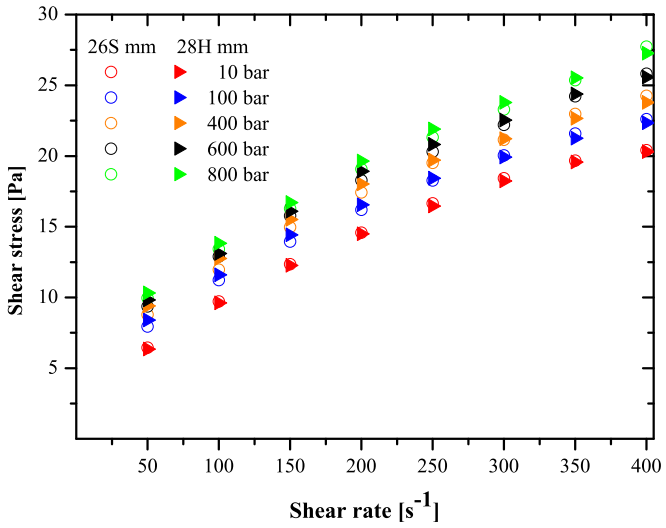

Source: Author (2021)

Figure A.4 – Comparison of flow curves with shear rate ramps and constant levels of shear rates for pressures of 10 and 600 bar at 25 ºC.

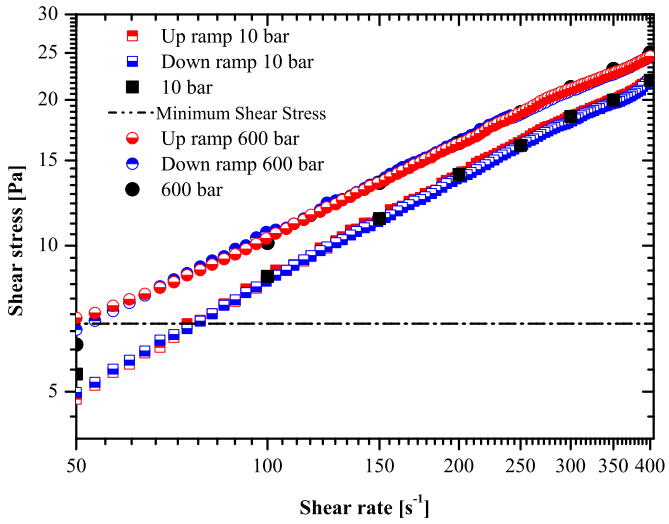

Source: Author (2021)

In conclusion, it was determined that the flow curves could be made with ramps or levels of deformation rates because the standard deviation of the measurements in the main rates was 0.18.

APPENDIX B - EFFECT OF WATER EVAPORATION

The following appendix discusses the evaporation of the water-based drilling fluid. Consequently, the use of temperature control systems Peltier-based with forced convection such as the Anton Paar MCR 702TD rheometer at high-temperature during long test times can generate evaporation. Evaporation occurs due to the high flow rate of air circulation over the sample, the air's low humidity, and the lack of concentration humidity in the atmosphere inside the protective chamber of the rheometer. The temperature control system's best configurations were evaluated of three different configurations, following the procedure in Figure B.1. Initially, the convection temperature control system is used, stabilizing the temperature at 25 ºC for 5 minutes, then a shear rate of 100 s^{-1} was imposed. The test time is defined as the average duration of the flow curve tests in a steady-state. Next, a test was carried out with the convection system off being controlled the temperature through Peltier-based, where the previous procedure was repeated. The last configuration was with the convection system off, but saturating the atmosphere inside the rheometer chamber, through cotton swabs moistened with water and controller the temperature Peltier-based.

In Figure B.2 (a) it was observed that the shear stress decreased for the first 200 seconds, caused by the breaking down of the fluid, as an effect of the imposed shear rate. As a consequence of the high airflow directed towards the sample, the shear stress begins to increase, reaching a maximum peak at 2000 seconds, probably caused by the evaporation. Evaporation occurs due to the high airflow received by the sample, which is found with a relative humidity of 22 $\pm 2\%$ measure through an Incoterm thermo-hygrometer. Furthermore, the rheometer's protective cover was an open system, so it is not easy to balance the moist air concentration. Therefore, air circulation removes water from the sample easily due to the suspensions' low absorption or osmotic forces. Intermolecular water was difficult to extract, capillary water that needs temperature for its extraction, and free water being the easiest to extract (CASTELLS, 2012). In this test, the extraction of free water was the one type that is likely to be occurring. One can notice that shear stress begins to decrease after 4000 seconds of testing. The test ended before completion for safety since the salt crystallized on the geometry is larger than the gap lateral. Therefore, using a Peltier-based forced convection temperature control system for water-based drilling fluids was not feasible. For the second condition, the shear stress takes approximately 4000 seconds to reach a constant value. In this case, the vaporization effect was observed but was slower. For the third experiment of Figure B.2 (c), the sample enters a steady-state with only 600 seconds, maintaining the shear stress stabilized throughout the test, with a possibility for executing this work.

Also, tests were carried out with a temperature of 55 ºC in order to verify the influence of a high temperature on water evaporation. Figure B.3 is shown the same three situations for a temperature of 55 ºC. In the first situation, it is interesting to note a higher shear stress peak than 25 ºC. Also, it was observed that in the next 200 seconds, after the peak, the shear stress is stabilized for 1000 seconds. Evaporation occurred more rapidly because the latent heat transfer is greater. Solids on top of the geometry were formed, having a smooth appearance. Salt crystallization was not perceived, as in the previous test.

For the second condition, the shear stress starts decreasing due to the breaking down of the sample and fluctuates for approximately 2200 seconds of the test, reaching a steady-state in the range of 2200 to 3800 seconds of the test. Then, the shear stress begins to increase after 4000 seconds, which can be concluded that the evaporation process begins, influenced by the temperature and the formation of solids on top of the geometry. Finally, the shear stress overtime for the experiment with the saturated

Figure B.1 – Procedure to identify evaporation in measurements.

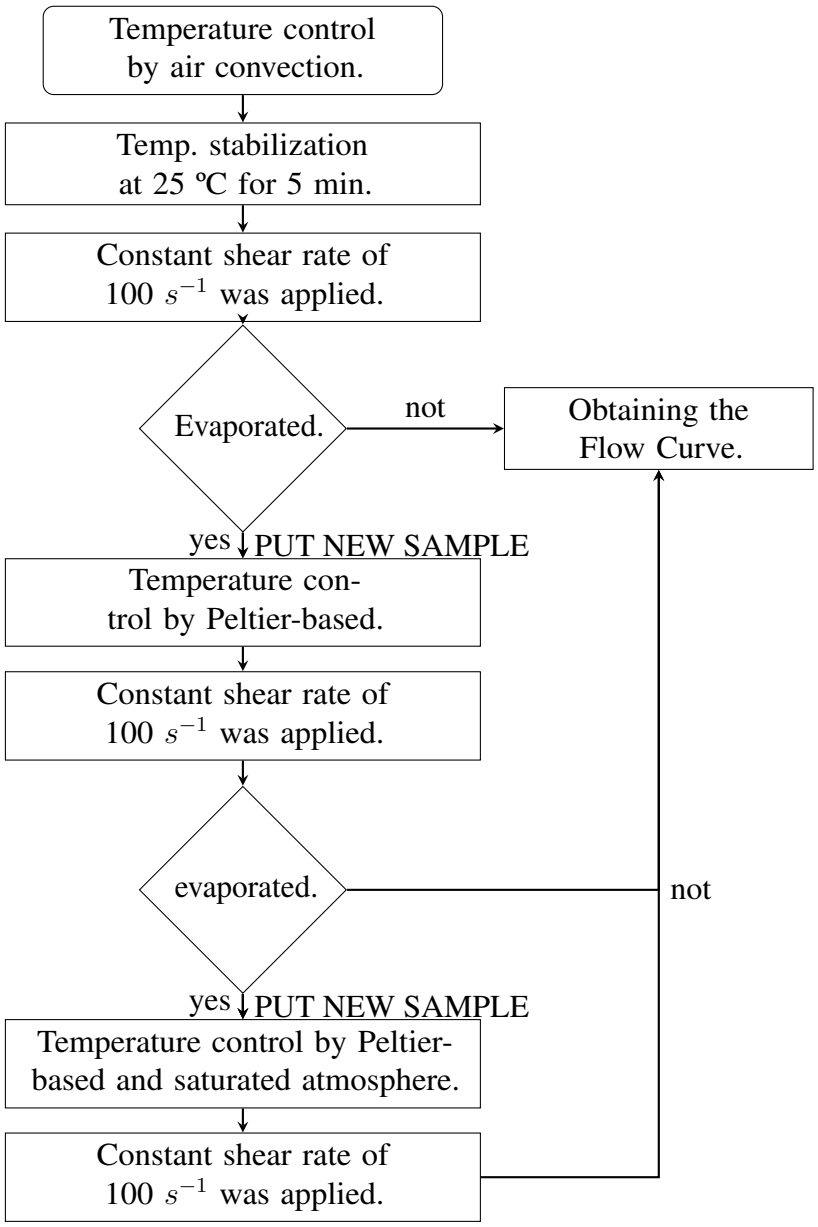

Source: Author (2021)

atmosphere is shown in Figure B.3 (c). One can see that the breaking down of the material takes 2000 seconds. After, the shear stress reaches a steady-state regime for the next 14000 seconds. A slight increase in shear stress was observed in the last 1000 seconds. At that moment, water in the pieces of cotton was evaporated, which started the evaporation of the sample's free water as it happened for the test at 25 ºC. When the stress is in a permanent regime, one can observe that the steady-state stress was smaller than the one for the second condition. The behavior is since there was a greater quantity of water at the borders of the sample.

The analysis suggests that the temperature control system with turned off convection and saturated atmosphere with temperature control by Peltier-based heating presents greater stability for

Figure B.2 – Shear stress at 25 ºC as a function of test time for shear rate levels of 100 s^{-1} with experimental conditions: (a) temperature control by convection, (b) convection turned off and (c) convection turned off and saturated atmosphere.

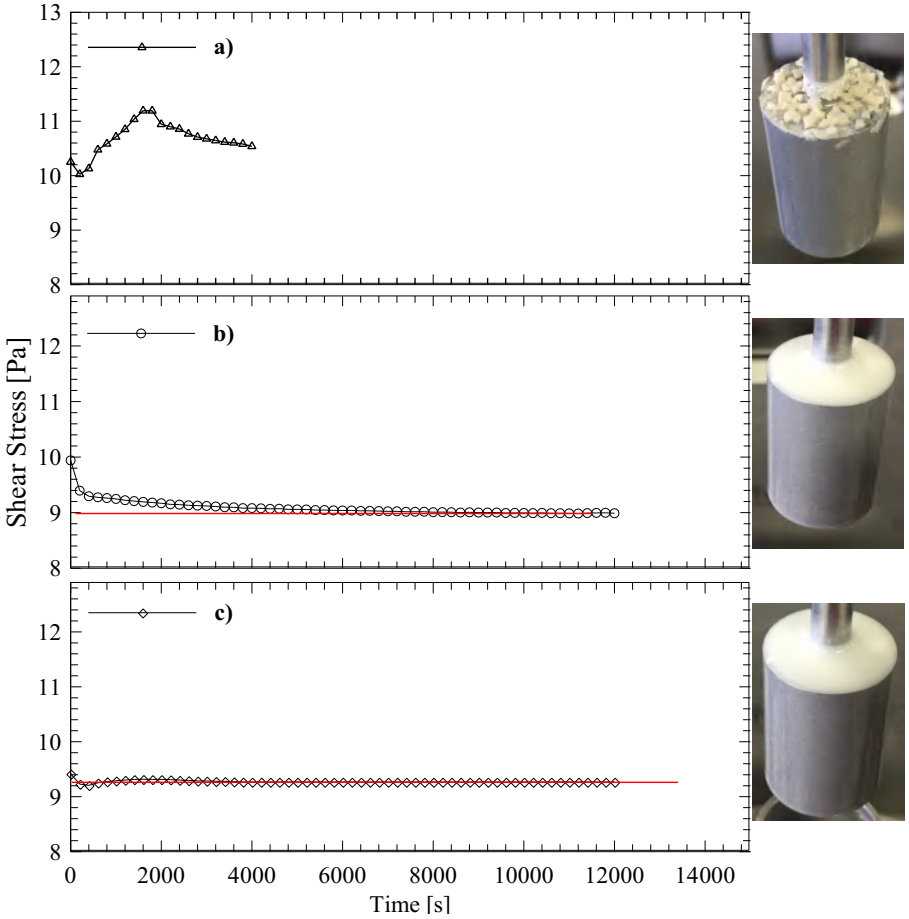

Source: Author (2021)

the acquisition of rheological data, especially in the flow curve that requires longer times and high temperatures. Therefore, this configuration was the one used in the subsequent tests.

Additionally, a comparison was made between the measurements obtained through the convection system off under saturated atmosphere and measurements through an invasive method that consists of placing a surface layer of a fluid with a lower density than of the sample to be measured, generating possible mixtures at high shear rate. In this case, SAE 25W-60 oil was used, which was placed 1 ml over the water-based drilling fluid sample to avoid evaporation. Figure B.4 shows that both methods provide similar data in the first 7000 seconds, then the oil layer method begins to present evaporation.

Figure B.3 – Shear stress at 55 ºC as a function of test time for shear rate levels of 100 s^{-1} with experimental conditions: (a) temperature control by convection, (b) convection off, and (c) convection turned off and saturated atmosphere.

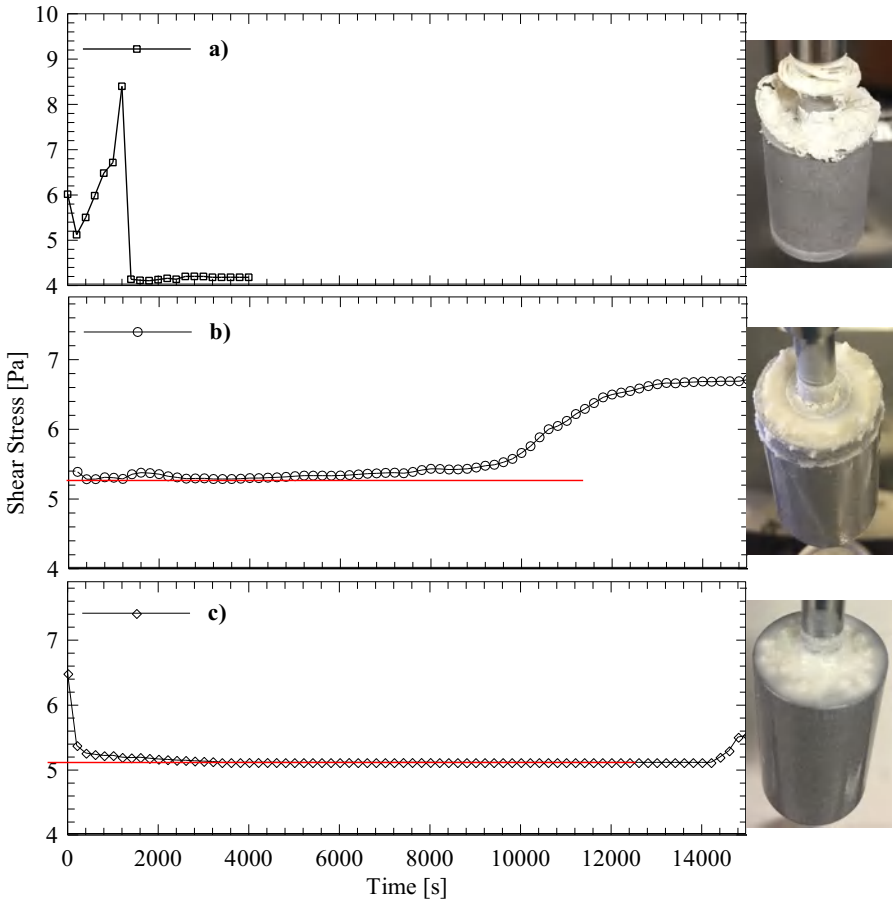

Source: Author (2021)

Figure B.4 – Comparison of measurements for the convection system off under saturated atmosphere and measurements through an invasive method of lower density surface layer fluid with temperature control by air convection at 25 ºC and a shear rate of 100 s^{-1}.

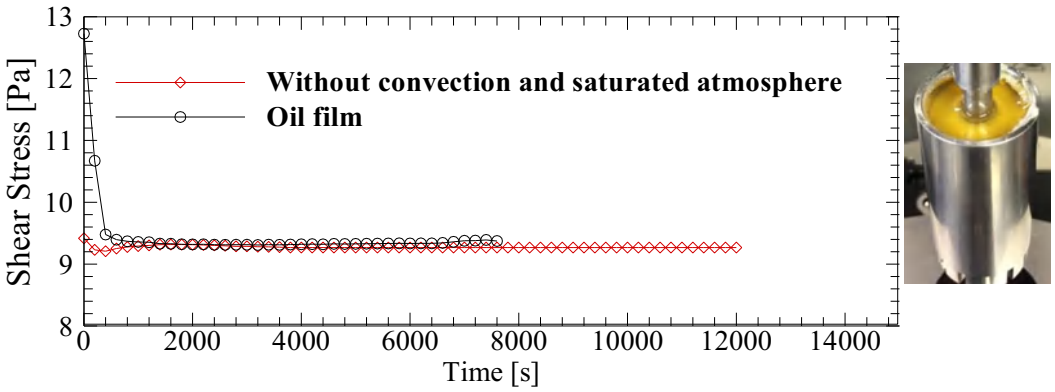

Source: Author (2021)

APPENDIX C - ORDER-DISORDER CONFORMATIONAL TRANSITION OF XANTHAN GUM SOLUTION

The validation was carried out according to the data shown by Pelletier et al. (2001), who measured the transition temperature of a xanthan gum solution of 1 % w/w and 0.008 M NaCl in distilled water, the procedure for preparing the sample consisted of initially mixing 400 ml of distilled water and 0.18 g of NaCl at 99 % purity for 10 minutes, then 4 g of xanthan gum were added homogenizing the sample for 5 minutes. The sample was heating under stirring for one hour at 80 °C to obtain complete dissolution and left overnight before any measurements were performed. The solutions can be considered to be in the "concentrated regime", the onset of which is defined by $C^{**} = 8/[\eta]$. C^{**} is calculated to be 0.27 % w/w (MILAS et al., 1990; PELLETIER et al., 2001).

In the case of the xanthan gum solution validation, a temperature ramp ranging from 25 to 80 ºC was imposed, and for the water-based drilling fluid, it was from 4 to 125ºC. The test starts by leaving an isotherm of 25 ºC for 2 minutes, and then the ramp is applied to a rate of 1 ºC/min^{-1}, then it was maintained at 80 ºC for 10 minutes, at the end of the previous interval a descending ramp to the same rate is imposed up to 25 ºC keeping it constant for 2 minutes. The measurements were repeated three times to check the repeatability. The order and disorder transition temperature for the xanthan gum and NaCl solution was determined by the exothermic peak in the temperature increase process resulting in a temperature of 51.8±0.48 ºC as can be seen in Figure C.1. The temperature range where the exothermic peak occurs begins more or less at 51.4 ºC and ends at 52.96 ºC and the absorbed heat flux was 1.9663 J/g. Comparing these data with those shown by Pelletier et al. (2001), where the exothermic peak obtained was 52 ºC, we can affirm that the methodology meets the adequate requirements for determining the transition temperature for drilling fluids with Xanthan gum.

Figure C.1 – Verification of the methodology used to measure the transition temperature with micro DCS for Xanthan gum + NaCl solution.

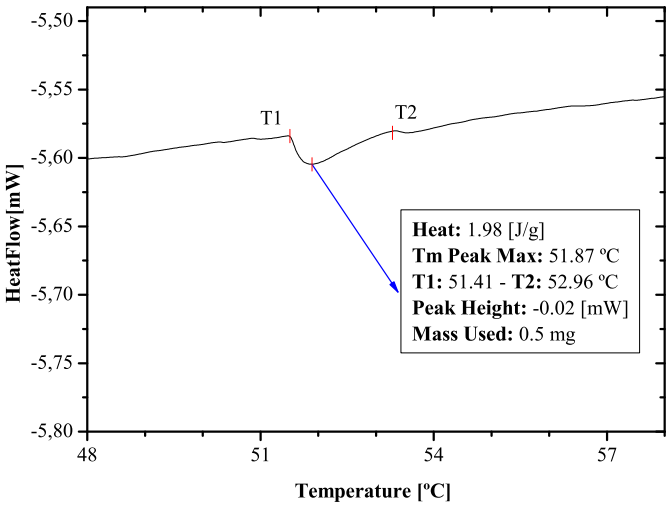

Source: Author (2021)

APPENDIX D - STATISTICAL ANALYSIS FOR HPHT MODELING

Next, the averages, the standard deviation, and the analysis of variation (ANOVA) of a single factor with a significance level of 95% are presented. In the first place, the statistical analysis was shown for the variations of the temperatures at atmospheric pressure, and in the second place, the results for high pressure and high temperature were presented.

D.1 **ANOVA for Different Temperature at Atmospheric Pressure.**

Table D.1 shows the averages and standard deviations of the measurements performed in duplicate to construct the flow curves for temperatures of 4, 10, 25, 40, 55, 70, 90, 100, and 125 °C at atmospheric pressure. The analysis of variance (ANOVA) was performed on the experimental data to evaluate any significant statistical difference between the repetitions' results for each temperature. At a significance level of 5% (value - P <0.05), the temperature effects are significant in the response variable up to the transition temperature.

Table D.1 – Experimental measurements of shear stress for temperatures of 4, 10, 25, 40, 55, 70, 90, 100, and 125 °C at atmospheric pressure with standard deviation for measurements obtained in duplicate.

Temperatures ºC	**4**	**10**	**25**	**40**	**55**	**70**	**90**	**100**	**125**
Shear Rate $[s^{-1}]$	**Shear Stress** [Pa]								
400	$27.35^{\pm 0.001}$	$25.13^{\pm 0.011}$	$24.30^{\pm 0.004}$	$19.60^{\pm 0.011}$	$15.72^{\pm 0.081}$	$10.74^{\pm 0.014}$	$4.32^{\pm 0.008}$	$2.35^{\pm 0.001}$	$1.30^{\pm 0.028}$
350	$25.88^{\pm 0.008}$	$23.68^{\pm 0.021}$	$22.92^{\pm 0.003}$	$18.23^{\pm 0.010}$	$14.15^{\pm 0.032}$	$9.44^{\pm 0.028}$	$3.99^{\pm 0.028}$	$2.10^{\pm 0.018}$	$1.09^{\pm 0.068}$
300	$24.05^{\pm 0.015}$	$21.91^{\pm 0.015}$	$21.25^{\pm 0.012}$	$16.74^{\pm 0.009}$	$12.78^{\pm 0.075}$	$8.73^{\pm 0.011}$	$3.64^{\pm 0.011}$	$1.83^{\pm 0.012}$	$0.89^{\pm 0.011}$
250	$21.82^{\pm 0.054}$	$19.97^{\pm 0.018}$	$19.35^{\pm 0.014}$	$15.10^{\pm 0.016}$	$11.36^{\pm 0.079}$	$7.56^{\pm 0.006}$	$3.19^{\pm 0.012}$	$1.53^{\pm 0.010}$	$0.77^{\pm 0.018}$
200	$19.27^{\pm 0.088}$	$17.69^{\pm 0.011}$	$17.20^{\pm 0.020}$	$13.27^{\pm 0.012}$	$9.83^{\pm 0.083}$	$6.18^{\pm 0.013}$	$2.64^{\pm 0.013}$	$1.31^{\pm 0.017}$	$0.65^{\pm 0.095}$
150	$16.34^{\pm 0.098}$	$15.06^{\pm 0.010}$	$14.71^{\pm 0.023}$	$11.20^{\pm 0.011}$	$8.16^{\pm 0.080}$	$5.83^{\pm 0.111}$	$2.15^{\pm 0.011}$	$1.05^{\pm 0.028}$	$0.51^{\pm 0.118}$
100	$13.15^{\pm 0.003}$	$11.93^{\pm 0.011}$	$11.53^{\pm 0.011}$	$8.79^{\pm 0.028}$	$6.24^{\pm 0.017}$	$3.92^{\pm 0.043}$	$1.57^{\pm 0.018}$	$0.80^{\pm 0.038}$	$0.37^{\pm 0.026}$
50	$8.81^{\pm 0.002}$	$7.97^{\pm 0.059}$	$7.69^{\pm 0.010}$	$5.82^{\pm 0.018}$	$3.96^{\pm 0.038}$	$2.20^{\pm 0.061}$	$0.99^{\pm 0.011}$	$0.50^{\pm 0.017}$	$0.26^{\pm 0.108}$
10	$3.86^{\pm 0.014}$	$3.53^{\pm 0.022}$	$3.24^{\pm 0.023}$	$2.31^{\pm 0.068}$	$1.43^{\pm 0.081}$	$0.83^{\pm 0.037}$	$0.43^{\pm 0.028}$	$0.19^{\pm 0.038}$	$0.11^{\pm 0.087}$
5	$2.88^{\pm 0.112}$	$2.68^{\pm 0.017}$	$2.48^{\pm 0.032}$	$1.58^{\pm 0.098}$	$0.91^{\pm 0.281}$	-	-	-	-
1	$1.59^{\pm 0.182}$	$1.42^{\pm 0.018}$	$1.32^{\pm 0.019}$	$0.85^{\pm 0.103}$	$0.5^{\pm 0.208}$	-	-	-	-
0.1	$0.84^{\pm 0.078}$	$0.77^{\pm 0.081}$	$0.68^{\pm 0.074}$	$0.45^{\pm 0.124}$	$0.25^{\pm 0.136}$	-	-	-	-

Source: Author (2021)

Table D.2 shows the factors obtained, which shows that the F parameters for all the tested temperatures were kept below the critical factor. The results showed that there is no statistically significant difference between the experimentally measured shear stress values.

Table D.2 – The ANOVA analysis factors for verifying of variations in the measurements at high temperature.

Temperature [℃]		**F**	$F_{critico}$
4			
10			
25	**Variation Source:**		
40			
55	**Shear Rate** $[s^{-1}]$	0,675	3.566
70			
90			
100			
125			

Source: Author (2021)

D.2 ANOVA for High Pressure and High-Temperature Measurements.

Table D.3 shows the average values and standard deviations of the experimental measurements carried out in duplicate for pressures of 10, 100, 400, 600, and 800 bar at temperatures of 25, 55, and 100 °C at a significance level of 5% (value - P <0.05), the effects of temperature and pressure factors are significant in the response variable.

On the other hand, Table D.4 shows the parameters obtained through the analysis of variance. No factor (F) was found lower than the critical factor by analyzing the results, indicating no significant differences in the measurements obtained.

The statistical analysis involved the fit of non-linear mathematical equations to the experimental results to validate the model through the analysis of variance (ANOVA). The correlation coefficient was used to verify the quality of the model generated by the data at a confidence level of 95% to assess all the terms of the model. The following shows the settings for the power-law and Herschel-Bulkley models for the pressure and temperature variation measurements. Table D.5 shows the consistency coefficient (m), flow behavior index (n), yield stress ($\dot{\gamma}$), and correlation coefficient (R^2) values obtained in the fit of the experimental data.

Table D.3 – Experimental measurements of shear stress for the pressure of 10, 100, 400, 600, and 800 bar at the temperature of 25, 55, and 100 ºC with standard deviation for measurements obtained in duplicate.

Temperature	**25** ºC				
Pressure [bar]	10	100	400	600	800
Shear Rate $[s^{-1}]$	Shear Stress [Pa]				
400	$23.48^{\pm 0.012}$	$23.34^{\pm 0.014}$	$23.77^{\pm 0.014}$	$25.58^{\pm 0.024}$	$27.26^{\pm 0.024}$
350	$22.10^{\pm 0.001}$	$22.28^{\pm 0.011}$	$22.66^{\pm 0.012}$	$24.38^{\pm 0.011}$	$25.51^{\pm 0.024}$
300	$20.49^{\pm 0.008}$	$20.92^{\pm 0.013}$	$21.22^{\pm 0.028}$	$22.53^{\pm 0.043}$	$23.79^{\pm 0.044}$
250	$18.75^{\pm 0.012}$	$18.92^{\pm 0.025}$	$19.70^{\pm 0.054}$	$20.80^{\pm 0.015}$	$21.89^{\pm 0.027}$
200	$16.73^{\pm 0.009}$	$16.95^{\pm 0.018}$	$18.01^{\pm 0.029}$	$18.91^{\pm 0.084}$	$19.63^{\pm 0.096}$
150	$14.37^{\pm 0.011}$	$14.42^{\pm 0.024}$	$15.50^{\pm 0.062}$	$16.09^{\pm 0.084}$	$16.70^{\pm 0.104}$
100	$11.47^{\pm 0.012}$	$11.60^{\pm 0.054}$	$12.75^{\pm 0.087}$	$13.10^{\pm 0.099}$	$13.82^{\pm 0.123}$
50	$7.75^{\pm 0.062}$	$8.40^{\pm 0.094}$	$9.41^{\pm 0.109}$	$9.81^{\pm 0.164}$	$10.31^{\pm 0.184}$
Temperature	**55** ºC				
Pressure [bar]	10	100	400	600	800
Shear Rate $[s^{-1}]$	Shear Stress [Pa]				
400	$11.56^{\pm 0.024}$	$13.58^{\pm 0.041}$	$14.82^{\pm 0.064}$	$15.60^{\pm 0.087}$	$16.63^{\pm 0.092}$
350	$10.30^{\pm 0.012}$	$12.41^{\pm 0.034}$	$13.79^{\pm 0.048}$	$14.89^{\pm 0.098}$	$16.19^{\pm 0.104}$
300	$9.28^{\pm 0.041}$	$11.28^{\pm 0.078}$	$12.82^{\pm 0.094}$	$14.19^{\pm 0.108}$	$15.49^{\pm 0.143}$
250	$7.85^{\pm 0.074}$	$9.91^{\pm 0.043}$	$11.95^{\pm 0.087}$	$13.50^{\pm 0.099}$	$14.74^{\pm 0.154}$
200	$6.68^{\pm 0.024}$	$8.58^{\pm 0.056}$	$10.69^{\pm 0.093}$	$12.73^{\pm 0.109}$	$13.88^{\pm 0.216}$
150	$5.29^{\pm 0.084}$	$6.99^{\pm 0.092}$	$9.28^{\pm 0.111}$	$11.37^{\pm 0.125}$	$12.69^{\pm 0.224}$
100	$3.49^{\pm 0.094}$	$4.97^{\pm 0.124}$	$6.95^{\pm 0.114}$	$9.80^{\pm 0.143}$	$10.93^{\pm 0.185}$
50	$1.49^{\pm 0.104}$	$2.79^{\pm 0.154}$	$4.46^{\pm 0.174}$	$7.51^{\pm 0.204}$	$8.49^{\pm 0.324}$
Temperature	**100** ºC				
Pressure [bar]	10	100	400	600	800
Shear Rate $[s^{-1}]$	Shear Stress [Pa]				
400	$2.351^{\pm 0.094}$	$3.843^{\pm 0.108}$	$4.841^{\pm 0.154}$	$7.010^{\pm 0.176}$	$8.115^{\pm 0.254}$
350	$2.01^{\pm 0.114}$	$3.35^{\pm 0.137}$	$4.55^{\pm 0.167}$	$6.60^{\pm 0.198}$	$7.80^{\pm 0.265}$
300	$1.53^{\pm 0.124}$	$3.11^{\pm 0.156}$	$4.31^{\pm 0.183}$	$6.42^{\pm 0.235}$	$7.54^{\pm 0.256}$
250	$1.35^{\pm 0.165}$	$2.89^{\pm 0.198}$	$4.08^{\pm 0.278}$	$6.10^{\pm 0.298}$	$7.10^{\pm 0.387}$
200	$1.11^{\pm 0.187}$	$2.35^{\pm 0.276}$	$3.35^{\pm 0.288}$	$5.60^{\pm 0.302}$	$6.60^{\pm 0.398}$
150	$1.05^{\pm 0.154}$	$2.13^{\pm 0.256}$	$2.91^{\pm 0.287}$	$5.05^{\pm 0.378}$	$6.05^{\pm 0.378}$
100	$0.60^{\pm 0.287}$	$1.73^{\pm 0.289}$	$2.50^{\pm 0.314}$	$4.37^{\pm 0.318}$	$5.37^{\pm 0.386}$
50	$0.50^{\pm 0.246}$	$1.37^{\pm 0.398}$	$1.87^{\pm 0.435}$	$3.48^{\pm 0.413}$	$4.48^{\pm 0.587}$

Source: Author (2021)

Table D.4 – The ANOVA analysis factors for verifying variations in the measurements at high-pressure and high-temperature.

Temperature		**25 ºC**		**55 ºC**		**100 ºC**	
Pressure [bar]		F	$F_{critico}$	F	$F_{critico}$	F	$F_{critico}$
10	Variation Source:						
100							
400	Shea Rate [s^{-1}]	0.489	4.145	0.501	3.167	0.096	4.156
600							
800							

Source: Author (2021)

Table D.5 – Parameters fitting of power-law and Herschel-Bulkley models at high-temperature.

	Power-law Model			**Herschel-Bulkley Model**			
Temperature (ºC)	m	n	R^2	m	n	$\dot{\gamma}$	R^2
4	1.15	0.53	0.99	0.98	0.55	0.48	0.99
10	1.04	0.53	0.99	1.08	0.52	0.18	0.98
25	0.70	0.51	0.99	1.02	0.52	0.11	0.98
40	0.52	0.57	0.99	0.57	0.58	0.19	0.98
55	0.30	0.65	0.99	0.26	0.67	0.19	0.97
70	0.11	0.75	0.97	0.11	0.75	0.15	0.97
90	0.06	0.70	0.99	0.04	0.75	0.13	0.97
100	0.021	0.784	0.99	0.01	0.89	0.13	0.96
125	0.006	0.88	0.98	7.38E-4	1	0.12527	0.87

Source: Author (2021)

Table D.6 – Parameters fitting of power-law and Herschel-Bulkley model at different pressures and temperatures.

	Power-law Model								
Temperature	**25 ºC**			**55 ºC**			**100 ºC**		
Pressure [bar]	m	n	R^2	m	n	R^2	m	n	R^2
10	1.005	0.52	0.99	0.06	0.86	0.99	0.01	0.90	0.99
100	1.18	0.50	0.99	0.18	0.71	0.99	0.15	0.52	0.96
400	1.66	0.44	0.99	0.65	0.52	0.99	0.27	0.48	0.99
600	1.52	0.47	0.99	2.32	0.31	0.99	0.92	0.33	0.99
800	1.53	0.48	0.99	2.90	0.29	0.99	1.34	0.30	0.99

	Herschel-Bulkley Model											
Temperature	**25 ºC**				**55 ºC**				**100 ºC**			
Pressure [bar]	m	n	$\dot{\gamma}$	R^2	m	n	$\dot{\gamma}$	R^2	m	n	$\dot{\gamma}$	R^2
10	0.78	0.54	0	0.98	0.06	0.86	1E-16	0.97	0.003	1	0.15	0.89
100	1.36	0.46	0	0.99	0.18	0.71	1E-16	0.98	0.05	0.68	0.44	0.95
400	1.66	0.44	0	0.99	0.55	0.54	0.35	0.99	0.26	0.48	0.01	0.95
600	1.52	0.47	0	0.98	1.13	0.41	2.25	0.99	0.92	0.33	0	0.96
800	1.08	0.52	1.62	0.98	1.51	0.37	2.41	0.98	1.34	0.30	0	0.94

Source: Author (2021)